National Library of Canada
Acquisitions and Bibliographic Services Branch
395 Wellington Street
Ottawa, Ontario
K1A 0N4

Bibliothèque nationale du Canada
Direction des acquisitions et des services bibliographiques
395, rue Wellington
Ottawa (Ontario)
K1A 0N4

Your file Votre référence

Our file Notre référence

NOTICE

The quality of this microform is heavily dependent upon the quality of the original thesis submitted for microfilming. Every effort has been made to ensure the highest quality of reproduction possible.

If pages are missing, contact the university which granted the degree.

Some pages may have indistinct print especially if the original pages were typed with a poor typewriter ribbon or if the university sent us an inferior photocopy.

AVIS

La qualité de cette microforme dépend grandement de la qualité de la thèse soumise au microfilmage. Nous avons tout fait pour assurer une qualité supérieure de reproduction.

S'il manque des pages, veuillez communiquer avec l'université qui a conféré le grade.

La qualité d'impression de certaines pages peut laisser à désirer, surtout si les pages originales ont été dactylographiées à l'aide d'un ruban usé ou si l'université nous a fait parvenir une photocopie de qualité inférieure.

Canada

Simulation of Ship-Ice Collision Dynamics

Development of ITHACA_SHIP, a Concept Exploration Model; and its Application in Predicting Hullgirder Stresses during Collisions with Multi-year Ice and Investigating the Influence of Transient Hydrodynamic and Ice Interaction Phenomena

by

Loyd D. Phillips

A Thesis Submitted to the Faculty of Graduate Studies of the University of Ottawa

In Partial Fulfillment of the Requirements for the Degree* of Doctor of Philosophy.

April 30, 1994

*A Joint Program with Carleton University Administered by the

Ottawa-Carlton Institute for Civil Engineering

ISBN 0-612-00492-9

Canada

UNIVERSITÉ D'OTTAWA
UNIVERSITY OF OTTAWA

Acknowledgment

The author would like to express his most profound gratitude to Hiroshi Tanaka for his excellent supervision and unwavering support throughout this journey. Without Professor Tanaka's insights and encouragement, the technical content of the research project would not have achieved its present depth. Nor would it have been personally so rewarding an experience.

A number of agencies have generously contributed funds for this research, without which the ITHACA_SHIP might have foundered. Ian Glen, as President of Fleet Technology Ltd., provided matching funds under an NSERC Industry-University Cooperation program. Ian Bayly from the Transportation Development Centre of Transport Canada is owed a special note of thanks for arranging a related research contract. Administrative support by Gilles Morier at the University Research Services has been greatly appreciated. Claude Daley and Sydney Mathews should also be thanked for their help in initiating the research project.

A great many individuals at the University or within the marine community have contributed to the development of the subject matter. In particular, Professor C. L. Tan provided an invaluable introduction to boundary integral equation methods. Bjarni Tryggvason has offered many pertinent suggestions, particularly concerning structural dynamics. For instilling an enduring interest in ship hydrodynamics and conceptual design methods, the author remains indebted to Charles C. Hsiung and Michael C. Eames at the Technical University of Nova Scotia.

Finally, every path of academic development has its darker moments. Those times were invariably brightened by the innumerable gestures of confidence and support from family and friends.

Abstract

The Canadian government has committed substantial research funds towards improving guidelines for the structural design of commercial ships operating in northern waterways. Of particular concern is the threat to survivability presented by head-on collision with multi-year ice or fragments of icebergs. The task of developing effective numerical models for studying the collision process has been hampered by the complexity of the physical interaction mechanisms. The present research considers the nonlinear and dynamic character of this problem.

A method for time-domain simulation of hullgirder stresses in icebreaking ships during collisions with multi-year ice is described. The model, ITHACA_SHIP, considers the transient ship-ice interaction and fluid-structure phenomena as strongly coupled through ship dynamics. Emphasis has therefore been placed on the development of hydrodynamic and ice force models.

Rigorous kinematic constraints at the interaction interface were identified as a critical factor in replicating the dynamic characteristics of prototype collision response. This led to the development of techniques for the three-dimensional mapping of the instantaneous ice boundary relative to the moving hull surface. The transient hydrodynamic force is also calculated directly, using boundary integral equation methods and a two-dimensional strip approach. The wave radiation problem for defining the free surface boundary of the fluid is based on a mixed Euler-Lagrange formulation.

The prediction of hullgirder stresses is carried out in two steps. Ice and fluid interaction forces are first determined from a rigid body motions simulation, and then subsequently applied as generalized forces in an analysis of flexural response. The hullgirder bending moments and stresses are extracted from the response. The modeling methodology has been verified by predicting simulated stress results for the *MV Arctic*, a multi-purpose bulk carrier. Good correlation was observed between the numerical predictions and corresponding results from physical model tests and full scale ramming trials. Further discussion is given concerning whipping indicated at higher impact speeds .

Nonlinearity of the ship-ice and fluid-structure interaction phenomena has been assessed by introducing progressively more complex representations of the physical mechanisms into the ITHACA_SHIP model. These studies found a high degree of coupling between the two effects. The transient hydrodynamic term was shown to be a significant factor, and the importance of the kinematic criteria confirmed. The indirect representation of collision interaction forces using conventional added mass and damping coefficients in the equations of motion was shown to be conceptually incorrect.

The present research has largely been limited to the development of the modeling methodology and examination of a number of suppositions concerning the collision process. But, interactive design software is available in the ITHACA_SHIP model which gives it a capacity for representing realistic ship forms. It may therefore be applied more generally as an engineering tool for conceptual design and parametric analysis; either to investigate collisions with ice, or other types of obstacles, such as mud banks and reefs.

Table of Contents

List of Figures

List of Tables

List of Symbols

A	Area, constant
AP	Aft perpendicular
A_s	Surface area
A_X, A_y	Projected area into Cartesian planes
B	Beam
BM	Bending moment
C_r	Generalized damping
CAC1	Canadian Arctic Class 1
CASPPR	Canadian Arctic Shipping Pollution Prevention Regulations
C_f	Coefficient of friction
CG	Centre of gravity
DK	Deck waterplane
E	Steel modulus
f	Friction
F	Freeboard, force
FP	Forward perpendicular
g	Gravitational acceleration
G	Centre of gravity
GM	Metacentric height
h	Heave
I	Section inertia
I_o	Mass moment of inertia
ITTC'57	International Towing Tank Convention, 1957
KG	Distance of centre of gravity above keel
K_r	Generalized stiffness

LBP	Length between perpendiculars
LCB	Longitudinal centre of buoyancy
LCG	Longitudinal centre of gravity
LOA	Length overall
m	Ship mass
m_i	Added mass
M	Moment, bending moment
M_r	Generalized mass
N_Z, N_Y	Normal force components
n_Z, n_Y	Unit normal x,y components
NA	Neutral axis
P	Pressure
q_r	generalized coordinates
Q_r	Generalized force
s	Surge
S	Section modulus
SWBM	Stillwater bending moment
T	Draft, kinetic energy
t	Time
V	Volume, velocity in knots, potential energy
VCG	Vertical centre of gravity
v_n	Normal velocity
WL	Water line
Y	Vertical displacement
Z	Surge displacement

λ	Model scale factor
β	Deadrise angle, coefficient
ε	Normal ice interface distance
ϕ	Mode shape, velocity potential
ψ	Admissible shape function
∇	Ship volume displacement
ρ	Water density
τ	Shear force
μ	Dynamic viscosity
σ	Stress
σ_{CR}	Uniaxial compressive strength
σ_6	Midship stress
σ_{max}	Maximum stress
θ	Pitch angle
ζ	Damping factor

Chapter 1 Introduction

1.1 General Background

The structural design of ships operating in Canada's northern waterways is governed by the Arctic Shipping Pollution Prevention Regulations, CASPPR. The need for scientific guidelines was first given impetus by the discovery of oil in 1968 at Prudhoe Bay on the Beaufort Sea coast of Alaska. The potential hazards of operating transportation routes through ice covered waters was investigated during the 1969 and 1970 voyages of the *SS Manhattan* through the Northwest Passage. Gray and Maybourne (1981), and Mookhoek et al (1981) have described the *Manhattan*'s conversion from a twin-screw tanker into an icebreaking vessel; and have summarized the experience gained from this project.

Most early experimental data had involved icebreakers, which are generally much smaller vessels, possessing distinct hullform geometries and structural properties which are significantly different from commercial cargo vessels or ocean-going tankers. It was found that the greater momentum of a massive icebreaking tanker, such as the *Manhattan*, allowed continuous mode operation in relatively thick ice; where most icebreakers would have been forced to operate in a ramming mode. The *Manhattan* voyages also demonstrated the limitations imposed by multi-year ice. In general, multi-year was avoided. But in one specific series of trials, the *Manhattan* rammed an ice island at speeds of up to five knots. The measured longitudinal bending stresses were well below the wave design criteria and not deemed to represent a problem. In contrast, the most severe damage

occurred during open water transit (at higher speed) of Davis Inlet. A large hole was punctured beneath the icebelt, caused by collision with a small growler or bergy bit.

Throughout the 1980's an Arctic Class 2 icebreaking cargo vessel, *MV Arctic*, provided a research platform for investigating structural design concepts and operational problems inherent in Arctic transportation. The *MV Arctic* was proposed in 1975 as a prototype for a growing fleet of commercial icebreaking cargo vessels. Consequently, the Canadian government and a group of shipping companies formed a consortium for its construction and operation. Hearnshaw et al (1981) have described the instrumentation system which was installed for measuring ice loads and longitudinal deck stresses. Multi-year ice ramming data for low speed impacts was collected from dedicated field trials in 1984. In conjunction with physical model tests and numerical modeling, this data has provided a basis for many of the changes included in the Proposed Modifications to the CASPPR Guidelines (1989).

Daley, St. John, et al (1984) have reported full scale trials data on global ice loads for large icebreakers. This was based on an experimental program involving the USCGC *Polar Sea* and *Polar Star*. Ghoneim et al (1984) have given a corresponding set of ice ramming results for the smaller icebreakers *Canmar Kigoriak* and *Robert Lemeur*.

The holings sustained during trials of both the *Manhattan* and the *MV Arctic* are examples of local failure of the exterior structure of the hull. As indicated by the extent of damage caused at relatively slow contact speed, this type of problem can be of significant concern. Its study involves predicting local ice pressures, and analyzing grillage and plating strength in terms of the detailed structural design of the sideshell. Research in this area has led to recommended design criteria for plating thickness in ice belts and other zones of the hull, as well as the more widespread usage of double skins.

Despite the acknowledged importance of protecting icebreaking ships from bow damage, such local plating failure is not generally believed to pose the gravest threat to survivability. Subdivision requirements, in combination with the use of double skins limits the extent of maximum flooding. It should be noted that the *Exxon Valdez* which grounded in Prince William Sound in 1989 was not an icebreaking tanker. Moore (1994) explains that double hulls only became mandatory in American territorial waters after the passage of the Oil Pollution Act of 1990.

Rather, the extreme damage scenario is believed to involve an accidental collision of a ship with a large growler or multi-year ice floe in an open water channel. It is feared that the global ice forces generated during such a collision at open water speeds could result in a catastrophic failure of the longitudinal hullgirder structure. This is the main problem addressed in the present work.

1.2 Ship-Ice Collision Dynamics.

The formulation of a collision theory for a ship striking a massive ice body is typically divided into two independent problems. One involves the computation of global response. The second addresses concerns about local structural damage. This separation corresponds to a parallel expression in the classical theory of ship collision dynamics dating from Minorski (1959). For a collision involving two ships the problem of outer dynamics concerns itself with the motions of the ships and the influence of the surrounding water. Inner dynamics considers the structural damage to the bow and sideshell of the two ships respectively. Petersen (1982) provides an excellent example of a classical outer dynamics problem; simulating structural deformations as nonlinear springs, and sectional hydrodynamic effects by means of unit response functions.

White (1965) has given a detailed mathematical treatment of the outer dynamics problem for an icebreaker during ramming interactions. He traced the historical development of ship-ice collision modeling from Runeberg's 1888 paper, through Kari and Simonson to Vinogradov's (1946) equations. A comprehensive assessment is given of several formulations based on Vinogradov's energy method by Jansson, Richardson (1959) and Milano (1973). Popov et al (1968) have shown a substantive parallel development of ship-ice collision models in the Russian literature.

White departed from earlier theory by formulating his model in terms of Newton's laws, rather than as an energy method. Despite the intrinsically dynamic nature of energy formulations, White found that these models had treated the ice forces as a static equilibrium process. In addition, an erroneous energy loss term was introduced at the instant of contact as a result of assuming a direct central impact. This assumption is invalid for most stem angles, at which the ice force normal vector is not aligned with the ship's center of gravity.

White introduced an acceleration term to account for the change in direction of the center of gravity. The normal ice force was comprised of a crushing term, given by the product of the projected area of indentation and the compressive ice strength, and two orthogonal friction components. This force was divided into vector components depending on the stem angle and instantaneous pitch.

White adopted the convention of separating the ramming process into two principal stages; a crushing phase and a sliding phase. He wrote linearized equations of rigid body motion for each of these phases and linked them using a kinematic constraint. The differential equations governing the crushing phase was solved by numerical integration, and the sliding phase initial value problem was included by means of Laplace Transforms.

The rift between energy methods and Newtonian approaches has been more visible in the literature of ice resistance modeling. Milano (1973) has described the advantages of an energy model in accounting for the energy balance associated with various components of a cycle of icebreaking which involves cusp failures. Naegle (1980) gives a Newtonian solution to the ice resistance problem, akin to White's model. Popov et al (1968) formulates both collision dynamics and ice resistance problems in terms of energy methods; but explains the importance of transforming the Lagrange function for the system into differential equations of motion using the Euler equations. Attempting to directly solve the energy equation for the minimum energy path leads to difficulties, especially as the number of degrees of freedom of the system increases.

Kashteljan et al (1968) signaled a trend towards semi-empirical models to address practical design considerations, and away from the simulation of response. Laskow (1982) describes parametric hullform optimization methods, and derives approximate expressions for various ice interaction parameters as a function of various ship and ice variables. These relations do not consider hydrodynamic effects.

Vaughan (1983) utilized dimensional methods to investigate the influence of salient physical parameters on hull bending moment; giving expressions for the required shear strength and section modulus of icebreaking ships. Crushing of ice was not considered in this model. Rather, the ice force is represented at initial contact by an impulse, and by a point load during the beaching phase. A controversial outcome of Vaughan's approach was that the maximum bending could occur at a critical impact speed, less than the maximum, which depended only on the ship dynamics.

1.3 Flexural Response Models

During the 1980's flexural dynamics during ramming interactions was recognized as an important modeling consideration for certain classes of Arctic shipping and icebreakers. Vaughan (1986) demonstrated the significance of ship flexibility by analyzing the deflection of a uniform beam in a free-pinned condition. The energy loss due to an impulse at the point of contact was interpreted as an upper bound on the energy available for flexural mode response. Despite its rather simple representation of the ice force and ship structural properties, Vaughan's model showed reasonable agreement with trends observed in full scale trials of the *Canmar Kigoriak* (Ghoneim et al, 1984).

Risse (1973), Varsta and Hakala (1983), Daley (1984), Matsuishi et al (1984), and Ghoneim et al (1984) have described models allowing analysis of flexural response and hullgirder stresses based on a finite element or lumped mass approximation to the ship's modal properties. Whereas Vaughan and Ghoneim studied the relatively small and stiff icebreaker *Kigoriak*, Matsuishi et al examined the collision response of large commercial icebreaking ships using a four flexural mode model. A thirty percent amplification factor was observed for the larger and more flexible ships.

Thompson (1981) and other standard references show the formulation of coupled equations of motion for an arbitrary structure and describe methods of mathematical treatment. With sufficient computational capacity, they can be solved directly in the time domain using energy or perturbation methods. In cases involving beam-like structures vibrating with relatively small motions, it is often possible to simplify the problem using the Euler equation of beam bending. If it is desired to include the effects of rotary inertia and shear deformation, Timoshenko's more general equation can be substituted. For these problems it is more expedient to solve the equations using normal mode methods.

In ship dynamics the methodology for determining modal response is divided into two camps, according to their treatment of hydrodynamic effects. Bishop and Price (1976,1979) presented a theory of mode superposition for hydroelastic response based on dry modes. In commentary to their first paper, Atkins argued for the usage of wet modes, in which fluid effects are included in the determination of the mode shapes. He presented a NASTRAN beam element representation of the stillwater bending moment and shear which showed good agreement with theory using eight distortion nodes. But, only hydrostatic effects were included. Betts, Bishop, and Price (1978) subsequently extended the dry mode analysis into a strip thereby involving to include generalized fluid forces. In this method the linear fluid force at a section depended critically on added mass and damping coefficients obtained using an expression given by Gerritsma and Beukelman (1964).

1.4 Ice Interaction Models

A limited understanding of ice failure mechanics has prevented a definitive formulation of the ship-ice problem. Sunder (1986) provides a summary of current limitations of ice load prediction models. He lists five principal areas of uncertainty; the mechanical properties of ice, analysis methods, interface modeling of contact forces, scale effects, and environmental factors.

Sunder is referring to the simpler problem of a cylinder indenting a continuous ice sheet. A number of models have been advanced using plasticity theory based on the von-Mises yield criterion given by Michel and Toussaint (1977), or a Tresca criterion suggested by Croasdale et al(1977), or a transversely isotropic yield function developed by Reinicke and Ralston (1977). He also reports

promising developments in the use of constitutive theories for describing mechanical ice properties, and in the application of finite element approaches.

The ship-ice collision is yet again a more complex problem, since dynamic response becomes a significant issue. This has encouraged the use of empirical models in design practice. Daley (1984), for example, has described the Baffin model, including an improved modeling of the ice force achieved by dividing the penetrated ice volume into a series of finite crushing layers.

White's projected area expression for the ice force involved only uniaxial crushing strength and friction. A number of researchers have proposed various methods for representing the mechanical properties of ice. For example, Kheysin (1966) introduced a nominal pressure based on elastoplastic theory. Varsta (1983) suggested a nominal ice pressure based on measured multiaxial ice strength. It included empirical coefficients for interaction factors, such as indentor geometry and contact surface, as well as the crushing strength. Riska and Frederking (1987) have extended this multiaxial approach. Riska (1987) has explored the use of infinite elements in determining nominal ice pressures; and Daley (1991) has advanced a model based on chaos theory. The evolution of methods for defining an effective, or nominal, ice contact pressure is discussed more fully in Chapter 4.

1.5 Hydrodyamic Force Models

A second fundamental difficulty in modeling ship-ice collisions involves the treatment of transient fluid forces. Risse's (1973) finite element analysis of a large icebreaking cargo vessel demonstrated this limitation. Following White's methodology for determining fluid forces, Risse found that the hydrodynamic mass was nearly equal to the inertial mass. Risse also investigated the effect of

varying the proportional damping applied to the modes. Although successful in defining general trends, Risse was unable to identify correct methods for computing the transient fluid forces.

Traditionally, the accepted method for handling hydrodynamic phenomena has involved a mechanical representation in terms of an added mass and damping component introduced into the equations of motion. Popov et al (1969) and others have given empirical added mass and damping relationships specifically for icebreaker hullforms. However, it is more common to express the hydrodynamic force in terms of two-dimensional, sectional added mass and damping coefficients. Lewis (1929), Grim (1957), Frank(1967), and Bishop et al (1978), among others, have defined procedures for evaluating these coefficients for heaving cylinders and more general section shapes.

Gerritsma and Beukelman (1963,1964) have conducted a series of oscillation tests on a segmented ship model which has shown reasonable correspondence between experimentally derived force components and analytic theory. Nonetheless, the Fourier separation of sine and cosine components into frequency domain added mass and damping coefficients is not strictly valid.

Second order theories have been developed by Parissis (1966), Lee (1968) and Potash (1971) for circular and U-shaped cylinders immersed in the free surface. Finite difference implementations for large amplitude motions of cylinders have been reported by Hausling et al (1975), Telste (1985), and Wang and Spaulding (1988). An extension of the method to analyze arbitrary section shape is given by Venkat and Spaulding (1990). The first, second and higher order harmonics of force determined by these numerical methods are generally reported to show good agreement with the corresponding theory. However, the exact physical meaning of these force harmonics is questionable. Only the first order Fourier component can be associated with added mass and damping in the classical sense of Frank's theory or Gerritsma and Beukelman's experiments.

Hydrodynamic added mass and damping coefficients are derived from potential theory. The mathematical techniques for different potential problems have defined theoretical ship hydrodynamics for the past fifty years. One branch of this field has emphasized the initial value or transient flow problems. Major contributors include: Ursell (1948,1953,1963), John (1949,1950), Finkelstein (1957), Stoker (1957), Wehausen (1967,1971) and Maskell (&Ursell,1970).

The mathematical complexity associated with these analytic formulations had long placed severe limitations on the generality of cases which could be studied. The recent advanced is finite element and boundary integral methods have greatly simplified the direct inclusion of the surrounding water within a structural response modeling process. For example, Hakala (1985) has reported a finite element approach for determining the dry modes of the ship as a Ritz function basis for determining the modal added mass and damping matrices from the fluid elements. This assumed only light coupling of the fluid and structure. Similarly, boundary elements applications on the free surface have become more accessible since the work of Longuet-Higgins and Cokelet (1976). The latter approach has been found useful in the basis for the current project, which is described more fully in Chapter 5.

1.6 *ITHACA_SHIP, A Concept Exploration Model*

The image of ITHACA_SHIP links modern scientific modeling to its origins in the remote past of Homer's Odessey, a seafaring tale that is poignant with the challenge of finding order amidst thecomplexity of human nature and world events. In the present context it is an acronym for the collision modeling process: 'Integrated Transient Hydrodynamic Arctic Collision Analysis - and SHIP design'.

ITHACA_SHIP has been developed as a concept exploration model for numerically investigating the nature of the ship-ice collision. Eames and Drummond (1976) have described the importance of introducing such methods at the earliest stages of a conceptual design and analysis process. Applications of this type will, in general, involve a broad range of parametric variations. It is therefore essential to establish an integrated approach which automates the individual design and analysis procedures; while adequately representing all of the pertinent physical mechanisms. Figure 1.1 illustrates the major components and organizational structure of the concept exploration model which has been developed.

The prediction of hullgirder stresses is reached through a three stage process. Its starting point is the interactive Hull Design Model. Realistic numerical ship sections are automatically generated from a small set of parameters. The basic geometry of the hullform is defined by specifying the principal dimensions, some angles, and the fractional length of the ship falling within bow, stern and parallel midbody regions. As a further refinement, it is possible to assign different mathematical curves to the sections in each of the regions. Structural properties and mass distribution are numerically implemented from standard methods in Naval Architecture (Comstock, 1967). In many cases, options are available for manual input or application of alternative formulations.

The second stage of the analysis involves the time-domain computation of interaction forces in the Rigid Motions Model. A fundamental characteristic of the present modeling methodology is its emphasis on the accurate kinematic mapping of displacements defining the ship-ice and fluid-structure interfaces. These interaction forces are dynamically coupled through the rigid body motions. A Lagrange equation formulation for the equations of motions has been employed; but the energy equations are interpreted in a manner virtually identical to a Newtonian analysis.

FIGURE 1.1 Major Components of the ITHACA_SHIP Model

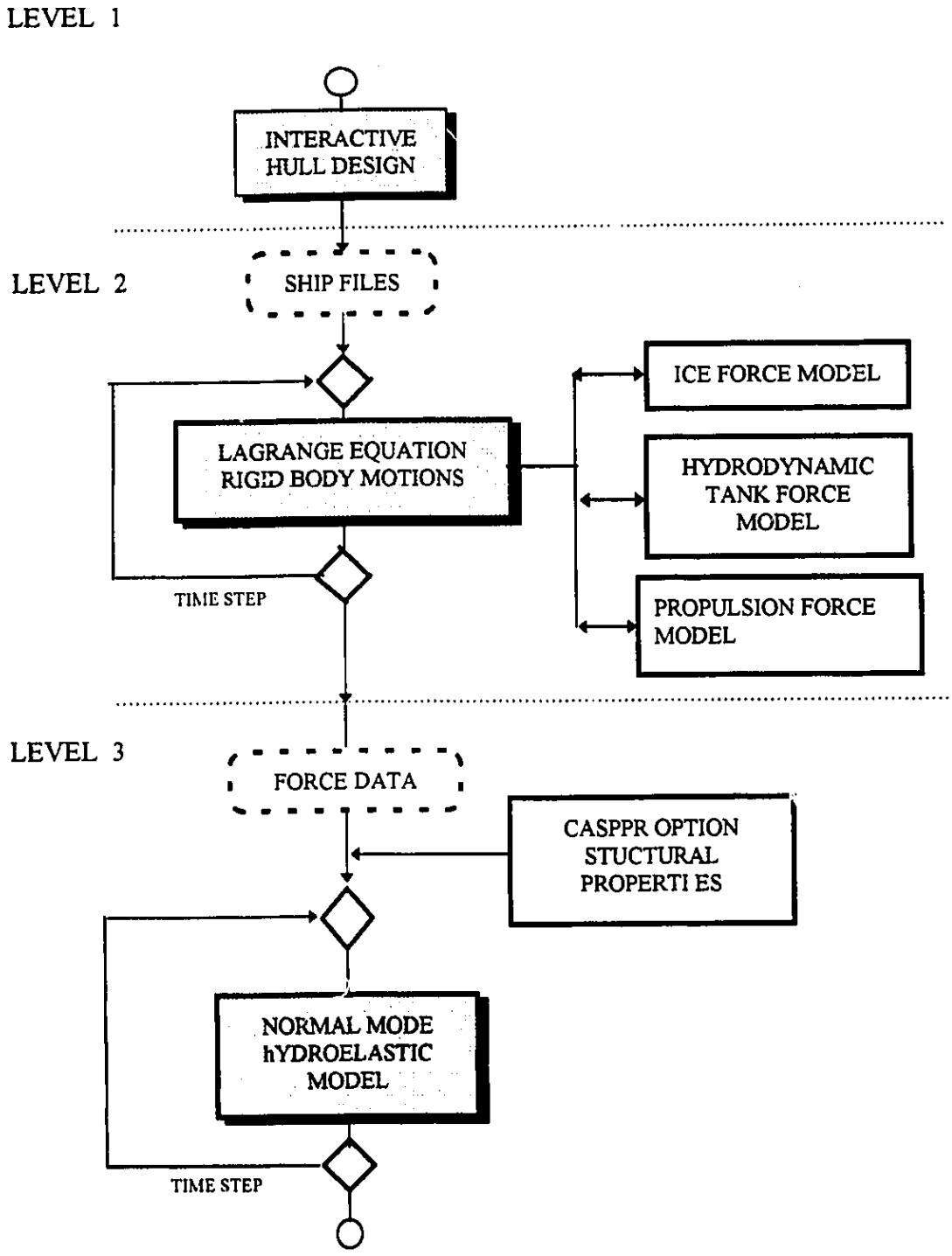

The ice modeling process starts from an assumption that the ice floe is of a sufficiently large size and thickness, such that it will not fail in shear and can be considered fixed throughout the collision. Ice forces are computed based on a three-dimensional ship-ice interface. Crushing is assumed as the dominant physical mechanism but additional elastoplastic characteristics are also included.

The hydrodynamic forces are generated in the BEM Numerical Wavetank by means of a strip approach. Independent sectional wavetanks are assigned to compute the transient pressures at each station along the hullform. Coupling and wave effects in the surge direction are neglected. The fluid is assumed to be incompressible and irrotational in accordance with generally accepted methodology. A boundary element method is used to solve for the unsteady pressure forces on the body boundary.

In accidental collisions, it is assumed that there will be a sudden loss of propulsive efficiency immediately after impact. This is caused by severe loading of the propeller. There is also a corresponding transient variation in surge hydrodynamic phenomena. But since the thrust and open water resistance are considered secondary and somewhat counterbalancing effects, they have not been included in the present model. Nevertheless, the magnitude of this effect can be examined using drag algorithms based on Michell's wavemaking theory and the ITTC'57 frictional resistance line.

The final stage in the modeling process is the Hydroelastic Model; which determines the flexural stresses from a time-domain simulation of the ship's normal mode

response. The interaction forces produced in the Rigid Motions Model are applied as generalized forces in a dry mode analysis. It should be remarked that the flexural response and stresses could have been computed directly, and without recourse to an intermediate, rigid motions step. But this would have precluded variation in section modulus using the same force results. Repeating the hydrodynamic force calculations for each section modulus would be very time consuming.

1.7 Scope of the Present Work

The ITHACA_SHIP model provides a basis for studying the nonlinear and dynamic characteristics of the collision process. The following chapters describe its major components, and their importance within the context of a numerical modeling methodology. Idealizations of physical mechanisms are explained, and salient features of the mathematical formulation and numerical implementation are given.

Chapter 2 describes the interactive Hull Design Model, its basic design options, and the steps required to produce realistic ship forms. The most important algorithms for implementing the mathematical characteristics of the hullform geometry and its corresponding structural properties are discussed. As an example of its application, the hullform geometry of the *MV Arctic* (as it existed at the time of the 1984 Trials) is developed.

The present research is limited to a treatment of the outer dynamics problem for a ship in a head-on collision with multi-year ice. Chapter 3 provides a theoretical basis for

the simulation of ship collision response in terms of a Lagrange equation formulation. This gives equations for the rigid body motions. A corresponding treatment for the normal mode flexural response and the longitudinal hullgirder stress is also developed. In both cases, the timestepping of spatial variables is accomplished by means of a Newmark $\beta = 1/4$, or constant average acceleration, method.

The definition of interaction forces and their inclusion in the simulation process is central to the overall modeling methodology. The equations of motion include the forces explicitly, rather than indirecly representing them by virtual coefficients in a mechanical representation. Abandonment of fluid added mass and damping, as well as ice spring stiffness, leads to the requirement for time-domain force models; and explains why the flexural response is formulated in terms of dry, rather than wet, modes.

Another question which is introduced at this stage concerns the accuracy and relative usefulness of bending moment and shear time histories generated by the rigid body motions, as opposed to those corresponding to flexural motions. This includes a comparison between the stillwater bending moment derived from hydrostatic equilibrium conditions and the corresponding distribution resulting from a dry mode flexural analysis.

Chapter 4 describes the conceptual development and numerical implementation of the ice model. Three progressive levels of modeling complexity have been considered. At each succeeding level there is greater accuracy in representing the contact interface forces. The simplest approach is based on the projected area of indentation of the ship bow into the ice. A dynamic profile contact area method is next introduced. It is defined by the instantaneous intersection of the bow profile and the centerline curve of the ice notch.

The most complete model gives a three dimensional representation of the contact interface. It correlates the relative displacements of elements from a variable size ship grid, and corresponding points on a mesh that defines the deformed ice surface.

The primary function of the ice model is viewed as the generation of dynamic contact forces within the broader context of the ship's rigid body or flexural response. This has led to a focus on accurate representation of geometrical and kinematic components of the interaction process. The mechanical modeling of ice properties has been kept deliberately simple. The ice force calculation emulates White's use of a pressure-area relationship based on uniaxial compressive strength. A normal friction component is also included. In addition, the mathematical modeling of several secondary interaction mechanisms are described.

At the end of Chapter 4 there is a continuation of the earlier discussion about the modeling of interaction forces within a Lagrange equation formulation. It involves a qualitative assessment of the ice interaction energies which can be derived from a detailed breakdown of the data at the ice interface. It should be remarked that the reference ice force data in the present study comes from the 1984 *MV Arctic* trials. These ramming tests were at quite low impact velocities and spanned a relatively narrow range. So it has not been considered worthwhile to extend the present analysis to consider the question of dependence of the ice pressure on strain rate or other variables.

Chapter 5 contains a description of the BEM Numerical Wavetank model which was developed for generating transient hydrodynamic forces. An introduction is given to the boundary element (or boundary integral equation) method. The kernel BEM

algorithms in the present model are adaptations from Tan (1987). A finite difference discretization of the Lagrange free surface wave condition has been used which derives from Chan (1987). A 4^{th} order Runge-Kutta integration method is used to advance the wave potentials in time. Fluid pressures on the body surface are derived from the potentials using the Bernoulli equation. A Taylor expansion process has been developed for extracting the transient pressure term.

The numerical tank implementation involved the creation of large data structures for controlling the transfer and storage of blocks of information at each boundary point. Its complexity is increased by a multiple path methodology for following individual fluid elements on the free surface. An expandable, Chebyshev interval grid on the free surface defines new sets of fluid paths at each instant. The key elements of this infrastructure and the boundary fitting technique are described.

The numerical tank was first configured as a piston-type wavemaker. This permitted an examination of the waves produced and a comparison with wavemaker theory, as described by Dean and Dalrymple (1984). A circular cylinder was subsequently half immersed in the free surface and subjected to periodic heave oscillation. The hydrodynamic force histories from the cylinder tests have served as a basis for discussing the accuracy and stability of the hydrodynamic results. The effect of variation in frequency and of large amplitude motions is examined.

Adapting the hydrodynamic model for use in the ITHACA_SHIP model involved a number of innovations. A few of the topics discussed are: scaling of the BEM Numerical Wavetank as a function of ship section dimensions, dynamic fitting of body grid points, a

Chebyshev distribution of strips along the ship, and treatment of section submergence and emergence. The significance of different hydrodynamic force components is quantified by comparing simulation results from different fluid models; including: buoyancy, dynamic pressures, and transient effects.

Chapter 6 documents an application of the ITHACA_SHIP model. The collision response of the *MV Arctic* is simulated over a broad range of contact velocities. Predicted hullgirder stresses are compared to physical model data reported by the author (Phillips et al, 1986; Daley and Phillips, 1986) and to an analysis of the 1984 full scale trials given by Melville/VTT (1984).

The strengths and limitations of the conceptual framework and basic methodology embodied in the ITHACA_SHIP model are summarized in Chapter 7. The principal results of the project are examined. In particular, the earlier discussions concerning the characteristics of the interaction forces, and appropriate method of representing the essential physical mechanisms, are completed.

Chapter 2 Hull Design Model

Conceptual ship design considers procedures for defining a basis ship whose general hullform particulars, structural properties and powering capacity satisfies a prescribed set of functional and operational criteria. Eames and Drummond (1976) have given a general methodology for identifying and systematically varying the significant parametric relationships which govern the ship design process. The first step in their approach was known as Concept Exploration. Its design spiral included algorithms for basic dimensions, hullform geometry, propulsion, ship and combat systems, weights and volumes, stability, flooding, structural strength, and seakeeping performance. Two subsequent steps involved Concept Development and Validification. This model was effective in optimizing the performance and other design characteristics of a particular class of warships by testing thousands of parametric variations.

The design of large icebreaking ships presents a number of difficulties at the concept exploration stage. Ship classes have traditionally evolved through incremental changes from previously existing designs. But proposed icebreaking tankers and cargo vessels are markedly different from either their open water counterparts, or from conventional icebreakers. Furthermore, the level ice performance is generally considered as the primary design problem. Some authors, such as Edwards, Jr. et al (1976) , have investigated the influence of icebreaker parameters and assigned empirical relationships for

their performance in level ice. But ramming and accidental collision have largely remained of secondary concern. So, at this time, formulating a concept exploration model which includes these types of interactions in terms of empirical relationships alone would not be a valid approach.

ITHACA_SHIP as a concept exploration model is more limited in scope than a complete design spiral for optimizing a commercial icebreaking ship. It considers only those elements necessary for analyzing the ramming performance, leaving aside any concerns about steady-state performance in level ice, open water, or waves. Emphasis is placed on flexible analysis of specific designs, rather than on optimization. Extensive use is made of analytic modeling and numerical simulation, since empirical relationships are seldom available.

2.1 Interactive Hull Design

The Hull Design Model denotes those software elements within the ITHACA_SHIP model that are used in the numerical development of realistic hullforms; and defining their hydrostatic, powering and structural characteristics. Its four principal modules are shown in Figure 2.1, together with an outline of their major components.

FIGURE 2.1
HULL DESIGN MODEL
OVERVIEW OF MAIN COMPONENTS

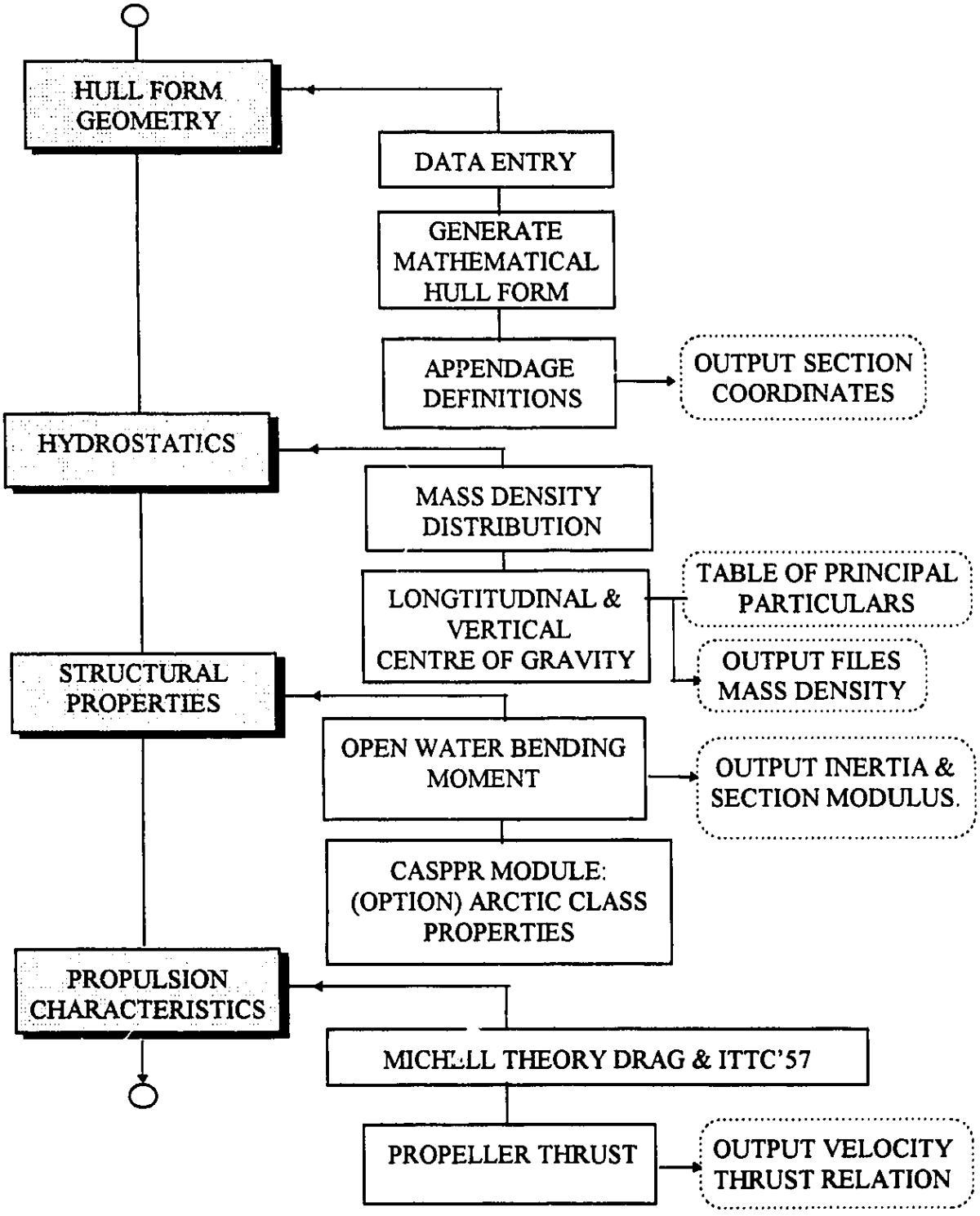

It should be remarked that the ship design process permits two independent modes of operation. For purposes of analysis, one might wish to investigate the collision response of a known ship. In this case, the model parameters would be selected to provide the closest numerical representation of the prototype hullform geometry and its various properties. This fitting process is simplified by interactive data entry procedures. Users either invoke default algorithms for computing required information in accordance with standard practice or theory, or optionally input data manually. However, incorrectly assigning properties such as mass distribution can lead to serious distortion and failure in the simulation programs. The second mode of operation involves defining a new basis ship and conducting a parametric investigation. In this case, there would be a more extensive use of the default calculations.

2.2 *Hullform Geometry*

The Design Model numerically generates curves defining cross-sections along the length of a ship. These section curves are automatically developed from a specified set of hullform parameters and mathematical relations. While output may be represented graphically, this process of mathematical hullform generation should not be confused with manually drawing lines plans and mechanically extracting coordinates.

Figure 2.2 illustrates the main divisions and elements of a simple representative hullform. The forward region of the ship is denoted as the forebody. The bow forms a

part of this division. At the opposite end is the aftbody, including the stern. A parallel midbody may be present, defining a region of the ship where the sections have identical dimensions and curvatures. The forward perpendicular (FP) is the point of intersection of the waterline and the bow profile. The corresponding intersection point at the stern is the aft perpendicular (AP). A fixed number of stations or cross-sections are traditionally defined between the forward and aft perpendicular.

The length between perpendiculars (LBP) is the distance along the waterline from forward to aft perpendicular. The length overall (LOA) is measured between opposite extremes of the ship along the deck centerline. The maximum or molded depth of the ship from the keel baseline to the deck is divided into two parts. The design draft (T) represents the maximum wetted depth of the ship when undisturbed in still water. The freeboard (F) represents the distance from the waterline to the deck. The beam (B) is the maximum width of the ship on the waterplane. In contrast, the section breadth gives the width at any section, irregardless of it being a maximum value.

A more detailed division of a ship is shown in Figure 2.3. The forebody is shown to consist of three distinct regions. The prow defines sections which are forward of the FP, and therefore entirely above the waterline. The bow defines a curved profile from the waterline to the baseline. It may also contain an iceknife. Sections in the forebase region have a finite width of flat bottom. Seen in the baseplane, waterplane or deckplane, the forebase curves towards a maximum width at the adjoining parallel midbody. This central region may, or may not, be wallsided depending on the selection of the maximum base width.

FIGURE 2.2
REPRESENTATION OF A SIMPLE HULLFORM

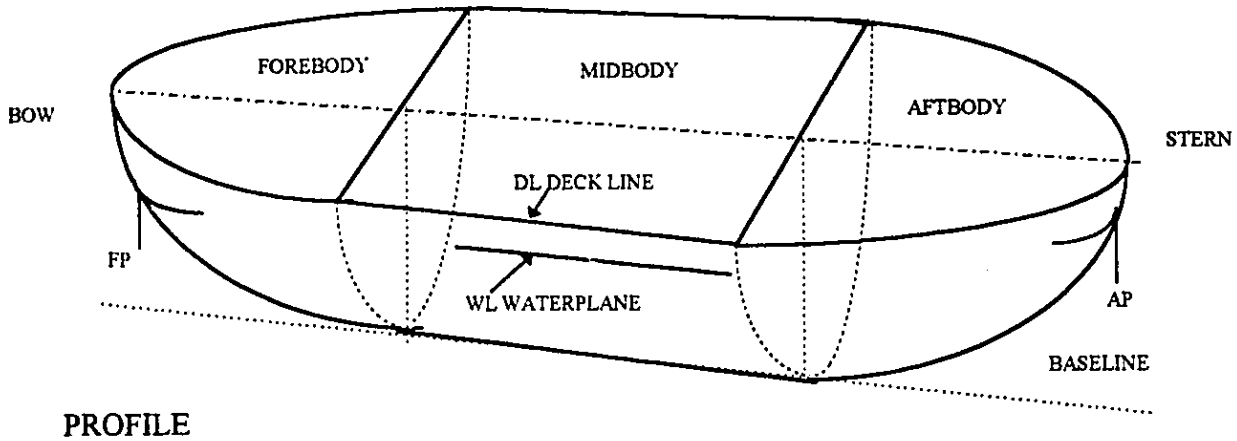

PROFILE

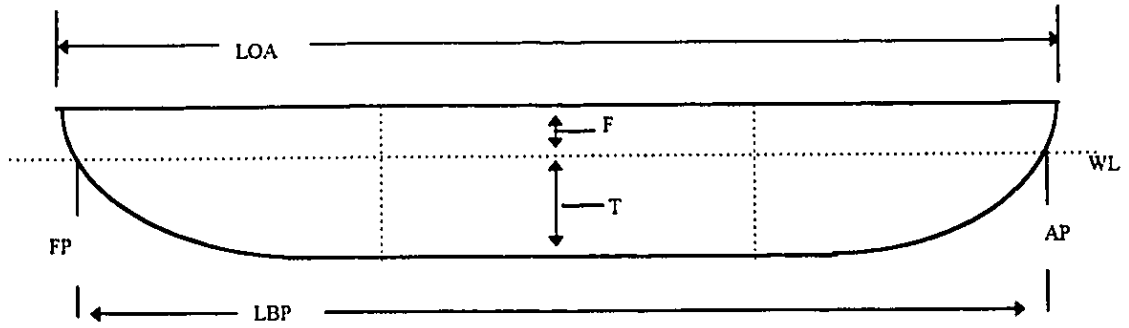

PLAN VIEW (Half Plane)

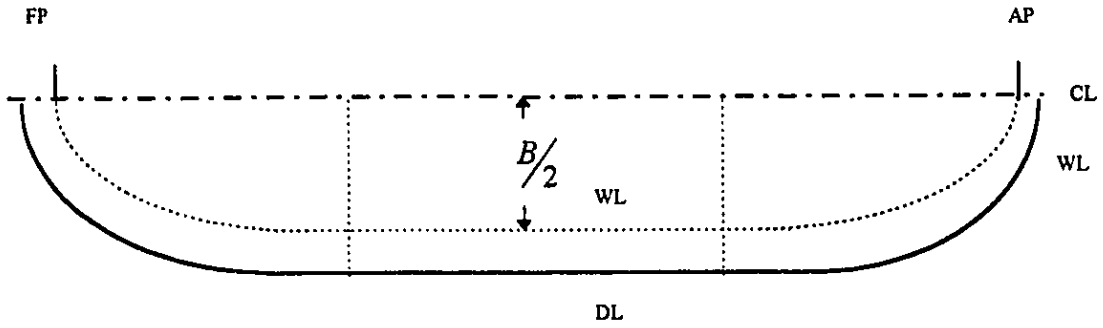

FIGURE 2.3
DEVELOPMENT OF A GENERAL SHIP FORM

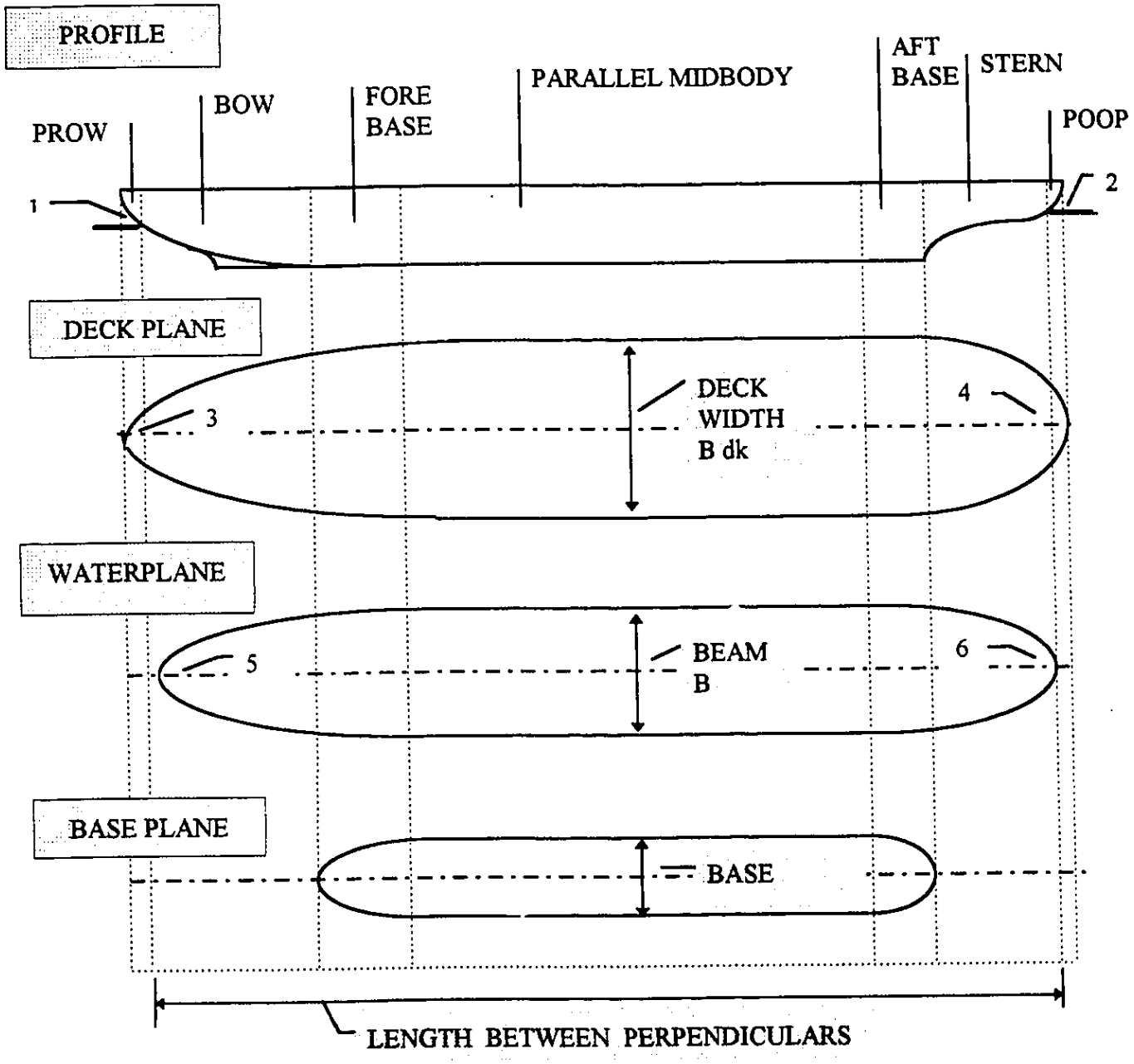

1. BOW PROFILE ANGLE	2. AFT KEEL PROFILE ANGLE
3. DECK ENTRANCE ANGLE	4. DECK EXIT ANGLE
5. WL ENTRANCE ANGLE	6. WL EXIT ANGLE

The principal angles defining the hull geometry are also shown in Figure 2.3. These include the half angles of entrance and exit for the deck and waterplane curves with respect to the centerline. The bow profile angle at the forward perpendicular and the stern profile angle at the aft perpendicular must also be specified.

Table 2.1 provides an example of the principal information required to develop the hull geometry. The interactive data entry process starts with the basic hullform dimensions. Fractions of the LBP are next input to define the major longitudinal divisions of the ship. Another fraction determines whether the maximum baseplane width is used, leading to wallsided midbody sections. Otherwise the midbody sections are curved. The bow profile is computed using a relationship of the form:

$$X = AY^B \tag{2.1}$$

which defines a parabolic rise from the baseline to the waterline over the length of the bow. An equivalent mathematical curve defines the stern profile. Their extension to the deck level marks the extremes of the ship, giving the LOA.

In an analogous manner, the waterplane entrance angle together with the beam and bow and forebase lengths are used in assigning a forward waterplane curve. The other angles and corresponding distances give the remaining curves of the waterplane and deck plane. The baseplane curves are approximated using the waterplane angles.

TABLE 2.1
SAMPLE OF SHIP DESIGN INPUT
MV ARCTIC DURING 1984 TRIALS

BASIC DIMENSIONS GIVEN BY PARAMETERS		
BEAM	22.9 m	WATERLINE BREADTH AT MIDSHIP
DRAFT	10.9 m	WETTED DEPTH AT MIDSHIP
LENGTH	196.6 m	LENGTH BETWEEN PERPENDICULARS ON WATERLINE
FREEBOARD	6.0 m	HEIGHT OF DECK ABOVE WATERLINE
FRACTIONS DEFINING DIVISIONS OF THE SHIP		
AFT - FRACT	0.050	WETTED STERN PART OF AFTBODY AS FRACTION OF LBP
BOW - FRACT	0.110	WETTED BOW PART OF FOREBODY AS FRACTION OF LBP
MID - FRACT	0.700	PARALLEL MIDBODY AS FRACTION OF LBP
SUBTOTAL	0.860	0.140 REMAINDER IS FOREBASE AND AFTBASE
BASE - FRACT	0.850	FLAT BOTTOM WIDTH OF MIDSHIP SECTION AS FRACTION OF MAXIMUM BASE WIDTH
ANGLES DEFINING THE SHAPE		
WL - ENT	32.8 deg	WATERPLANE HALF ENTRANCE ANGLE
DK - ENT	36.0 deg	DECK PLANE HALF ENTRANCE ANGLE
STEM - ENT	30.0 deg	BOW PROFILE ANGLE AT FP
WL - EXIT	60.0 deg	WATERPLANE ANGLE AT STERN
DK - EXIT	60.0 deg	DECK PLANE ANGLE AT STERN
KEEL - EXIT	55.0 deg	KEEL PROFILE ANGLE AT AP
WALL - SIDE	85.0 deg	SIDESHELL ANGLE OF MIDSHIP SECTION AT WL
TYPE OF SECTION CURVES FOR THE DIVISIONS		
BOW	5	[2 - 6] WHERE 5 IS POWER FUNCTION
FOREBASE	5	[2 - 5]
MIDBODY	5	[1 OR 5]
AFT - BASE	5	[2 - 5]
STERN	5	[2 - 6]

The bow profile can be modified to include an iceknife. This is illustrated in Figure 2.4. The depth at which the iceknife curvature starts must be specified, as well as the horizontal distance over which curves to the baseline. Its curvature can be changed from linear to highly curved by modifying a squashing coefficient to a cosine based function. The iceknife width is assigned a constant value, but it can be revised in the simulation model. There is a similar option for modifying the stern curvature to include a cutup zone. This affords a more realistic aftbody geometry, allowing for a propeller race. A skeg can be affixed along the centerline of the cutup zone if the ship is a twin-screw design.

Stations giving the locations of cross-sections are specified at distances along the ship. There are typically 11 to 21 stations between perpendiculars. Half stations are traditionally added between the first two stations closest to the FP and AP, giving better resolution of the bow and stern shape. The Design Model automatically assigns three equi-spaced stations at either extremity, defining the prow and poop. These stations are sites for calculating the hydrodynamic force distribution in the rigid body motions and flexural response models. Greater accuracy in numerically integrating the global forces and moments can be realized by increasing the number of section. But the corresponding computational effort will increase linearly. A trade-off is achieved by assigning the stations between perpendiculars at Chebyshev intervals. This concentrates more stations in the forebody and aftbody regions where the shape is changing rapidly, and fewer along the parallel midbody.

FIGURE 2.4
APPENDAGE MODIFICATIONS

1. ICE KNIFE

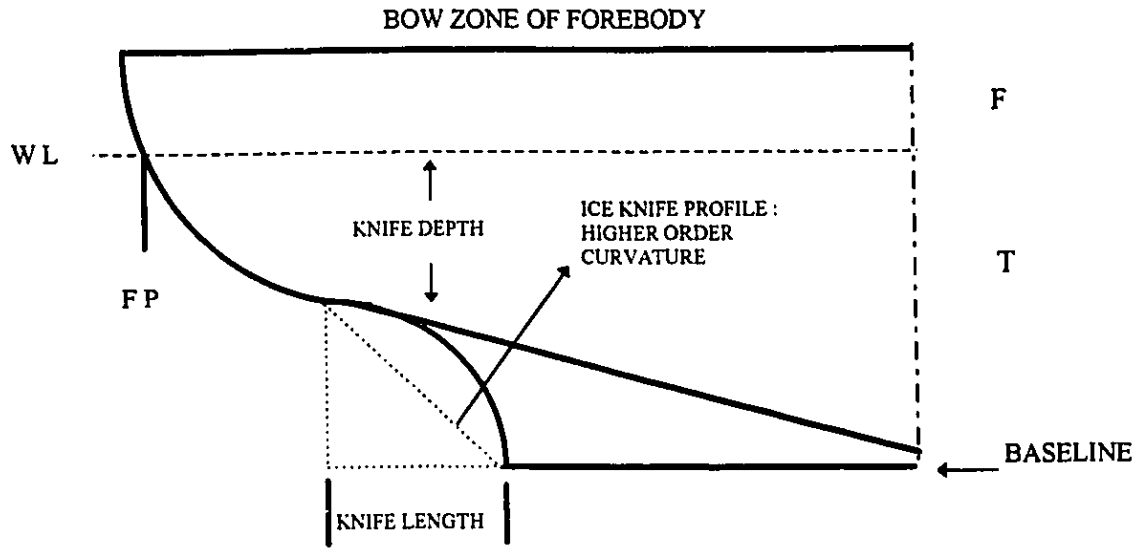

2. SKEG & CUTUP PROFILE

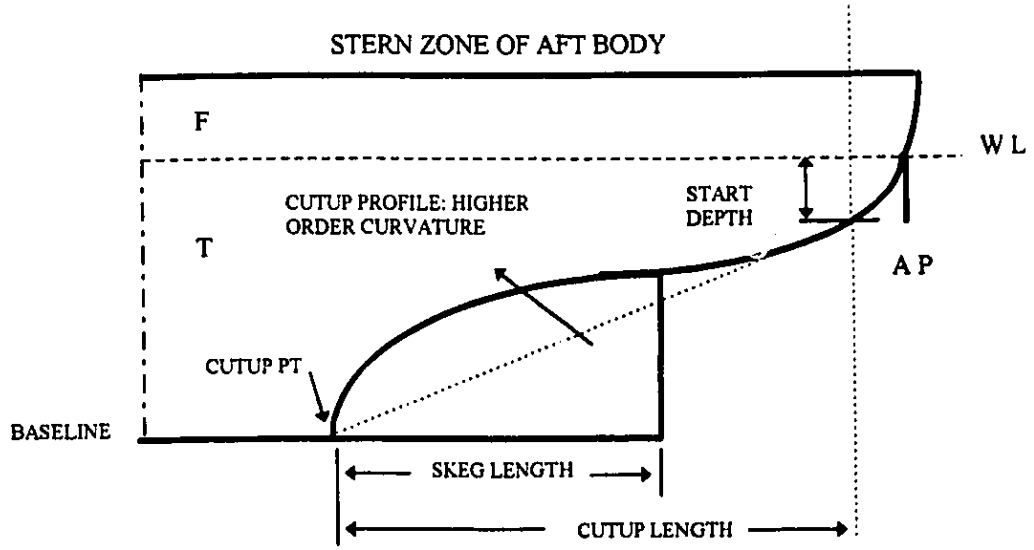

The section dimensions at the stations are uniquely determined in the vertical centerplane by the bow and stern profile equations. Their lateral extent is defined by the baseplane, waterplane, and deck level equations. Curvature of sections in the lateral plane depends on the local deck breadth, waterline breadth, and base width; as well as the freeboard and wetted section draft. The origin of the section equations is at the lateral extremity, giving a vertical angle at the deck.

Table 2 2 lists the different types of section curves which are available to the user. Parabolic, tertiary and quartic polynomial functions offer progressively rounder curves. These equations allow refinement in the shape of the forebody and aftbody sections. The exponential equation allows the sharpest bilge, but is more prone to failure. The power function is the most versatile curve, and can be applied to all of the ship divisions. The linear equation is limited to the wallsided option for the midbody stations.

The circular cylinder equation is a special case. Its use is reserved for the development of cylindrical bodies of rotation. These forms have a cylindrical midbody, and circular profiles at bow and stern. They are not intended as realistic ship forms, but rather are used for testing of hydrodynamic concepts and other special applications.

TABLE 2. 2
MATHEMATICAL SECTION CURVES

TYPE *	DESCRIPTION	GENERAL FORM †
1	LINEAR	$X = AY + B$
2	PARABOLIC	$X = AY^2 + BY$
3	TERTIARY	$X = AY^3 + BY$
4	QUARTIC	$X = AY^4 + BY^2$
5	POWER	$X = AY^B$
6	EXPONENTIAL	$X = A[EXP(BY) - 1]$
7	CIRCULAR	$X = \sqrt{B^2 - Y^2}$

* The program limits the curve-types available to each division of the ship.
- TYPE 1 Only available for parallel midbody sections.
- TYPE 6 May fail for some angle combinations.
- TYPE 7 Only available if a Body of Rotation is selected, rather than a General Ship Form.

† Specific algorithms for mathematical section curves account for bottom width and other geometric factors. Special section coordinates (X,Y) are referenced to a fixed origin on the deck at maximum half breadth. Y is positive downward, X laterally inboard. Regular coordinates are referenced to origin on the baseline at the ship centreline.

Figure 2.5 describes the various types of numerical sideshell curves which are developed from the mathematical section forms. A smooth sideshell is characteristic of the prow or bow divisions of the forebody. The stern and poop sections may also use this type of curve. Section coordinates are determined by dividing the horizontal domain

(from the centerline to the local deck halfbreadth) according to a two-sided Chebyshev spacing. Corresponding abscissa values are computed from the mathematical equations.

An iceknife appendage can be attached onto a smooth sideshell. This process of merging curves is shown in more detail in Figure 2.6. Two sets of points at Chebyshev spacings are defined over the two separate domains. The inner extent of the smooth sideshell is shifted laterally outward by an amount corresponding to the half-width of the iceknife. The section curve for the iceknife can be varied from nearly linear to an almost rectangular shape by specifying higher order constants on a cosine based function. The abscissa values for each domain are computed and the two sets of coordinates are linked into a single set.

The mathematical shape of forebase, aftbase, and parallel midbody sections all exhibit flat bottoms. For numerical purposes, these curves are modified to give a monotonically increasing curve from the keel centerline to the deck. An arbitrary bilge point is assigned as the abscissa at the point where the section baseplane reaches its maximum half width. A fourth order polynomial through this point is prescribed, replacing the flat bottom. The sidewall is replaced by a power function from the deck and waterline breadth to the bilge point. The bottom curve is discretized along the lateral x axis to give a one-sided Chebyshev spacing, which has its widest intervals near the centerline. The sidewall curve uses a two-sided spacing.

FIGURE 2.5
DEVELOPMENT OF NUMERICAL SECTIONS CURVES

1 : SMOOTH SIDESHELL

SINGLE SET OF POINTS AT A TWO SIDED CHEBYSHEV SPACING

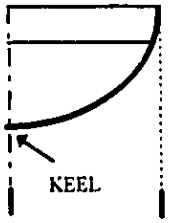

2 : ICEKNIFE SECTION

TWO SETS OF POINTS FOR COSINE FUNCTION LINKED TO A SMOOTH SIDESHELL CURVE

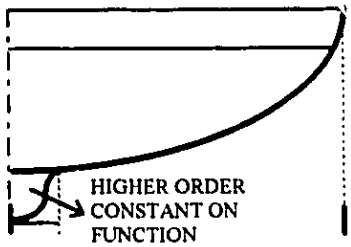

3 : MIDBODY SECTION

TWO SETS OF POINTS FOR A BILGE CURVATURE FUNCTION LINKED TO SMOOTH SIDEWALL CURVE

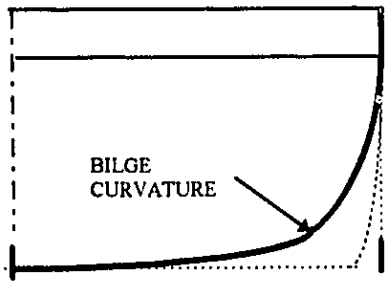

4 : SKEG STERN SECTION

TWO SETS OF POINTS FOR A COSINE FUNCTION LINKED TO THE STERN CUTUP SECTION CURVE

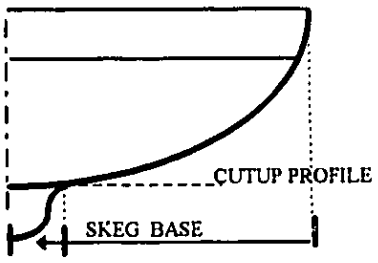

5 : STERN CUTUP SECTION

SINGLE SET OF POINTS ON MEAN CURVE OF ORIGINAL SECTION AND A FOURTH ORDER POLYNOMIAL

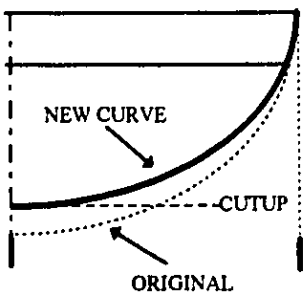

FIGURE 2.6
NUMERICAL SECTION CURVES:
DETAIL OF MERGING CURVE REGIONS

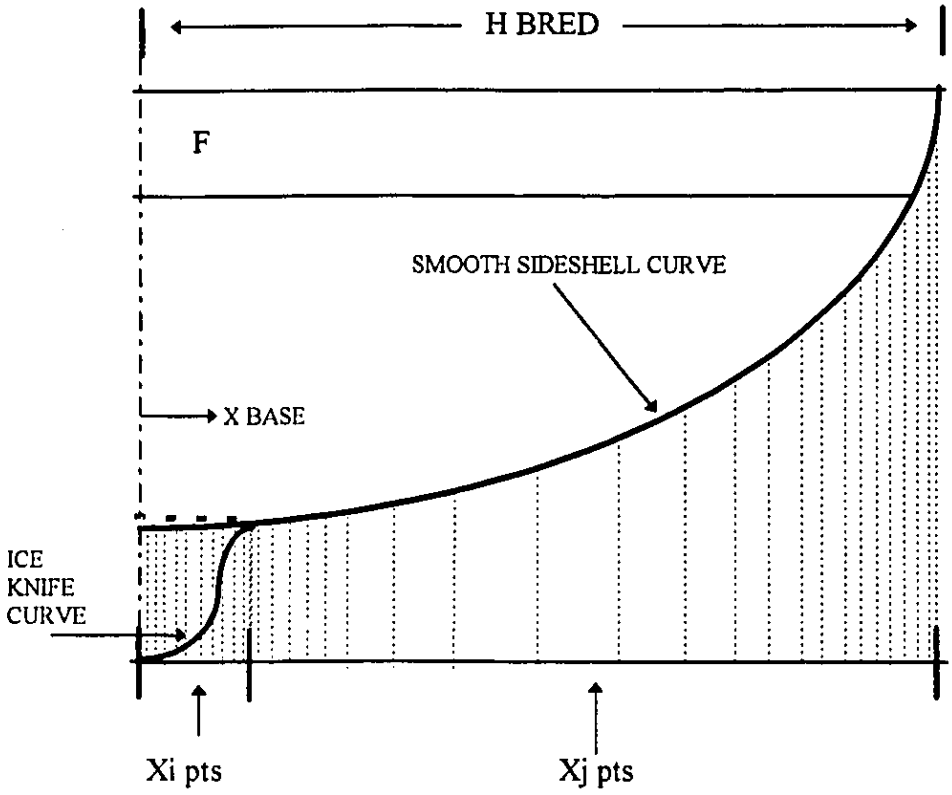

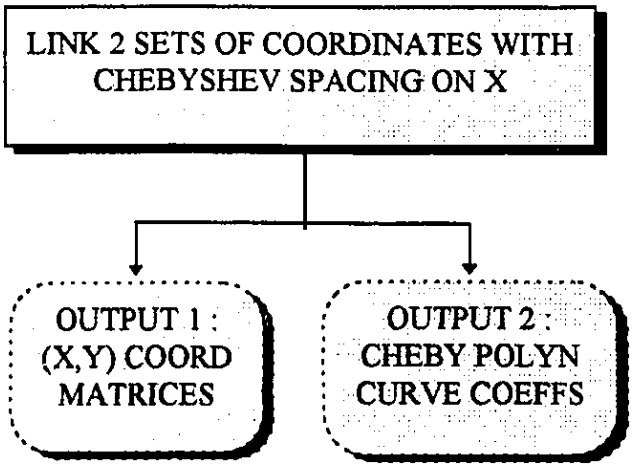

The stern of the ship may have been altered by inclusion of a cutup zone. In this case, the original mathematical section curves for this division will be modified using a fourth order curve which preserves the deck and waterplane breadths, and which ends on the cutup profile. This keel coordinate is computed from the cutup profile equation. The new curve is developed in two parts, and linked at the intersection point of the fourth order modifying equation and a reference line laterally outward from the local cutup depth. Inboard from the intersection point, the curve is defined by the mean of the modifying equation and the lateral line. Beyond this point, it is the numerical mean of the modifying equation and the original mathematical curve. A single set of two-side Chebyshev spaced points is used in discretizing this mean curve.

The attachment of a skeg onto the cutup centerline is analogous to the treatment of iceknife sections. It is again a process of linking a smooth sideshell and an appendage. In this case the smooth sideshell is replaced with the mean cutup section curve. The skeg curvature is again represented by a cosine based function. Linkage of the two domains proceeds as before.

The domain and abscissa values from each of the stations along the ship are output in coordinate matrices. They were also translated into a condensed mathematical form as coefficients of Chebyshev polynomials representing the section coordinates, integrated areas, and derivative curves. This format was found particularly convenient in the drag module and motions programs for simplifying certain repeated calculations, such as integrating the sectional buoyancy forces. However, the Chebyshev algorithm's

dependence on spline interpolation can lead to failures at sharper curvatures. So, the body boundary element coordinates in the hydrodynamics model are formed directly from the section coordinate matrices using simpler linear and parabolic interpolation schemes.

2.3 Hydrostatics and Weights

The vertical alignment of the ship's longitudinal centre of gravity (LCG) and centre of buoyancy (LCB) is a prerequisite for a ship to lie at its design longitudinal waterline. The moment balance depends on the distributed buoyancy forces and corresponding curve of weights. Defining the actual mass distribution of a ship is a complex problem, depending on many factors, such as the detailed hull and deck structure, subdivision, cargo, ballasting and location of propulsion machinery. In applications where the actual distribution of weights is known the direct data entry option may be used. But for concept exploration it was necessary to define a reasonable and systematic approximation method.

In the present work, the weight curve is modeled by adjusting the lineal mass density of the ship, starting from a uniform density distribution. The initial density is defined by dividing the overall ship mass by the volume contained within the hullform. The ship's mass displacement simply corresponds to the integrated volume of displaced water at the design waterline. Figure 2.7 illustrates the numerical implementation of the method of shifting mass elements to achieve an equilibrium situation. It is assumed that the LCG coincides with the LCB. The initial moment imbalance between weight and buoyancy distributions is then computed based on the uniform ship density. This involves

algorithms for calculating buoyancy forces and gravitational weights at each of the individual sections, and their corresponding incremental moments with respect to the LCG. The total moments are defined by numerical integration over the length of the ship.

An iterative process is used to progressively reduce the moment imbalance by shifting elements of mass. At each step a sinusoidal distribution of mass is shifted, sufficient to almost offset the moment imbalance. Of course, the buoyancy moment remains constant, since the design waterline is not changed. The mass transfer gradually changes both the ship density distribution and the mass density. Once the imbalance is reduced to within an acceptable limit, the LCG position is recalculated by integration of mass moments with respect to the forward perpendicular. This gives a check on numerical accuracy. The mass moment of inertia, I, about the LCG is also computed for subsequent use in the rigid body motions simulation.

FIGURE 2.7
MASS DENSITY BALANCING METHOD

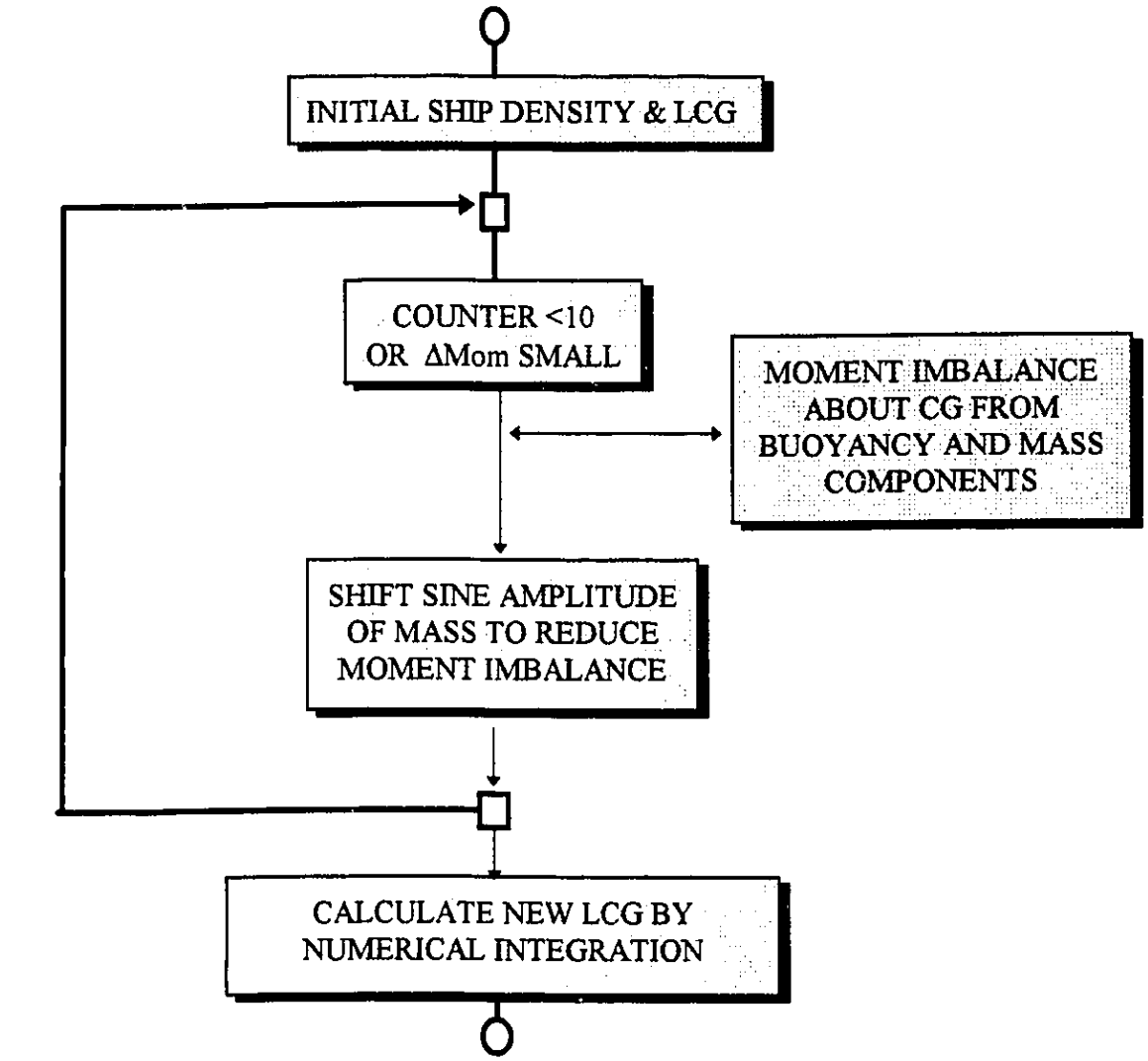

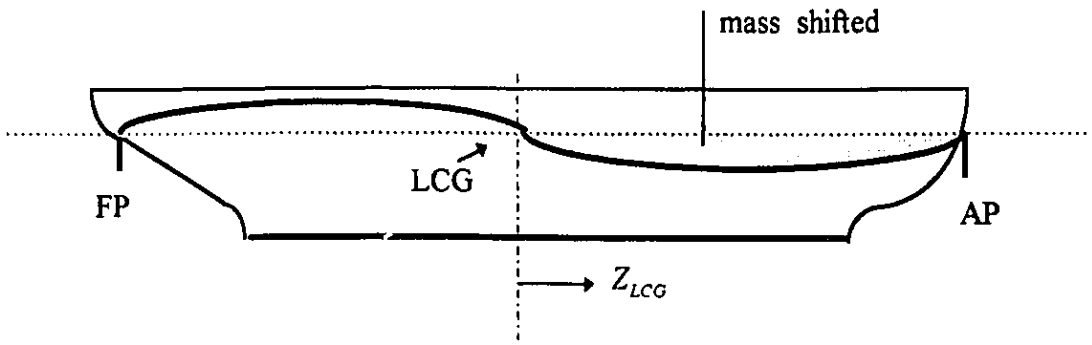

An approximation to the position of the vertical centre of gravity (VCG) is automatically generated by a default calculation, if the user does not directly assign it. Figure 2.8 shows the steps in this process. The distance KB from keel to the vertical centre of buoyancy (LCB or B) is given by Morrish's Rule:

$$T - KB = \left(\frac{T}{2} + \frac{V}{A}\right) \times c \qquad (2.2)$$

where the constant c is 1/3 if draft T expressed in units of feet. V and A are the displaced volume and area of waterplane respectively. This equation is deemed reasonable for larger, flat bottomed ships. The transverse metacentric radius, BM, is found by dividing the displaced volume by the moment of inertia of the waterplane about the centerline axis. KG from the keel baseline to the VCG is then defined to satisfy a minimum stability condition; whereby the metacentric height, GM, is greater than one meter.

2.4 Structural Properties

The main contributions to the longitudinal strength of icebreaking ships are assumed to come from the shell, framing, inner bottom and deck. There is no provision for directly including these structural elements within the present conceptual modeling process. Rather, the section modulus distribution corresponding to these elements is approximated according to a methodology shown in Figure 2.9.

FIGURE 2.8
VERTICAL CENTER OF GRAVITY, VCG
ASSUMING TRANSVERSE STABILITY CONDITION

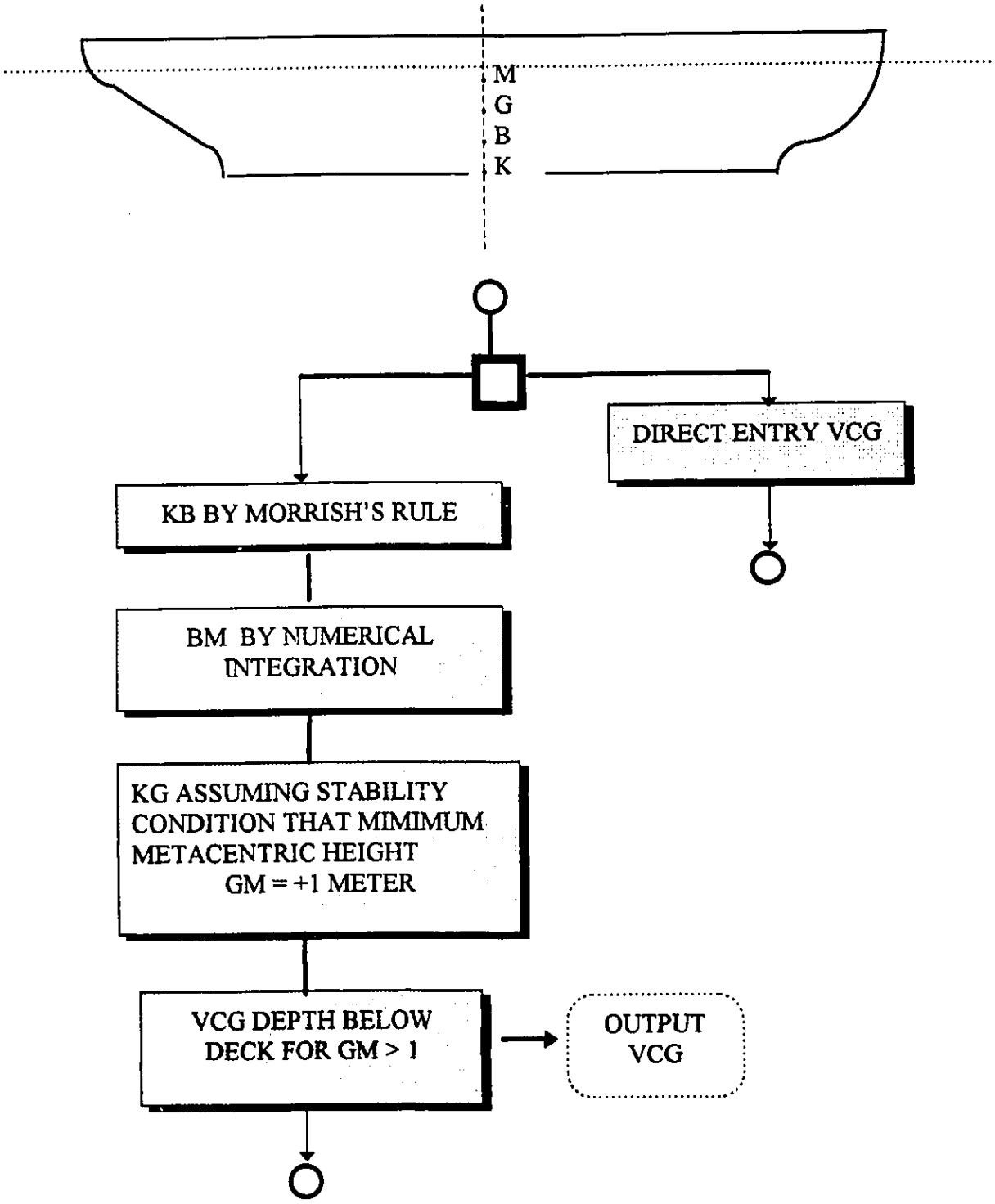

FIGURE 2.9
OPEN WATER STRUCTURAL PROPERTIES

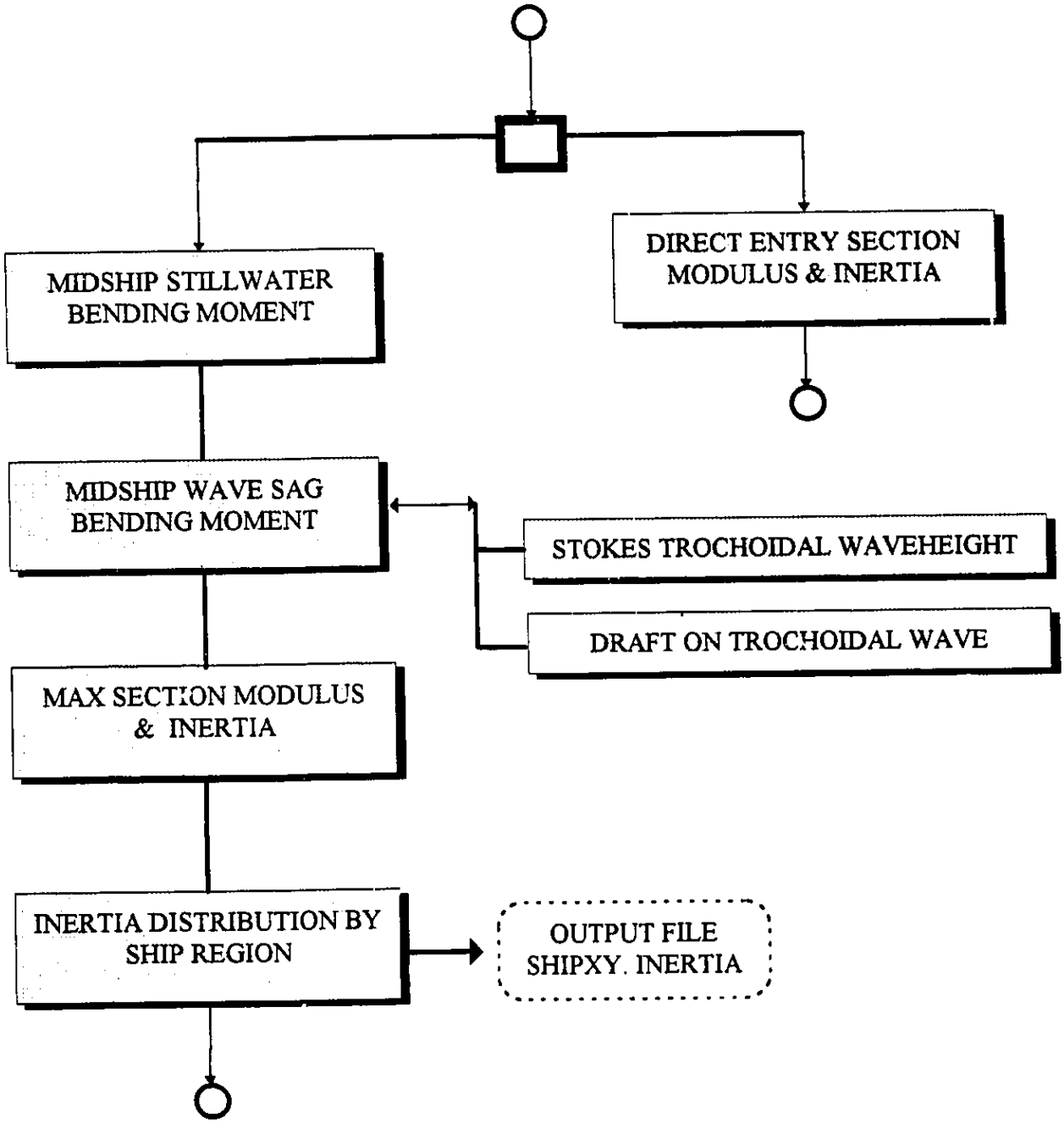

The traditional method for ensuring adequate longitudinal strength in open water operations involves a two step process. The stillwater bending moment distribution is first calculated by hydrostatic procedures, which define the shear and bending moments in terms of the section buoyancy and weights. The sagging bending moment distribution is then analyzed by statically placing the ship on an L/20 trochoidal wave. This leaves the ship supported by the wave at the ends and unsupported in the amidships region. The actual expression for commercial ships used in the Design Model gives the waveheight as

$$\lambda = 1.1\ (LBP)^{0.5} \text{ (in Imperial units).} \qquad (2.3)$$

For computational purposes a Stokes 2nd order trochoidal equation given by Newman (1977) has been used to determine the amplitude of the wave at the ship sections.

2.5 Arctic Class Properties

CASPPR provides guidelines for the structural design of icebreaking ships which operate in Canada's northern waters. Corresponding regulatory requirements have been proposed by a number of classification agencies, including Lloyd's Registry, the American Bureau of Shipping, Det Norske Veritas, the Russian Federation, and the Finnish-Swedish Board of Navigation. CASPPR originally recognized nine Arctic Classes and four Baltic types. The intervening years since its inception in 1972 have seen considerable research

and development of Arctic shipping technologies by government agencies and private industry. This resulted in the 1989 proposed revisions to CASPPR, which recommend four Arctic Classes and five Baltic types. Table 2.3 lists these categories and describes their limiting ice conditions.

TABLE 2.3
CANADIAN ARCTIC CLASS SHIPPING
(PROPOSED 1989)

CATEGORY	LIMITING ICE CONDITIONS
CAC 1	No Limiting Ice Types
CAC 2	Multi-year Ice
CAC 3	Second Year Ice
CAC 4	Thick First Year Ice
TYPE A	Medium First Year Ice
OTHER	Open Water or Type B, C, D, E

Most of the revised structural design criteria are concerned with effects of local ice pressures on plates, stringers and frames. Only in the case of the strongest category, CAC1, are there guidelines for the section modulus of the hullgirder. For all other classes and types, it is left to the discretion of the designer. The ITHACA_SHIP model considers two different approaches for determining section modulus. In the first case, the section modulus and neutral axis at the amidships section, or its distribution along the ship is

known. Equivalently the entire distribution of inertia may be specified; in which case it can be entered directly. If only the midship modulus is known, it can be used to proportionately modify the inertia distribution computed according to open water criteria.

For purposes of concept exploration, it is assumed that no section modulus information is available. Or only data for the basis ship used in a parametric study. In this case, a systematic approximation for icebreaking section modulus is applied according to the procedures outlined in Figure 2.10. This process starts with a determination of the stillwater and L/20 wave bending moments which have been described as a basis for designing open water ship structures. A minimum strength condition in ramming is then introduced. This is based on the assumption that all classes and types of icebreaking ships are equally likely to suffer unintended collisions in nearly open water. A midship ramming moment is computed which considers the ship as beached on the ice. In the present model this is a static calculation. It assumes that the bow (at the FP) is raised so that the baseline emerges as far as the waterline; and the stern finds its own equilibrium position. The model takes the larger of the stillwater and ramming moments, and combines it with the wave sagging moment to determine the minimum amidships bending moment for a Type A ship. The section modulus for the four Arctic Class categories are computed as a proportional variation from this minimum to the CAC1 maximum, which is specified by an empirical powering relationship.

FIGURE 2.10
ARCTIC CLASS STRUCTURAL PROPERTIES

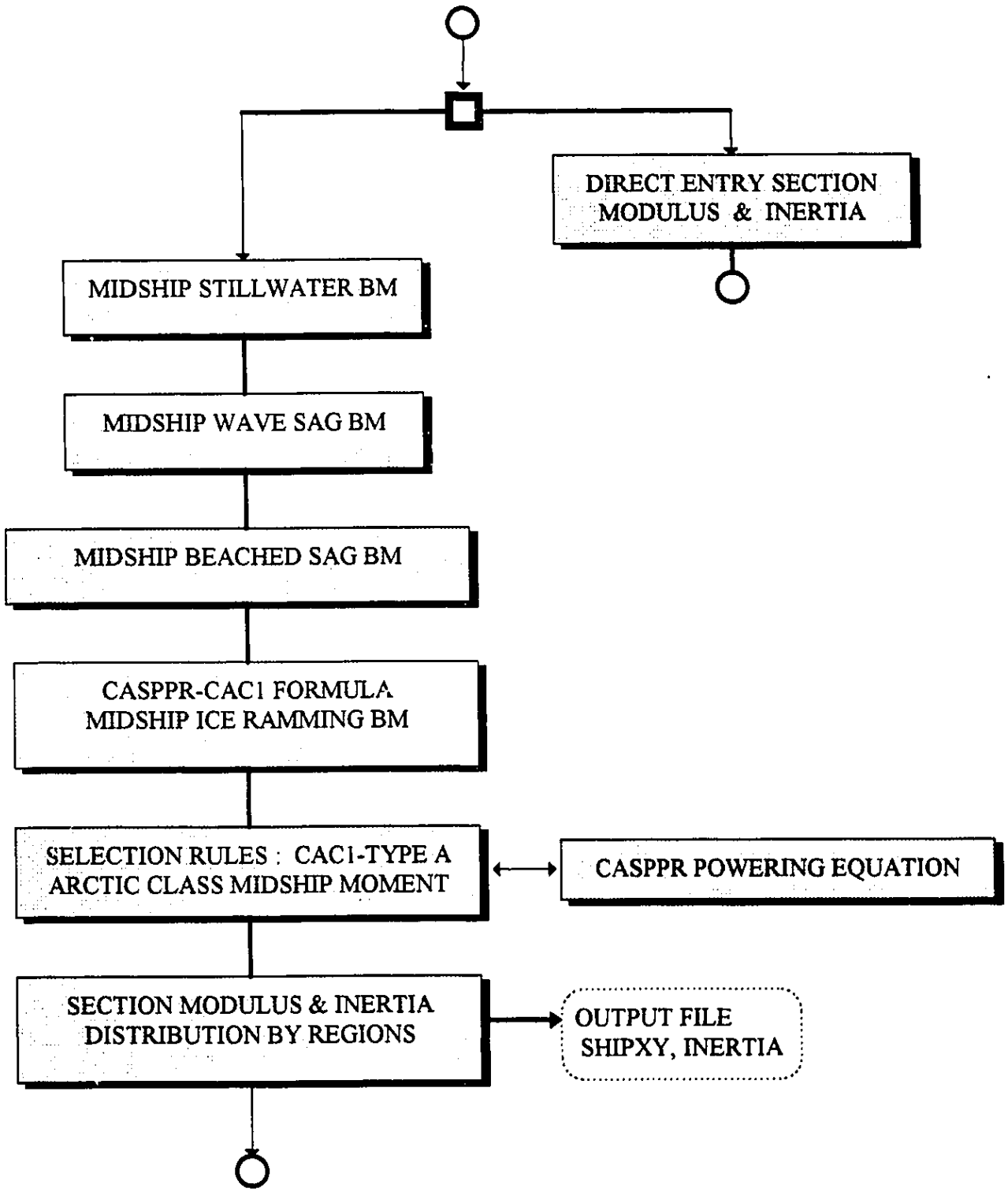

2.6 Sample of Ship Design Output

Table 2.4 presents the principal particulars which result from using the ship design parameters specified in Table 2.1 for representing the *MV Arctic*. The basic dimensions (with the exception of freeboard) and the forebody angles are those reported by Hearnshaw et al (1984) for the prototype; and correspond closely to those used by the author in designing earlier physical model tests. The aftbody angles are rougher approximations taken from illustrations, since the complete lines plans were not available. It is nevertheless observed that the simulated hullform geometry and mass displacement are in good agreement with the prototype.

The same hullform has been generated using a small, medium and large number of stations between the ship perpendiculars. In each case, the stations between perpendiculars are located according to a Chebyshev spacing. And extra end sections are included as described previously. The accuracy of the principal particulars is largely dependent on the numerical integration of area at each section, and the integration of variables over the stations defining the ship length. Because of concern over possible spline instabilities in the more sophisticated Chebyshev integration scheme when the number of data points is small, a trapezoidal failsafe algorithm has been included as a check. With this methodology, it is found that increasing the number of stations (between perpendiculars) from 11 to 21 causes less than one percent variation in the particulars. Hearnshaw gives the prototype mass displacement at the summer draft of 10.82 metres as

37,728 tonnes. The numerical, mean wetted volume displacement of 37,120 cubic metres at a draft of 10.90 corresponds to a mass of 37,524 tonnes; assuming that the specific gravity of seawater is 1.020 and correcting for the difference from the summer draft. The block coefficient of the numerical ship also shows good agreement. It has an average value of 0.757 which is only marginally greater than the prototype at 0.753.

TABLE 2.4
SAMPLE OF PRINCIPAL PARTICULARS
MV ARCTIC in 1984 Trials Condition

PRINCIPAL PARTICULAR		NUMBER OF SECTIONS BETWEEN PERPENDICULARS †			
		n = 11	n = 15	n = 21	UNITS
V_{WL}	Wetted Vol Displ.	37111	37065	37261	m^3
V_{DK}	Total Vol Displ.	63614	63850	63846	m^3
A_{WP}	Waterplane Area	4134	4141	4164	m^2
C_B	Block Coef.	0.756	0.755	0.759	
C_{WA}	Waterplane Coef.	0.918	0.928	0.925	
C_{CP}	Vert. Prism Coef.	0.823	0.821	0.821	
$L/V^{1/3}$	Slenderness Coef.	0.170	0.170	0.170	
I	Inertia	$9.59\,e^{10}$	$9.66\,e^{10}$	$9.70\,e^{10}$	m^4

† A two-sided Tchebychev distribution of (n - 2) sections, plus a half station section at each perpendicular. Three additional Prow and Poop sections at the ends. Total sections = n+8.

Figure 2.11 shows the curves of the main variables governing the geometry of the hullform. These include sectional draft, waterplane halfbreadth, deckplane halfbreadth, and baseplane half-width. It should be remarked that the origin for length along the ship is at the forward perpendicular. Negative distances refer to the prow extension of the bow from the FP. The poop extension of the stern past the AP leads to distances greater that the LBP of 196.6 meters. The area and property distributions resulting from the selection process are shown in Figure 2.13. In the case shown, the amidships inertia (about $200m^4$) is for a much stronger ship and does not correspond to the expected section modulus of 14.2 m^3 for the *MV Arctic* in the 1984 summer trials condition.

A sample of a numerically developed body plan is given in Figure 2.14. Forebody and aftbody sections are plotted for a Chebyshev spacing of the stations between perpendiculars. It can be seen that with this method of spacing, 10 of the 17 sections lie outside of the parallel midbody; thereby providing better resolution at the end regions. The midbody sections also display one weakness of the Hull Model. Sideshell curves are not as nearly vertical as in a wallsided prototype, because the spline algorithms are not sufficiently robust to handle a sharper bilge angle. This has necessitated a slight distortion in the fractional length of midbody to account for the volume lost by the more slender bilges. Another effect that can be observed is the modification of the stern sections by the cutup zone in the aft body plan. The nearly straight AP section curve reflects the definition of sections in the stern division sections as power functions, rather than as quartic or exponential. The prow and poop sections have not been included on this graph.

FIGURE 2.11
SHIP GEOMETRY AND PROPERTY DISTRIBUTIONS - 1

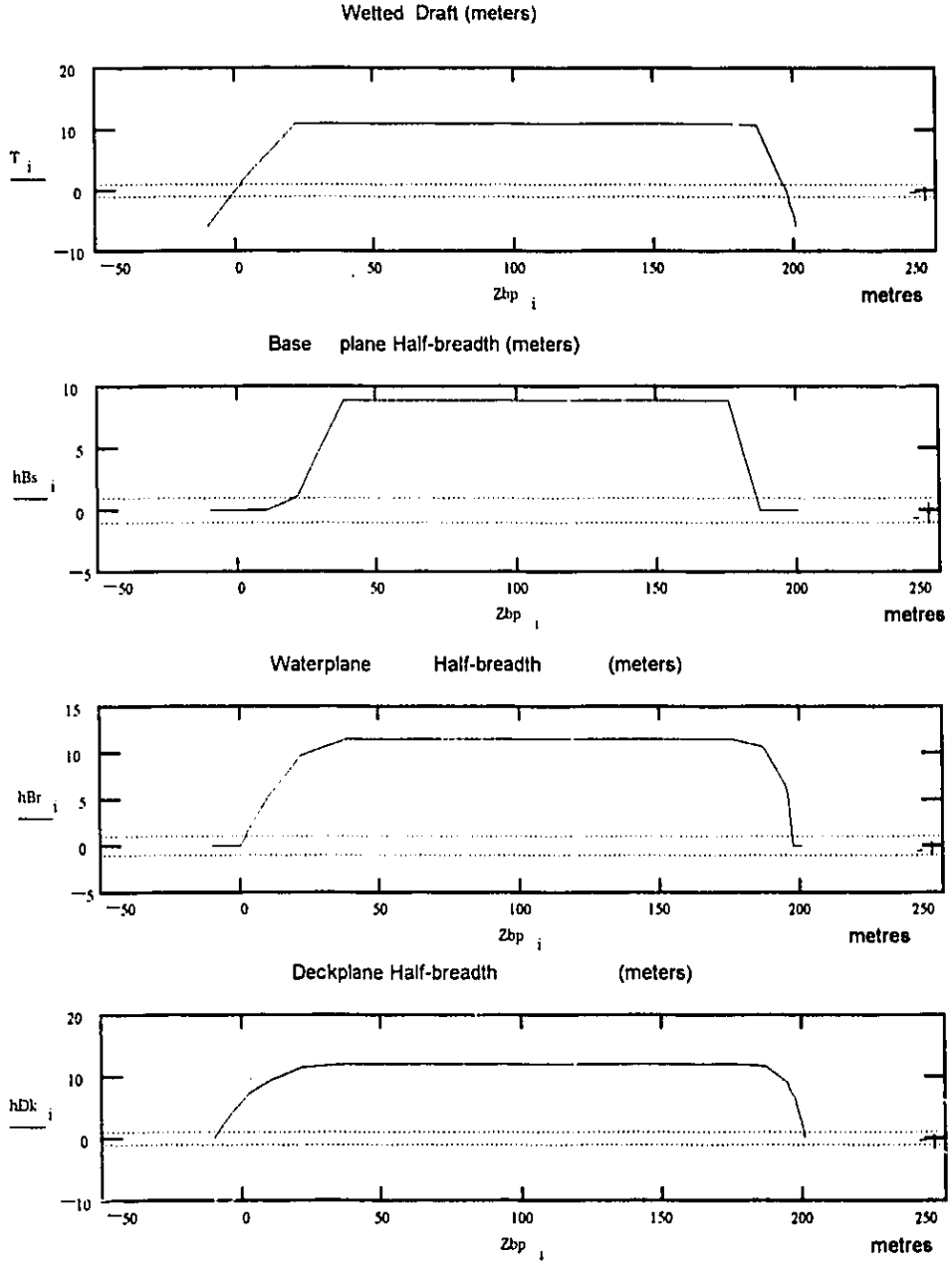

FIGURE 2.12
SHIP GEOMETRY AND PROPERTY DISTRIBUTIONS - 2

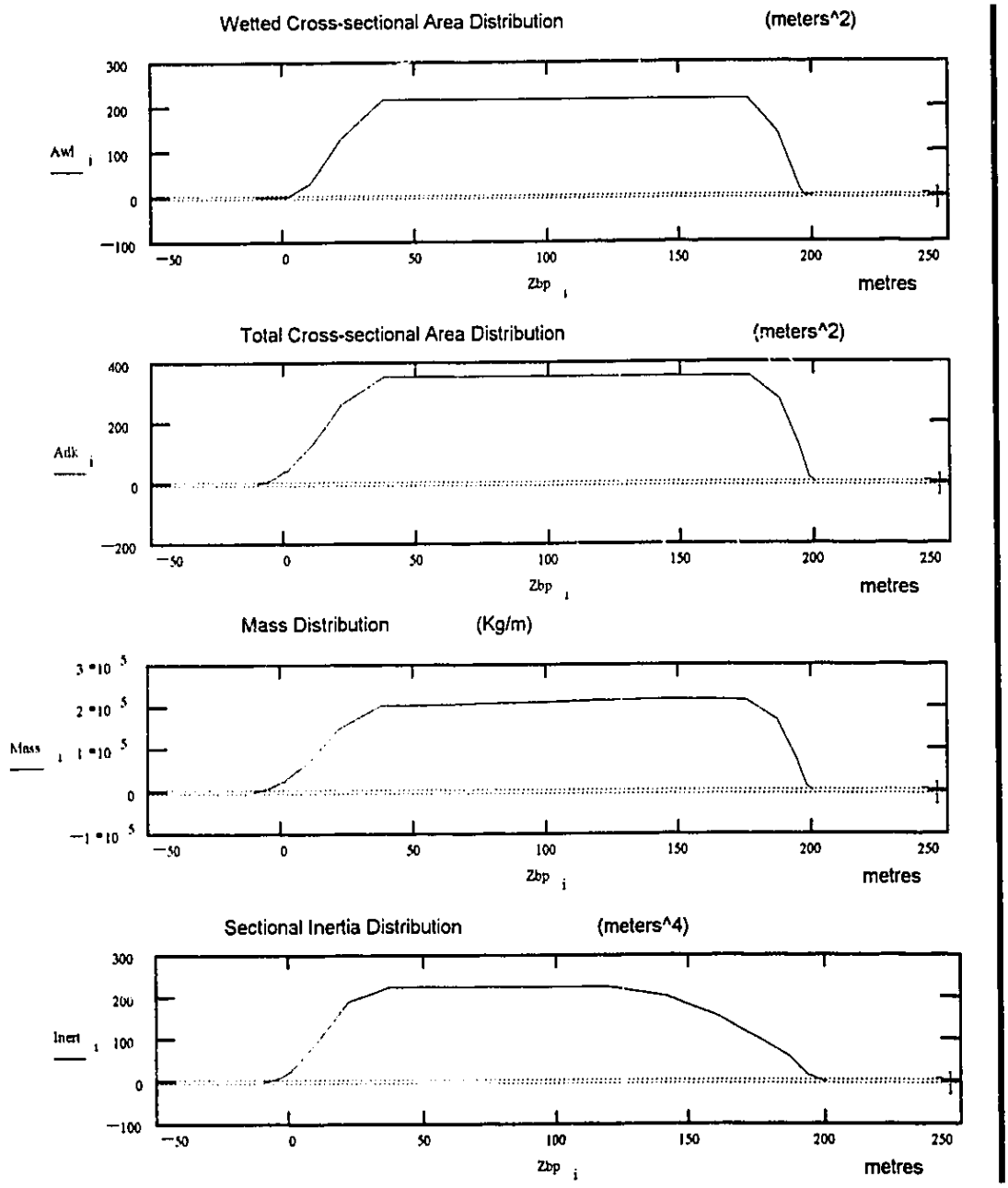

FIGURE 2.13
SAMPLE OF SIMULATED BODY PLAN

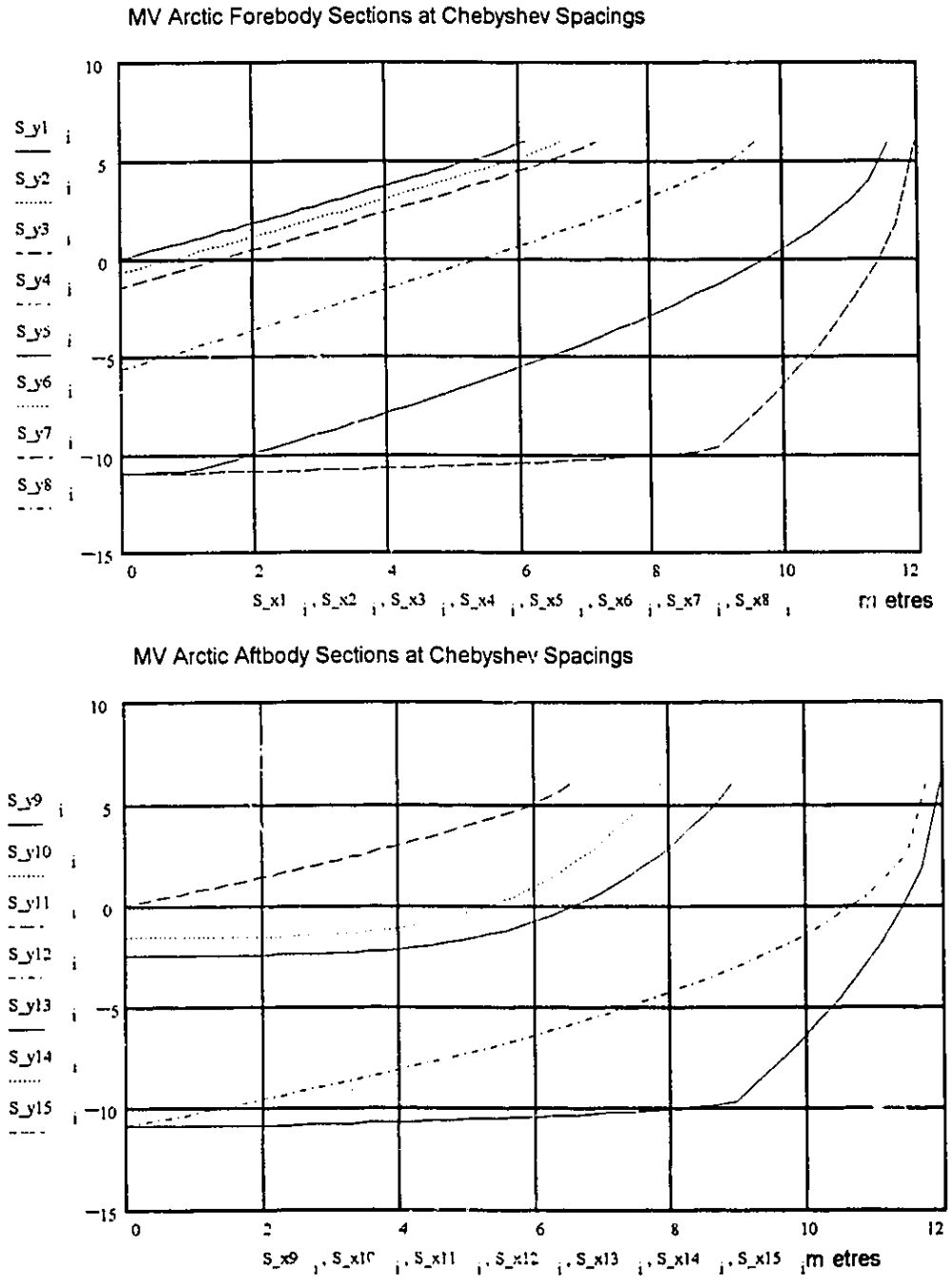

Chapter 3 Simulation of Motions and Stresses

This chapter discusses the theory and numerical implementation of procedures for time-domain simulation in the ITHACA_SHIP Rigid Motions Model and Hydroelastic Response Model. The analysis of stress follows directly from these response calculations. The rigid body equations of motions are first developed, based on a Lagrange equation energy formulation. The method of including interaction forces is explained, describing their dynamic relationship through the ship motions. The flexural response is determined independently in a second step; based on small amplitude beam theory and using the force time-histories from the rigid body analysis. At the level of precision sought in concept exploration studies, this two-step procedure is not expected to prejudice the maximum stress prediction, nor to distort trends. If a more detailed analysis is required; then the rotary inertia and shear deformation should be modeled, and whipping effects accounted for by directly simulating the flexural response in a single step. The method of determining the bending moment and stress distributions is subsequently described, as well as the importance of the stillwater bending moment.

3.1 Response Modeling Methods

Prediction of bending stresses in the extreme fibres of the hullgirder during a ramming interaction is the principal objective of the present computational model. The

maximum stress provides an inverse measure a ship's resilience to a global failure of its structural elements. Phillips and Daley (1985, 1986) have shown that the stress, as a function of impact velocity, exhibits a significant oscillation about its mean trend. In consequence, the maximum stress may not occur at the design open water velocity, but at a lesser speed. These variations in the stress curve are associated with an initial peak in the stress time-history which occurs immediately after the instant of contact. Its magnitude is observed to be strongly dependent on rigid body and flexural dynamics. In its turn, the ship response during this initial period depends on the nature of the distributed ice and fluid forces acting on the hull.

It is postulated that conventional added mass treatments will be inadequate to represent large amplitude, transient motions of a ship, when subject to the coupling effect of contact with ice. Figure 3.1 illustrates two candidate methods of modeling the dynamics of the system. A mechanical representation is first considered, in which the fluid effects are replaced with springs, dampers and added mass. The ice interaction properties are shown modeled by vertical and horizontal springs, but mass and damping effects should perhaps also be included. While the diagram indicates only heave and pitch modes of response, an analogous situation holds for higher, flexural modes.

FIGURE 3.1COLLISION MODELLING METHODS

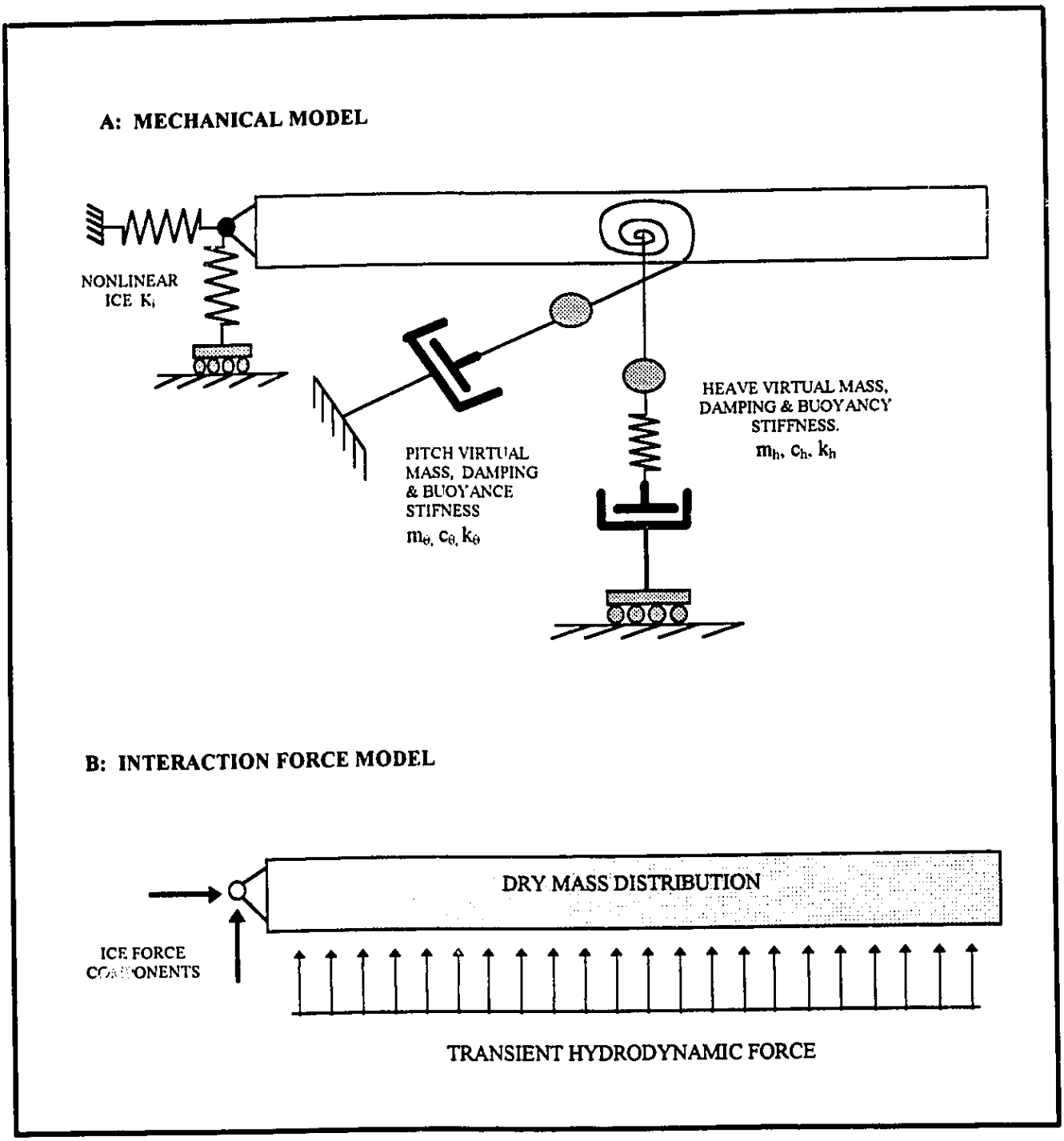

The equations of motion could be written in terms of generalized coordinates and mechanical properties as:

$$m_i\left(1+u_m\right)\ddot{q}_j+c_i\left(1+u_c\right)\dot{q}_i+k_i\left(1+u_k\right)q_i=F_j \qquad (3.1)$$

On the left-hand side of the equation, the coefficients, u_m, u_c, and u_k have been introduced to represent modification to the modal mass, damping and stiffness of the dry ship, so as to account for fluid and ice effects. Techniques have been reported in several seakeeping strip theories for determining the first two coefficients. The ship added mass and damping are usually expressed in terms of local sectional added mass and damping coefficients; and are both frequency and velocity dependent. The effect of large amplitude motions on the restoring stiffness term is usually neglected. However, it is not a straightforward process to extend these arguments to account for the presence of ice and the transient hydrodynamic phenomena observed in a ship-ice collision.

Phillips and Menon (1987) have analyzed the hydrodynamic force from *MV Arctic* physical model tests, showing its predominantly transient behaviour. Howard and Menon (1987) present further evidence from model scale shaker tests suggesting that harmonic added mass and damping coefficients should not be applied to the transient ice collision problem. They observed that the added mass for periodic oscillations in an ice cover could be greater than in open water by a factor of two or three. The major increase was attributable to the rigid body mode; and its effect was most pronounced at the bow. Riska (1987) has extracted a nonlinear expression for spring stiffness from a particular set

of MV Arctic physical model tests. But in general there is no accepted methodology for defining these coefficients within the broader context of a ship-ice-fluid system. Neither the mechanical properties associated with the ice interaction process, nor the transient added mass and damping characteristics are well understood.

Second order hydrodynamic theories have been proposed by Lee (1968) and Potash (1971) as a means of considering large amplitude response. Results have subsequently been reported from several numerical implementations; giving the magnitude and phase of higher order harmonics of the hydrodynamic force. Nevertheless, it is by definition only the first order force harmonics which can be interpreted as added mass and damping. So wet modes reflecting the dynamic system behaviour cannot be properly formulated in terms of these coefficients.

Figure 3.1b shows an interaction force modeling of the collision process. It represents the dry mode approach which has been adopted in the present model. All of the interaction forces acting on the ship are explicitly calculated in time-domain models; and their combined effect is expressed as a generalized force which is retained on the right side of the equations of motion. In this case, the mass, damping and stiffness refer to the dry ship modal properties alone, rather than virtual properties. The fluid and ice forces are coupled through a time-domain simulation of the instantaneous ship motions.

3.2 Lagrange Equation Formulation of Rigid Body Motions

The ship motions are formulated in terms of Lagrange's equations, which can be derived from the principle of virtual displacement or from Hamilton's principle. They are commonly expressed in terms of derivatives of the kinetic energy, T, and the potential energy, V. For the n generalized coordinates, q_i, of a NDOF system; this takes the form:

$$\frac{d}{dt}\left(\frac{\partial T}{\partial \dot{q}_i}\right) - \frac{\partial T}{\partial q_i} + \frac{\partial V}{\partial q_i} = Q_i \quad , i=1,2,...,n \tag{3.2}$$

It is assumed that the derivative terms are defined analytically, rather than solving the quotients numerically. The generalized force, Q_i , is typically non-conservative and gives a virtual work, W_i , as a result of acting through a virtual displacement, δq_i.

Two coordinate frames are introduced for defining motions of the ship. One is an absolute frame of reference on the undisturbed free surface at the ice edge. Its axes define Cartesian coordinates in the horizontal Z, vertical Y, and lateral X directions. A ship-based reference frame describes the position of points on the body with respect to a origin fixed at the centre of gravity, CG. In this case, the longitudinal distance along the ship is z, and the transverse coordinate is y. The x coordinate is laterally outward from the ship centerplane. The rigid body motions of the ship with respect to the absolute reference frame are traditionally expressed in terms of three independent coordinates: surge, heave and pitch; represented by s, h and θ.

A direct numerical treatment of the energy balance is generally impractical in ship motion simulation problems, since the path of least energy must be explicitly derived for all of the independent coordinates. Rather, a Lagrange Equation formulation is preferred, in which the derivatives implicitly account for the minimizing of energy. The total kinetic energy is a function of the ship mass and its mass moment of inertia, I_0; as well as velocities in surge, heave, and pitch. It is given by:

$$T = \frac{1}{2} m\left(\dot{Y}^2 + \dot{Z}^2\right) + \frac{1}{2} I_0 \dot{\theta}^2 \tag{3.3}$$

The potential energy is defined by the vertical shift of the mass centre within the gravitational field. It is expressed with respect to its initial position in the undisturbed free surface as:

$$V = mgh \tag{3.4}$$

The generalized force, Q_i , for each rigid body mode is extracted from the interaction forces. For example, the hydrostatic buoyancy force gives rise to a vertical force at the CG and a rotational moment. Expressed in terms of a double integration along the ship of the individual wetted areas given by the section curves, the buoyancy terms are:

$$F_{B_y} = -\rho g \int_L \int_y x(y)\, dy\, dz \tag{3.5a}$$

and

$$M_{B_\theta} = -2\rho g \int_L z\left\{\int_y x(y) dy\right\} dz \tag{3.5b}$$

For small amplitude motions the functional relationship x(y), defining the section coordinate curve, can be replaced by the constant section halfbreadth, x_i. But in the present large amplitude model, it is necessary at each instant to reconstruct the wetted section areas by integration over the section curves. In the equation, ρ and g are water density and gravitational acceleration respectively.

The hydrodynamic pressures distributed over the wetted hull sections contribute a second set of force and moment terms. These pressures are integrated over each section to give a force for that strip. The instantaneous global vertical force and moment are given by:

$$F_{H_y} = \int_L \delta F_{H_y}(z)dz \tag{3.6a}$$

and

$$M_{H_y} = \int_L z\,\delta F_{H_y}(z)dz \tag{3.6b}$$

Similarly, the Ice Interaction Model generates individual icemesh force elements which are summed to give a resultant global force component in vertical and horizontal directions, and a corresponding moment about the CG. These are denoted by F_{Iz}, F_{Iy}, and $M_{I\theta}$.

Additionally, force and moment terms may be included to account for the variation in propeller thrust during the collision interaction. It is assumed that the thrust acts longitudinally, and its magnitude is given by the total of the ship's open water wavemaking resistance and its frictional resistance. The wavemaking component is determined from

Michell's Thin Ship theory. The numerical algorithms developed for its solution are based on a particular form of Michell's integral given by Newman (1977). The frictional component is calculated according to a nondimensional relationship established by the 1957 International Towing Tank Convention. The thrust is given by the total of these two resistance components. But, its variation during a collision interaction is poorly understood, since the sudden loading of the propeller causes a significant reduction in propulsive efficiency. In addition, the thrust is a secondary term as compared to the ice force. So this term has been ignored in the Rigid Motions Model, although an optional calculation of the drag as a function of velocity is available.

Once the derivatives in the Lagrange equations are defined, it is found that the equations reduce to a form equivalent to a Newtonian formulation, where:

$$m\ddot{s} = F_{I_s} \tag{3.7a}$$

$$m\ddot{h} = \left(F_{I_Y} + F_{H_Y} + F_{B_Y}\right) - mg \tag{3.7b}$$

$$I_o\ddot{\theta} = M_{I_\theta} + M_{H_\theta} + M_{B_\theta} \quad . \tag{3.7c}$$

3.3 Implementation of Rigid Motions Algorithms

Figure 3.2 provides an overview of the basic data flow in the Rigid Motions Model. The program starts by retrieving hullform geometry and physical properties which must have previously been created in the Hull Design Model. A number of run options must be assigned to define the particular conditions under which the collision is

occurring. The physical parameters include impact velocity, time-step size, maximum collision duration, ice strength, and iceknife width. It is also necessary to specify the type of hydrodynamic and ice modeling which will be used.

During the initial time step, corrective offsets for the vertical force and the corresponding moment with respect to the LCG are determined. A check on the hydrostatic moment balance negates concerns over numerical error. These could be introduced by minor differences in algorithms representing section shapes in the Hull Design and Rigid Motions models. The kinematic orientation of the ship in the free surface is established in terms of the intersection of the keel profile and the waterline. It initially corresponds to the forward and aft perpendiculars. At subsequent times, the orientation of the forward and aft profile curves are functions of the instantaneous surge, heave and pitch. Their intersection with the waterline is determined by a combined Newton-Raphson and bisection root-finding algorithm given by Press et al (1987). The points of contact between the bow and the upper ice surface, and further aft at the ice edge, are computed in a similar manner.

FIGURE 3.2 RIGID MOTIONS MODEL

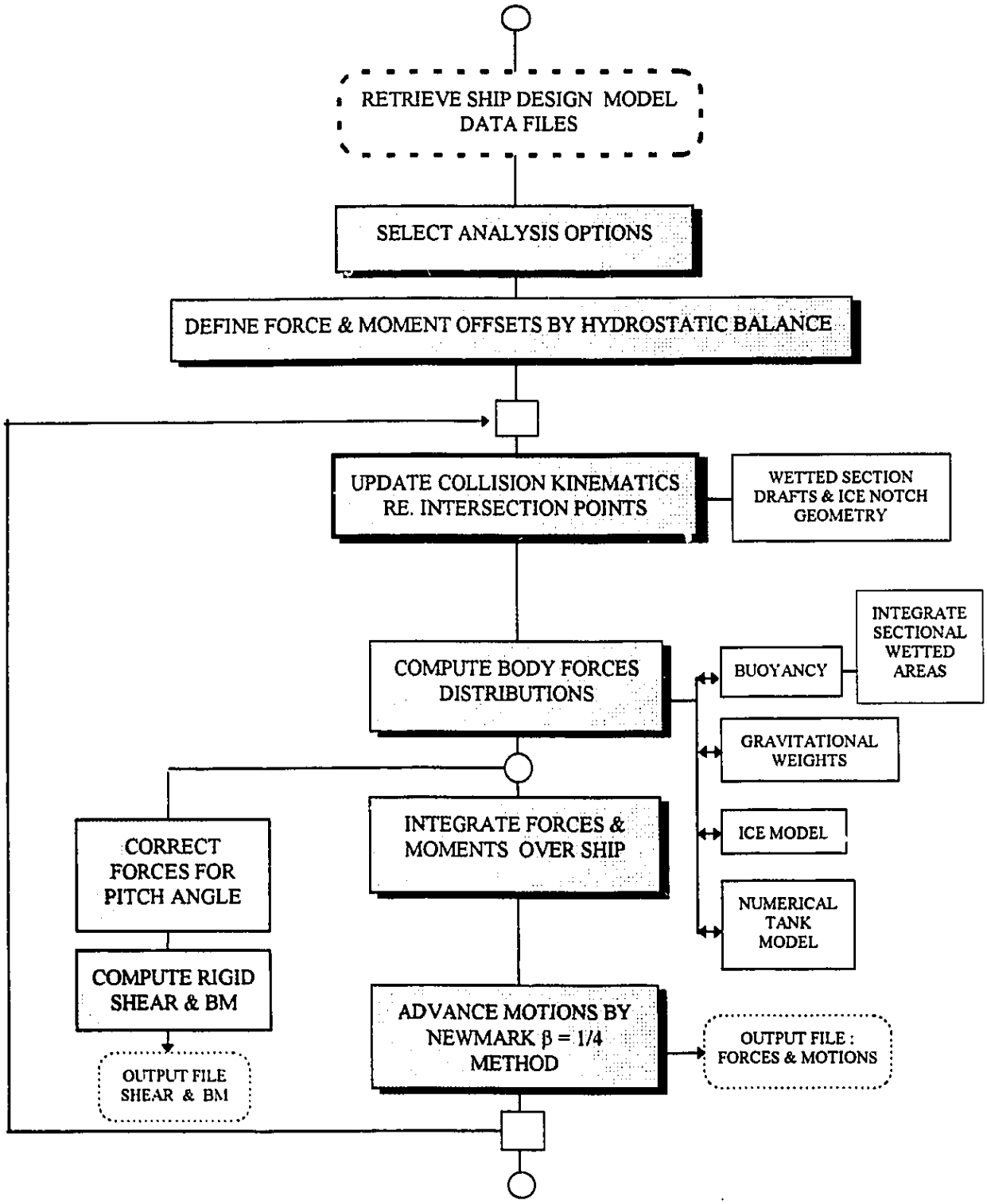

Next, the instantaneous body forces acting on the ship are determined. The distribution of gravitational forces remains unchanged with time. The sectional buoyancy and hydrodynamic forces are calculated at the wetted sections between the forward and aft intersection points. The resultant vertical and horizontal components of the ice force are also extracted. (A detailed description of the Ice Interaction Model and the BEM Numerical Wavetank will be given in later chapters.) The force distributions are summed at individual sections and integrated over the ship's length, giving the total force acting in heave. A similar moment integration of forces with respect to the LCG results in the total moment acting in the pitch mode. With the forces and moments defined, it is then possible to advance the motions according to equation (3.7). This is accomplished by means of the Newmark $\beta = \frac{1}{4}$ Method.

It should be remarked that the timestep integration process is effectively governed by the hydrodynamic model which uses a 4^{th} order Runge-Kutta scheme. This introduces four mini-steps per time step. For practical purposes this precludes any time-stepping scheme for the equations of motion which would require a second level of iteration in the hydrodynamics calculations. The Newmark $\beta = \frac{1}{4}$ Method provides a direct solution with good stability. It is derived on the assumption that the average acceleration remains constant over a time-step. Table 3.1 summarizes the recursive equations given by Craig (1981) for advancing of the motions in time. These have been modified by the assumption of a proportional damping. A particular advantage of the Newmark method is that it only requires motions data, in conjunction with force data, from one step to predict the next.

At each timestep, the force distributions are also corrected for pitch angle and then used to determine the longitudinal shear and bending moment distributions. The algorithms for shear and bending moment are adapted from common engineering methods for analyzing static structures. The starting point is the instantaneous loading distribution acting on the ship; including gravitational weights, buoyancy forces, inertial forces and the ice force. A lumped mass approximation is assumed for the distributions. The ice force is treated as a point load. Shear is obtained by integrating the loads over the ship's length. The bending moment distribution is realized after a second integration.

TABLE 3.1 CONSTANT AVERAGE ACCELERATION METHOD*
or NEWMARK β = 1/4 METHOD

1.	$\ddot{q}+(2\omega)\dot{q}+\omega^2 q=\frac{pt}{m}$	Equation for proportional damping
2.	$\ddot{q}(t)=\frac{1}{2}\left(\ddot{q}_i+\ddot{q}_{i+1}\right)$	Average acceleration assumption
3.a	$\dot{q}_{i+1}=\dot{q}_i+\left(\frac{\Delta t}{2}\right)\left(\ddot{q}_i+\ddot{q}_{i+1}\right)$	Integration gives velocity
b	$q_{i+1}=q_i+\dot{q}_i\,\Delta t+\left(\frac{\Delta t^2}{4}\right)\left(\ddot{q}_i+\ddot{q}_{i+1}\right)$	Second integration gives motion
4.a	$\Delta\ddot{q}_i=\left(\frac{4}{\Delta t^2}\right)\left(\Delta q_i-\dot{q}_i\Delta t\right)-2\ddot{q}_i$	Solve for old incremental accel.
b	$\Delta\dot{q}_i=\left(\frac{2}{\Delta t}\right)\left(\Delta q_i\right)-2\dot{q}_i$	Solve for old incremental velocity
5.	$\Delta\ddot{q}_i+(2\zeta\omega)\,\Delta\dot{q}_i+\omega^2\Delta q_i=\frac{\Delta p(t)}{m}$	Incremental equation of motion
6.a	$k_i^*\Delta q_i=\Delta p_i^*$	Modified incremental equation
b	$k_i^*=\omega^2+\left(\frac{4\zeta\omega}{\Delta t}\right)+\left(\frac{4}{\Delta t^2}\right)$	Stiffness term in modified equation
c	$\Delta p^*=\frac{\Delta p_i}{m}+\left[\left(\frac{4}{\Delta t}\right)+(4\zeta\omega)\right]\dot{q}_i+2\ddot{q}_i$	Load term in modified equation
7.a	$q_{i+1}=q_i+\Delta q_i$	Update motion, velocity, acceleration
b	$\dot{q}_{i+1}=\dot{q}_i+\Delta\dot{q}_i$	
c	$\ddot{q}_{i+1}=\ddot{q}_i+\Delta\ddot{q}_i$	

* Note: Modified from Craig (1981), assuming proportional damping.

3.4 Flexural Response by Normal Mode Methods

The flexural response and stresses in the extreme fibres of the hullgirder are determined by a normal mode analysis. Figure 3.3 illustrates the main steps in this process. It consists primarily of a determination of the modal properties for the ship, and a time-domain simulation of flexural response based on the use of mode superposition techniques. This is followed by an extraction of stress results from the flexural motions.

The hydroelastic motions in the present model are dependent upon structural properties assigned in the Hull Design Model, and ice forces and hydrodynamic data produced in the Rigid Motions Model. The dependence of the flexural analysis on force time-histories from the rigid motions simulation limits it to the same collision parameters and ship geometry. The impact speed, uniaxial ice strength, iceknife width, time-step and run duration must correspond exactly. Only structural parameters, such as the section modulus and steel modulus can be varied. The section modulus can be proportionally scaled according to a desired midship value. And CASPPR, a module for approximating to Arctic Class structural properties, can be run prior to the flexural analysis.

FIGURE 3.3

FLEXURAL RESPONSE BY NORMAL MODE SUPERPOSITION METHODS

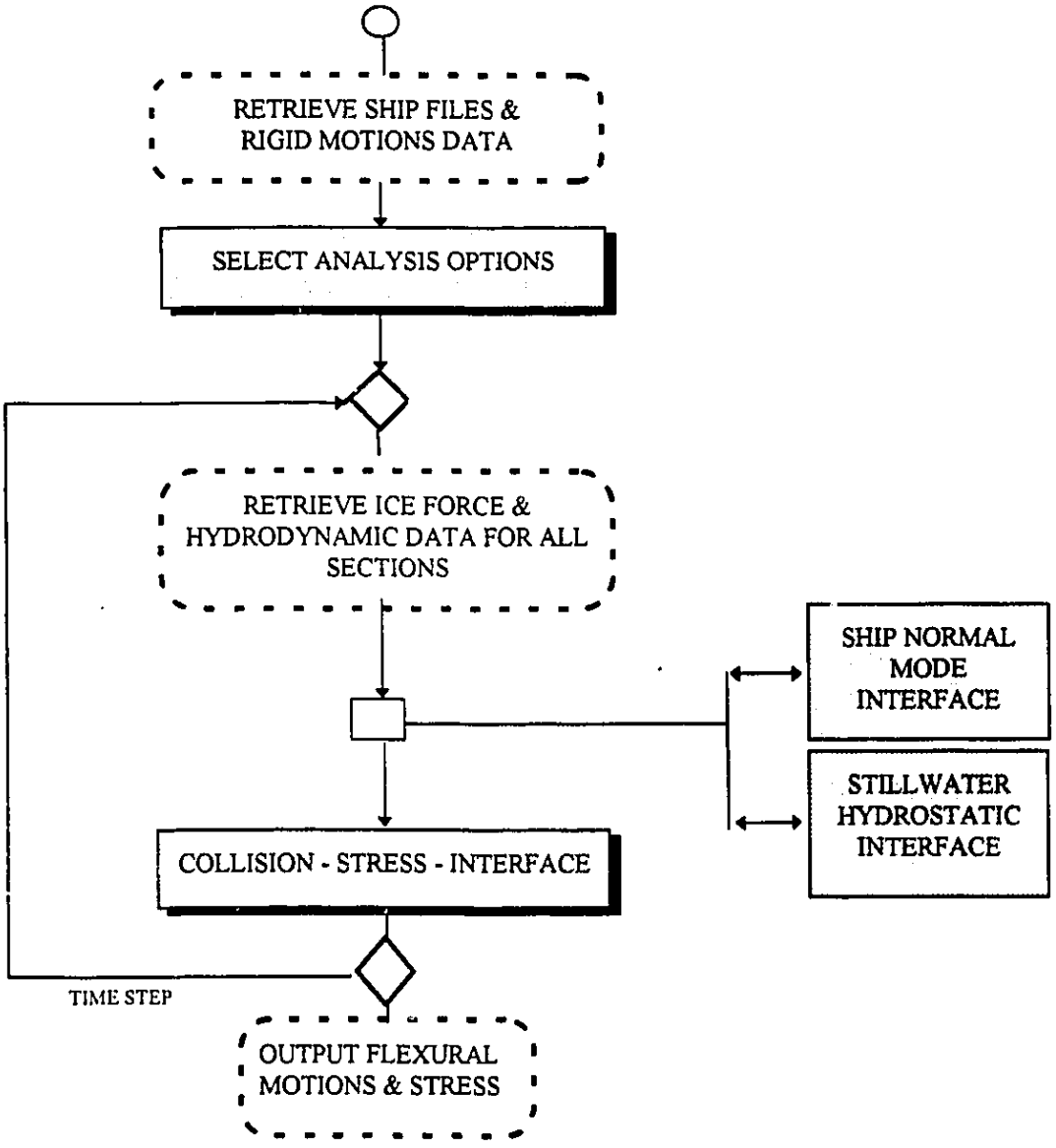

The decision to adopt a dry mode means that free-free mode shapes for the dry ship are calculated, rather than wet modes. As explained in the introductory comments, this choice is premised on the need to accurately include the transient hydrodynamic and ice interaction forces. While an elastic foundation model can produce wet mode shapes and frequencies corresponding to values measured in vibration tests on actual ships; the hydrodynamic phenomena associated with large amplitude motions is not included. In contrast, the dry mode shapes and frequencies cannot be measured directly (since the ship is floating); but any arbitrary distribution of forces acting on the hull can be included through the computation of generalized modal forces. This is consistent with the methodology recommended by Betts et al (1978) .

Figure 3.4 charts the main procedures for solving the eigenvector problem and defining the modal properties of the ship. The determination of mode shapes is based on an admissible shape function methodology. Cosine and sine functions spanning the range $(0,2\pi)$ and alternating in a Fourier sequence are used as admissible functions. The maximum number of shape functions is limited by the number of sections along the ship at which property information is available. In practice, it must be less than the number of stations, excluding the end sections which are very closely spaced.

FIGURE 3.4

SHAPEFUNCTION NORMAL MODE INTERFACE

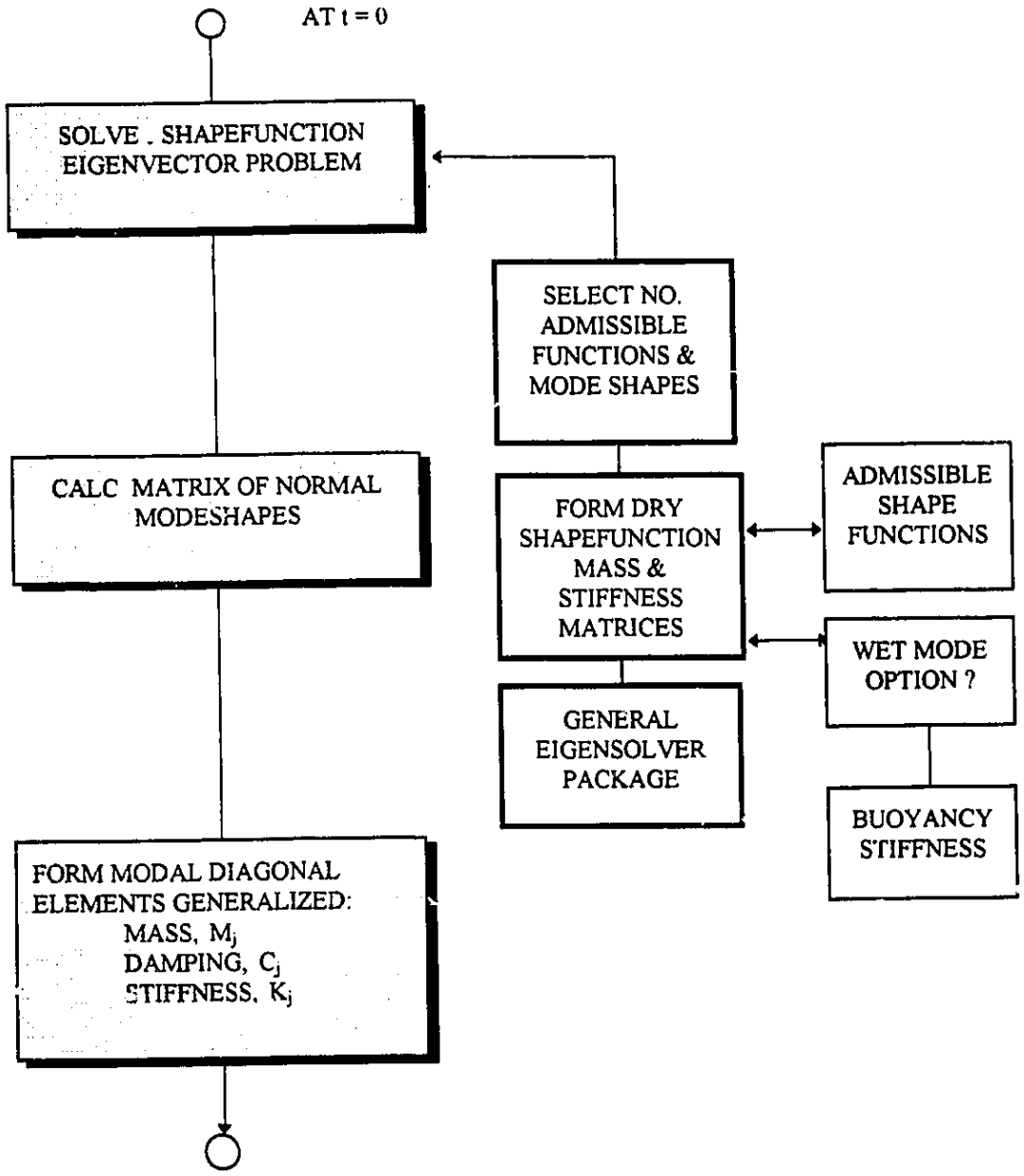

The transverse displacement u(t) is sought for the NDOF model representing the ship as a continuous beam structure. The known mass and inertia distributions are used to form a shape function mass and bending stiffness matrix. Their elements can be developed from virtual energy considerations, (see Craig, 1981 or Bathe 1982), and are commonly expressed in integral form as:

$$m_{ij} = \int_0^L m(z)\Psi_i\Psi_j dz \tag{3.8a}$$

and

$$k_{ij} = \int_0^L EI\,\Psi_i''(z)\Psi_j''(z)dz \ . \tag{3.8b}$$

A buoyancy term would be added to the stiffness equation if the wet modes, as well as the dry modes, were being sought.

Since the matrices will contain off-diagonal terms it is neither possible to directly employ the shape functions as single degree of freedom analogues of the NDOF system, nor to approximate the hullgirder response by a linear superposition of shape functions of the form:

$$u(z,t) = \sum_{i=j}^{n} \Psi_j(x)\,u_j(t) \ . \tag{3.9}$$

Instead it is necessary to translate the admissible shape functions into normal mode shapes by solving the eigenvector problem. The eigenvalues giving the modal frequencies can be found by simple, conventional methods. But the determination of the

corresponding eigenvectors is not a trivial problem. Recourse has been made to a general eigensolver routine originating in the Argonne Laboratory handbook. It produces both eigenvalues and eigenvectors for the given matrices. The elements of the eigenvectors, w_{ir}, act as weights on the shape function amplitudes in defining the mode shapes, $\Phi_r(z)$, according to the summation:

$$\Phi_{jr} = \sum_{i=1}^{r} \Psi_{ji} w_{ir} \quad , \; j = 1,.., n \, . \tag{3.10}$$

Each of the mode shapes is subsequently normalized by its maximum amplitude. A truncated set of terms is retained as the normal modes. The precise number of modes that is used depends on several factors, but it will approximate to one third of the number of shape functions.

The diagonal elements of the normal matrices, representing the generalized mass and stiffness, can then be formed in terms of the mode shapes. This transformation can be written:

$$M_r = \left[\Phi_{jr}\right]^T \left[m_{ij}\right]\left[\Phi_{jr}\right] = \int_0^L m(z)\Phi_r^2(z)\, dz \tag{3.11a}$$

and

$$K_r = \omega_r^2 M_r \tag{3.11b}$$

In practice there is no need to carry out the integrations using the mode shapes, since the generalized mass elements can be reconstructed from the existing shape functions mass matrix elements. The corresponding stiffness terms can immediately be deduced

from the mass and the corresponding modal frequency, ω_r. An error algorithm is included to verify that the mode shape truncation process does not distort these properties.

The generalized damping, C_r, is based on Craig's discussion of proportional damping using a Raleigh approximation. It presumes some knowledge or estimation of the damping factors at two lower modes. While considerable shaker test data is available for the prototype MV Arctic in situ, there is no information about damping for the dry condition. A typical value of first flexural mode damping for a large steel structure such as tall building might be 0.01, i.e. 1 percent of critical. In the present model, the first flexural mode is arbitrarily assigned a value of 0.02 and the second mode 0.05. These values refer to the structural damping only, without concern for ice and fluid effects. For higher modes the generalized damping is given in terms of its estimated damping factor, ζ_r, as:

$$C_r = 2M_r\omega_r \quad \zeta_r \tag{3.12a}$$

with

$$\zeta_r = \frac{1}{2}\left(\frac{A}{\omega_r} + B\omega_r\right). \tag{3.12b}$$

The constants A and B are solved simultaneously using the assumed damping factors for the two lowest flexural modes. Admittedly, the selection of these damping factors is somewhat arbitrary. But the higher mode dynamics are considered to play a less significant role in the investigation of large amplitude global response, than in an analysis of vibration phenomena.

Figure 3.5 graphically presents the time-domain procedures for computing the flexural response by means of mode superposition. The formation of normalized mode shapes and corresponding vectors of generalized mass, damping and stiffness has effectively translated the multi-degree of freedom system into an equivalent set of single degree of freedom problems. At each time-step the generalized force for each mode is calculated from the instantaneous force data retrieved from the rigid body analysis. It depends on the distribution of hydrodynamic and buoyancy forces at the sections and the vertical component of the resultant ice force; and takes the form:

$$F_r = \int_0^L \left\{ \sum F(z) \right\} \Phi_r(z)\, dz \ . \tag{3.13}$$

In practice, while the ice force is known, its location may not exactly correspond to the stations at which the elements of the mode shape vectors are explicitly known. So an interpolation process must be used to compute the mode shape value at this location.

Each of the single degree of freedom normal modes can be expressed in a form analogous to that of a rigid body mechanical system. This can be written in terms of coordinate motion, velocity and acceleration; and their corresponding generalized stiffness, damping and mass as:

$$M_r \ddot{q}_r + C_r \dot{q}_r + K_r q_r = F_r \ . \tag{3.14}$$

FIGURE 3.5

DETAIL OF COLLISION STRESS INTERFACE IN HYDROELASTIC MODEL

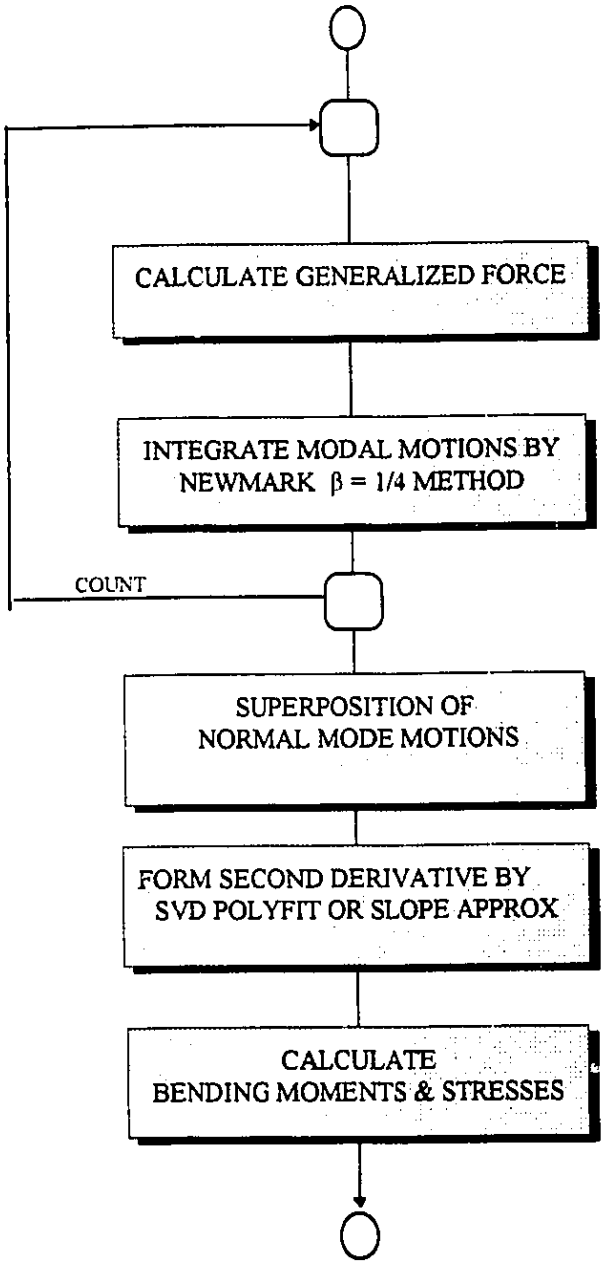

This set of modal equations is solved, as in the case of rigid body motions, by applying the Newmark β = ¼ Method. Each equation is solved independently. The resulting amplitudes of each coordinate motion are summed in a linear combination which includes the mode shapes as weighting functions. This gives the overall transverse displacement, u(z) or response, y(z) as a function of longitudinal distance along the ship.

$$y(z) = \sum_r q_r \Phi_r(z) \tag{3.15}$$

In the numerical algorithms, this summation takes place at each of the i ship sections.

3.5 Hullgirder Stress Calculations

If the detailed structural design of a ship was known, it would be possible to extract the various stresses in a particular member through a finite element modeling process. But at the concept exploration stage it is assumed that only approximate section modulus information is available. This limits the present analysis to an estimation of the hullgirder stress in the extreme fibres of an equivalent longitudinal beam representing the general structural features. The stress is calculated from the instantaneous bending moment along the ship according to the usual engineering stress-moment relationship. Expressed as a function of longitudinal position the stress, $\sigma(z)$ is:

$$\sigma = \frac{Mc}{I} \quad (3.16)$$

where c is the transverse distance from the neutral axis to the extreme fibre. The section modulus is I/c.

The bending moment expresses the transverse curvature of the deck or baseline associated with the displacements arising from the normal mode analysis. This curvature can be taken from the elastic flexure equation for beams in bending as:

$$M/EI = -\frac{d^2y}{dz^2} \quad (3.17)$$

where E is the steel modulus. The moment distribution depends on the second order spatial derivative of the response, which is approximated by a least squares polynomial fit. This is implemented using a singular value decomposition technique, with a simpler linear slope calculation as a check.

3.6 Discussion of Rigid Body Shear and Bending Moment

Figure 3.6 and Figure 3.7 present examples of longitudinal shear and bending moment curves at various time-steps during a collision, as derived from a rigid body analysis. The accuracy of these results is limited because of the effect on the quasi-static analysis algorithms of rapid variations in the magnitude of the ice force. The dynamic response of the ship motions may bring the bow into full contact with the ice at one instant, but at the next it may be nearly free. The discontinuities of this mechanism are

discussed more fully in the following chapter. In contrast, the sectional accelerations associated with the lumped inertial force elements reflect the cumulative effect over time of all forces acting on the body, rather than responding instantaneously to the ice force variations. So the instantaneous loading distribution can be badly skewed by the ice force variations, leading to large offsets and errors in the derived shears and moments. At any particular station, this could introduce a high frequency distortion into the derived time-histories of shear and bending moment. This problem is corrected somewhat by a smoothing process, which averages the ice force over two consecutive time steps.

The bending moment distribution along the ship is characterized by a maximum amplitude near the midship section. At the ends the moment and shear are zero. During the collision, the entire distribution increases in magnitude in response to the variations in the forces. Figure 3.8 shows a corresponding time-history of the bending moment at the midship section. It shows an initial large amplitude peak which drops back to the stillwater value. This is followed by a gradual buildup throughout the remainder of the collision interaction.

FIGURE 3.6

RIGID SHEAR FORCE DISTRIBUTIONS

Ship M15V Longitudinal distribution at fixed times
3-D ICEMESH MODEL and BEM Wavetank
Impact velocity = 4 knots, Ice strength = 1.5 MPa

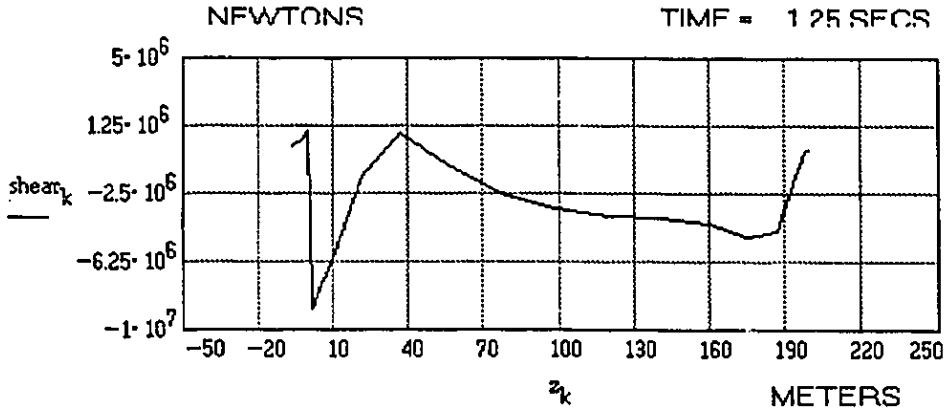

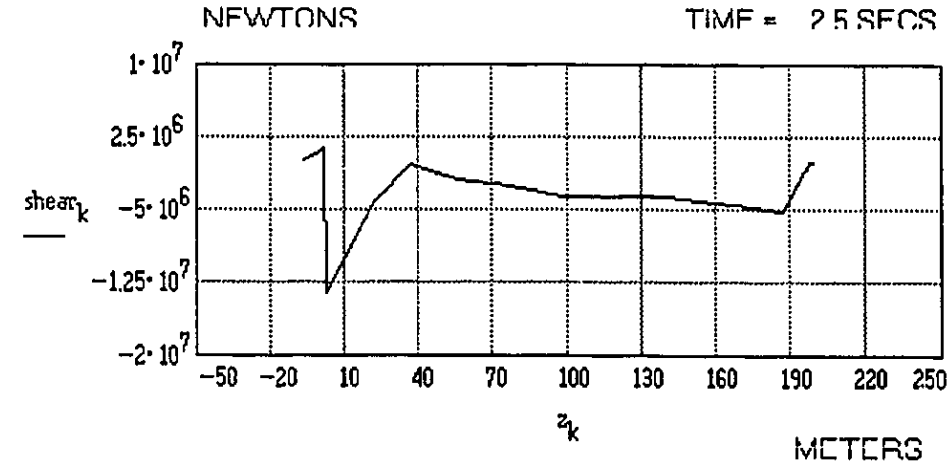

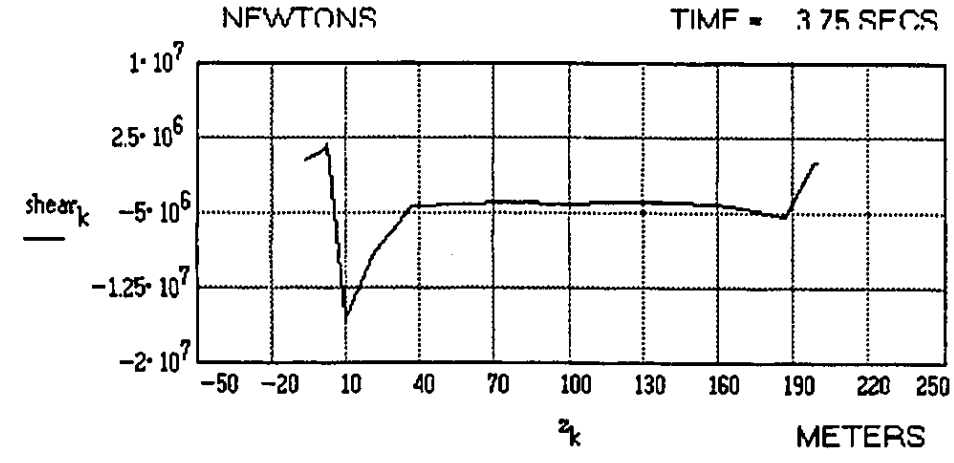

FIGURE 3.7

RIGID BENDING MOMENT DISTRIBUTIONS

Ship M15V Longitudinal distribution at fixed times

3-D ICEMESH MODEL and BEM Wavetank

Impact velocity = 4 knots, Ice strength = 1.5 MPa

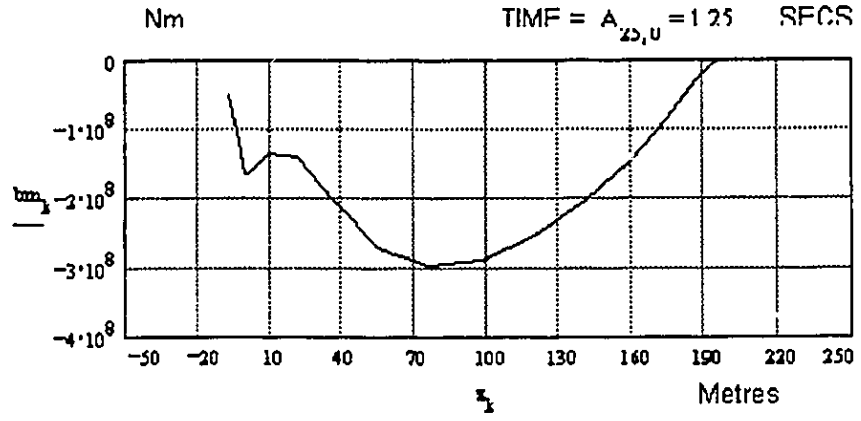

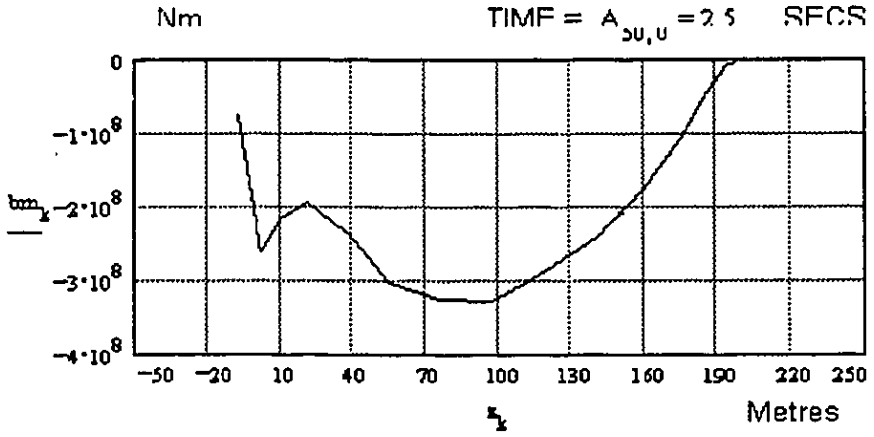

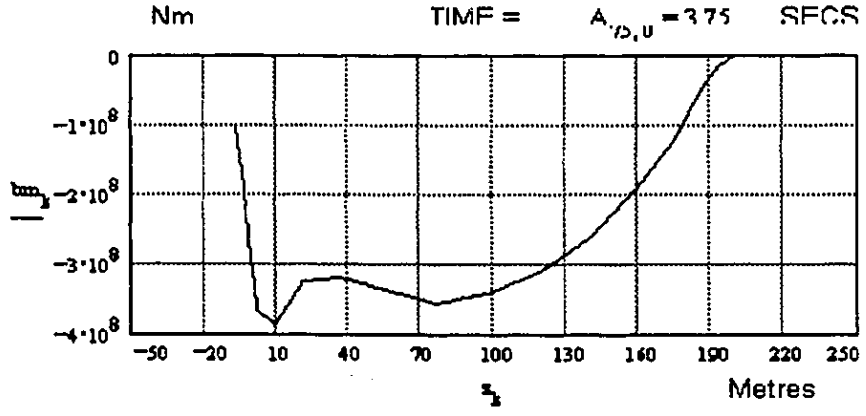

Figure 3.9 presents a corresponding set of flexural bending moment distributions, extracted at a number of intervals during a collision. The time-history of the flexural midship bending moment is shown in Figure 3.10. It exhibits a smooth curve; indicating that the flexural analysis more adequately treats the dynamics of the collision process. As in the rigid ship case, there is an initial peak with a corresponding magnitude. But the subsequent phase also exhibits significant dynamic response, rather than showing a gradual and modest buildup.

In the case of flexural bending moments, the time-histories give the magnitudes at the midship (or other sections) corrected for the stillwater bending moment. This represents a significant offset, which must be included in any comparison to the results of a quasi-static calculation. The stillwater bending moment is computed at the beginning of the normal mode stress analysis process. It uses the same basic algorithms, but is entirely distinct from the flexural response simulation. In this case, an arbitrary time period is specified for the ship to reach the stillwater equilibrium condition. The gravitational weights and initial sectional buoyancy forces are applied in exponentially increasing increments, such that:

$$F_{APPLIED} = \left(1 - e^{\beta}\right) \bullet F_{TOTAL} \quad \text{with} \quad \beta = -4\left(n/n_{max}\right). \tag{3.18}$$

The constant -4.0 in the exponent, β, gives 86 percent of the force at one-half of the maximum number of time steps, n_{max}.

FIGURE 3.8

MIDSHIP RIGID SHEAR & BENDING MOMENT
Ship M15V Run HO-A-04
BEM Numerical Wavetank & 3-D ICEMESH MODEL
Impact velocity = 4 knots, Ice strength = 1.5 MPa

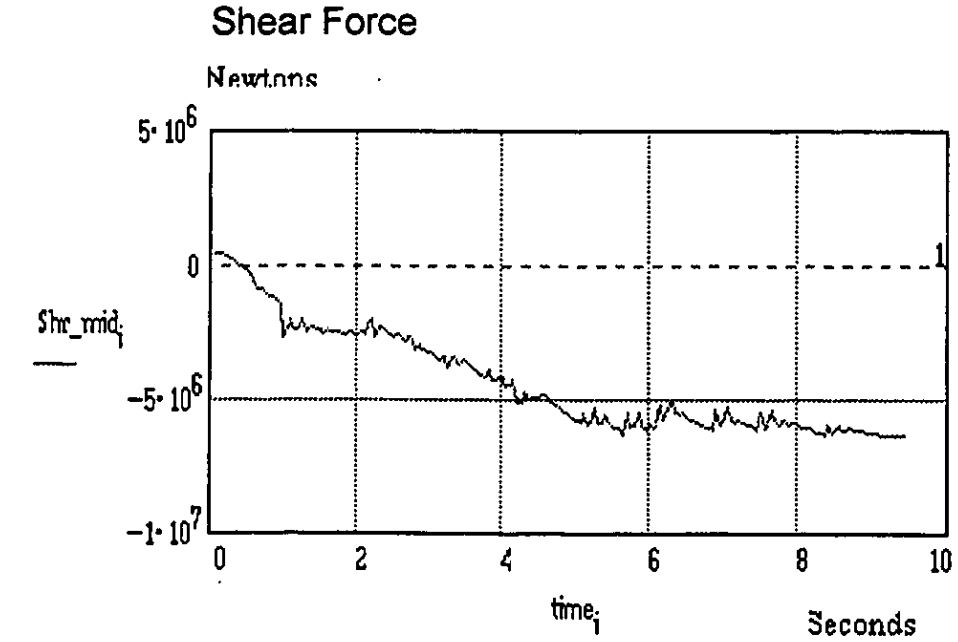

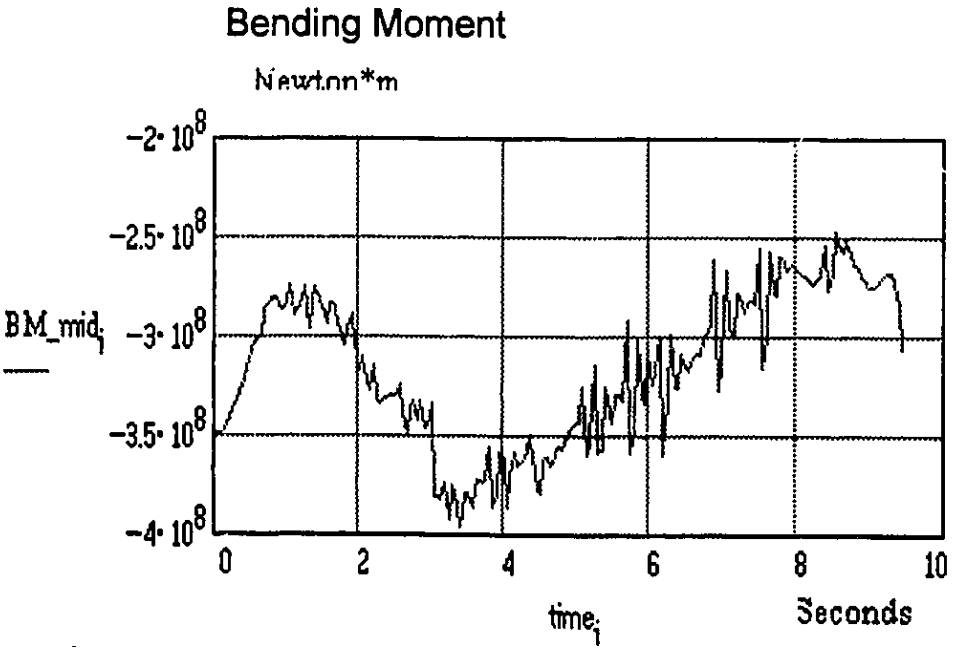

FIGURE 3.9
FLEXURAL BENDING MOMENT DISTRIBUTIONS

BEM Numerical Wavetank & 3-D ICEMESH MODEL
IMPACT SPEED 4 Knots
Sect_mod = 14.2 m3 Shapefuncs = 16 Modes = 5

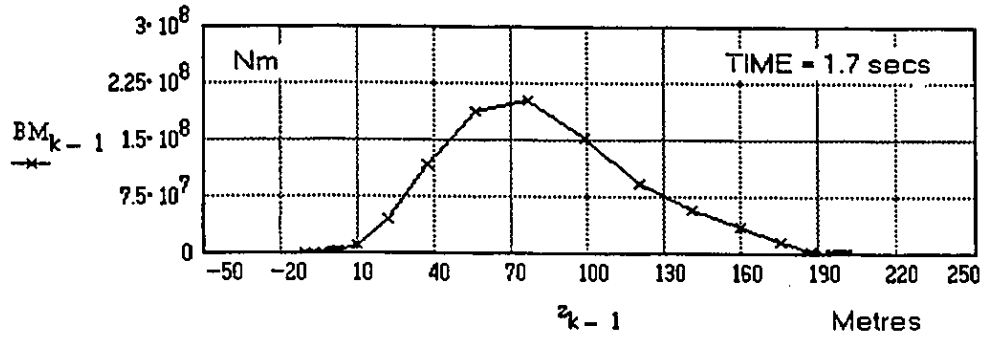

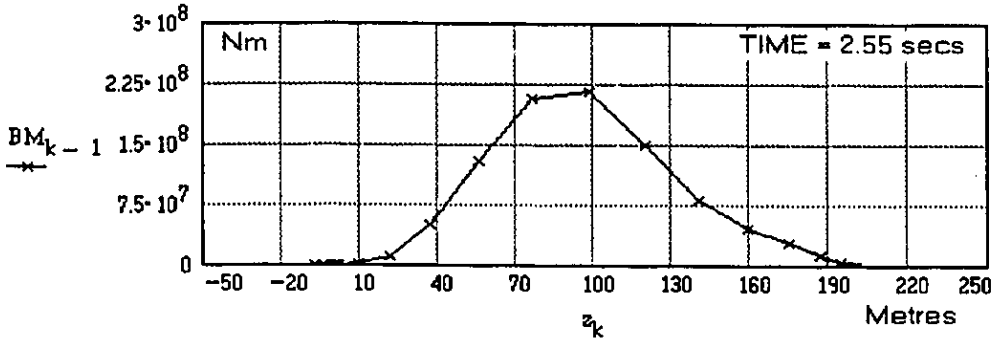

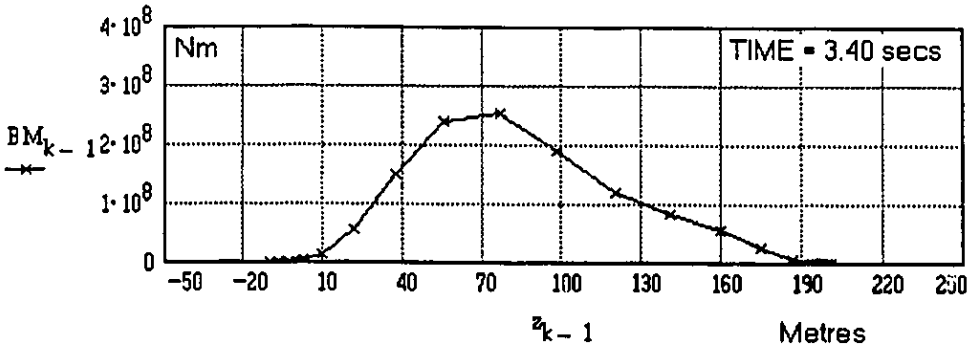

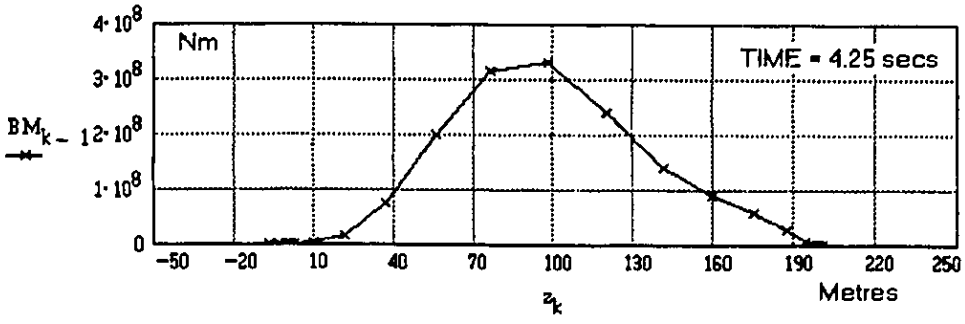

FIGURE 3.10
FLEXURAL STRESS & BENDING MOMENT

BEM Numerical Wavetank & 3-D ICEMESH MODEL
IMPACT SPEED 4 Knots
Sect_mod = 14.2 m3 Shapefuncs = 16 Modes = 5

max(BM_mid) = $4.36 \cdot 10^8$ Newton*m

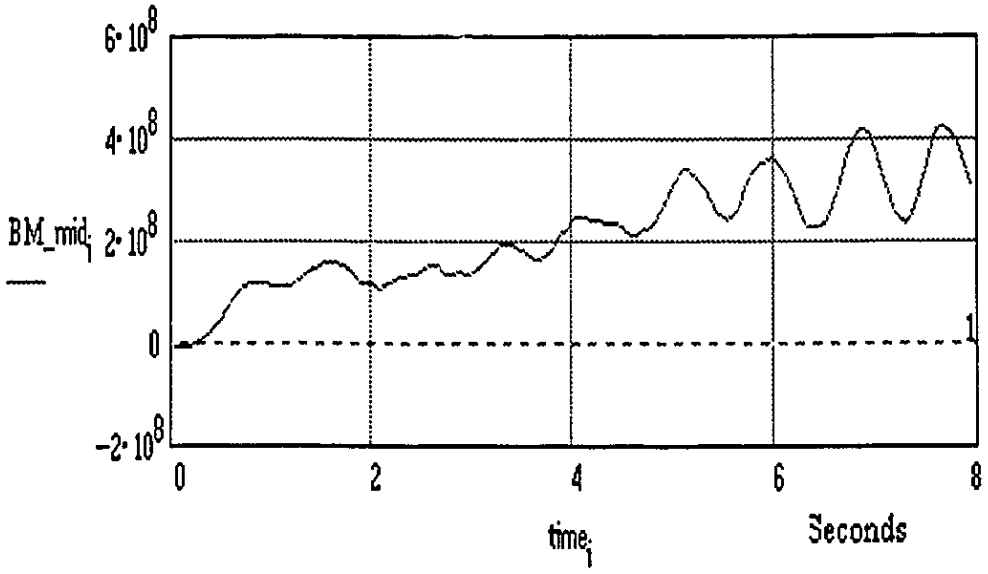

max(Str_mid) = $3.071 \cdot 10^7$ Newtons/m^2

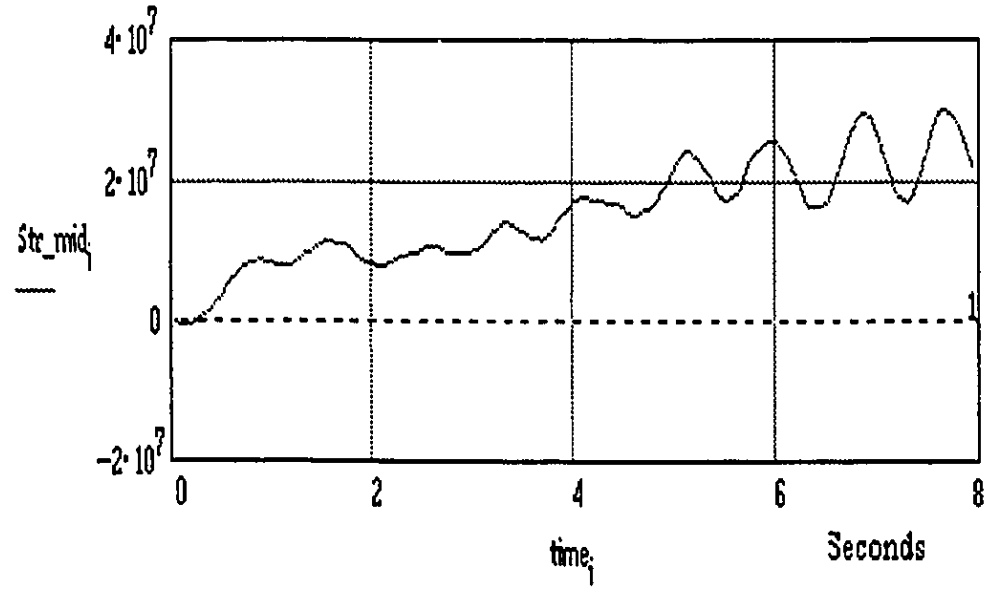

Figure 3.11 shows the results of a time-domain simulation of the modal stillwater moment at the midship section. For comparison, it also shows the corresponding distribution along the ship resulting from a hydrostatic calculation. The gradual application of the equilibrium force distribution avoids ringing in the numerical calculation. After completion of the stillwater calculation, all force data for the collision time-stepping is corrected to remove the stillwater component. Good agreement is observed between the bending moment derived from the dynamic methods, and that given by the reference hydrostatic calculation. A further comparison of the relative magnitudes of the stillwater and the ramming components (e.g. Figure 3.10) shows that the former plays a significant role, and must not be neglected in a valid analysis of collision stresses.

FIGURE 3.11
MIDSHIP STILLWATER BENDING MOMENT

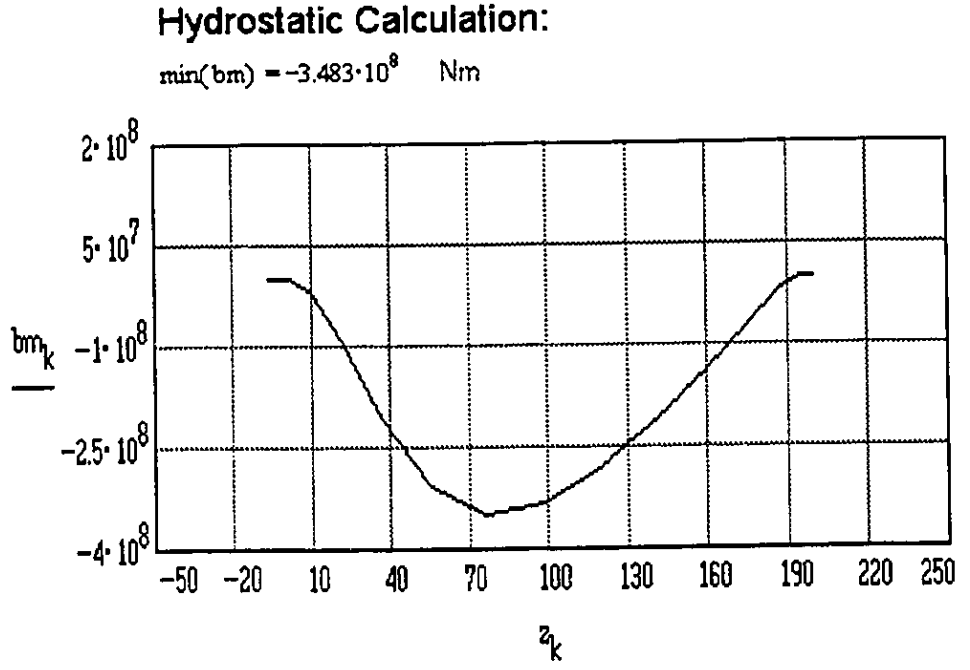

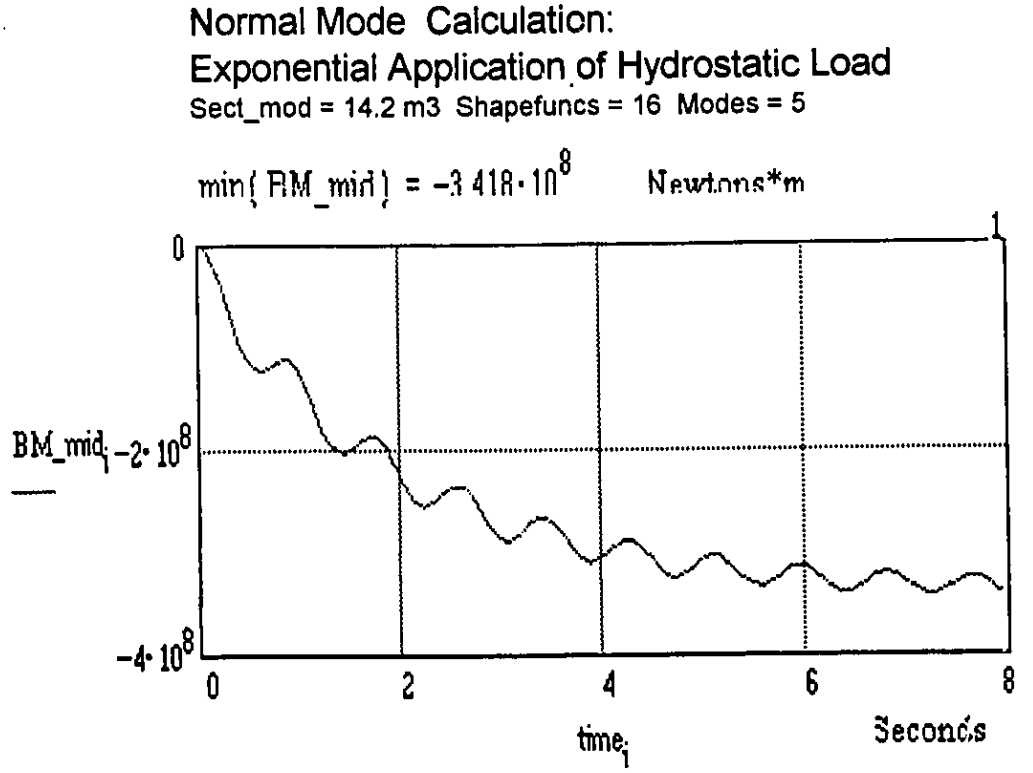

Chapter 4 The Ice Interaction Model

The determination of global ice loads and hullgirder stresses is critically dependent upon the limiting assumptions and mathematical idealizations which are imposed in modeling the ice failure process. Its inherent complexity can be reduced by a judicious selection of system parameters which account for the significant physical mechanisms. But this representation must preserve the characteristic nonlinear dynamics of the overall system. In this respect, the collision case is quite different from the interaction between fixed, rigid structures and slowly moving ice sheets. It demands a unified approach which integrates contributions associated with the mechanical ice properties and those due to the kinematic displacements of the ice interface.

The present chapter starts with a discussion of the basic assumptions and idealizations which have been embedded in the ITHACA_SHIP Ice Interaction Model. This is followed by a description of three progressive stages of modeling complexity that have been implemented. The contact force components are first defined in terms of the projected areas of indentation mapped onto the horizontal and vertical planes. The concept of a dynamic profile contact area is then introduced, giving effective projected areas that reflect the instantaneous kinematic condition of the system. Lastly, the kinematic description is extended to include mapping displacements of two surfaces comprising a three-dimensional interaction interface. This multi-tiered approach permits a

later assessment of the importance of including or neglecting different physical mechanisms.

The methodology for determining the effective contact pressure is subsequently explained. This includes discussion and development of mathematical representations for different elastoplastic mechanisms contributing to the ice interaction forces. The corresponding interaction energies resulting from the time-domain analysis are also described.

4.1 Modeling Ice Interface Dynamics

According to Andronov et al (1966), a physical interaction such as a ship-ice collision can only be adequately represented as a nonlinear, non-conservative system. And it is dissipative because of the energy losses associated with the ice failure process. In terms of the Lagrange equation formulation of motions in Chapter 2, this means that the ice force cannot be represented as a potential function. It must be retained as a generalized force on the right side of equation (2.1). The implications of this statement will be returned to in the next chapter—in regard to attempts to lump together all of the external interaction mechanisms into pseudo added mass and damping coefficients. In modeling nonlinear dynamics, the idealizations which Andronov accepts as permissible are those which 'consider the problem in its entirely'. This involves the questions asked, as well as the system properties.

The complexity of the ice interaction process stems from the variety of states in which multi-year ice can exist. Sinha (1978) has likened ice to a crystalline metal, existing in a high temperature state close to its melting point. By definition, multi-year ice has undergone at least two annual cycles of melting and recrystallization. This leads to a tough interwoven matrix of crystals, quite unlike the more regular alignment of first year sea ice.

Its physical properties depend on a range of environmental factors associated with its formation and subsequent history. Experimental data have been reported by Riska and Frederking (1987) based on uniaxial, biaxial and triaxial tests. Above a strain rate of $10^{-3}s^{-1}$ it was found that multi-year ice exhibited decidedly brittle characteristics. The stress-strain plots show a characteristic initial stress peak which ends abruptly at a certain strain limit. This maximum is followed by lower stresses associated with indentation through broken ice. The maximum stress increases nonlinearly with lower strain rates, but becomes more linear at higher rates. The uniaxial compressive stress varied from 1 MPa to about 10 MPa at the highest strain rate. Time to failure decreased over the same range. Confinement in the triaxial tests produced a fractional reduction in the measured stresses. Unfortunately the experimental procedures cannot handle strain rates above $10^{-2}s^{-1}$ So there is limited information on strain rate behaviour in the range corresponding to ship collision dynamics.

It should not be surprising that the ship designer and regulator's requirement for more accurate prediction of global ice loading has prodded the modeling process towards nonlinear dynamics. Earlier models were satisfied with estimations based on the limited

case of parameters which did not depend on the instantaneous state of the system. Ice crushing strength was considered as a constant. This gave linear differential equations, which often could be solved analytically. Theoretical developments of ice resistance and ramming models by Kasteljan et al (1968) and White (1968) consider ice properties in this way. But the need for more specific design information has demanded more complex mathematical representations.

Daley (1991) has documented the trend in ice failure modeling towards nonlinear dynamics as supportive discussion for his application of Chaos Theory, which is itself a component of nonlinear dynamics. As a starting point he cites the work of Kheysin (1966), who extended the concept of a viscoelastic interface from plasticity theory to ice mechanics. Kheysin proposed that an intermediate layer of pulverized and fluidized ice is formed between the hull and the elastic zone below. This allowed an approximation for the global loading dependent on the ship's mass and the relative contact velocity. It was noted that the global force was not strongly dependent on the magnitude of the crushing strength. Furthermore, any hypothesis leading to a reasonable contact duration was thought to give a good result.

Daley ascribes the first process model to Matlock, Hawkins and Panak (1969, 1971). It represented the failure interaction of an ice sheet with a structure as a series of brittle fractures. In contrast, Croasdale (1980) introduced a series of consecutive shear failures throughout the indentation period. Other models have introduced independent failure zones with a finite failure distance; asychronous failure; assumed instantaneous pulverization; or combined constitutive property models with damage mechanics. These

models have generally attempted to satisfy Kheysin's criterion of a reasonable contact duration by including physical mechanisms identified as being significant in pulverization or uniaxial crushing tests.

In modeling ice sheets impacting slowly on rigid structures the emphasis is reasonably placed on improving the representation of the ice failure mechanism. But in a collision process the requirement of nonlinear dynamics to 'consider the problem in its entirety' suggests that the kinematic representation of the contact surface displacements warrants careful modeling. (A rigorous treatment of techniques in theoretical kinematics is given by Bottema and Roth, 1979). In fact, Kheysin's conclusions indicate that variations in ice strength may be a less significant factor than the accurate modeling of system parameters.

Similar concerns over limitations in the existing knowledge about ice failure properties can be seen in physical model testing reported by Phillips and Daley (1985, 1986) and Riska (1987). In each case, flexural models of the MV Arctic were constructed and tested in simulated multi-year ice. It was accepted that some scaling distortions would be introduced through assumptions about the nature of the ice failure process. Attempts were made to minimize scale effects by tailoring ice modeling materials to replicate trends in full scale trials data. There was less concern for retaining micromechanical properties.

In the former case, a synthetic wax-like material was used. A crushing strength relationship was experimentally determined such that Froude (or dynamic) scaling for the overall collision process was preserved. This calibration established a geometric (linear)

scaling between the model scale indentations and corresponding MV Arctic ramming trials data. It was observed that the resulting ice force components and the collision duration were in good agreement with the prototype data.

In marked contrast, Riska first tested his physical model using a light density concrete. In this case, emphasis was placed on scaling the brittle ice failure at the prototype impact velocity; rather than on maintaining dynamic similarity over an extended velocity range. In this case, indentations were not geometrically scaled. Riska subsequently extended the testing to higher velocities by using blocks of fine grained saline ice.

In summary there is only limited collision data as a basis for defining explicit ice strength relationships; and there is an inherent uncertainty about scale effects in applying sample ice properties to prototype applications, especially where high strain rates are involved. Verification of any mathematical representation of the prototype ice failure process will, at best, be very weak. In the context of a concept exploration model it has not seemed worthwhile to concentrate on the ice properties question. So a constant ice strength assumption has been used. It is further assumed that the ice body remains fixed, and is a homogeneous and isotropic material. Nevertheless, a number of physical mechanisms introducing elastoplastic properties have been included.

A consequence of the foregoing considerations concerning nonlinear dynamics is that the kinematic representation of the instantaneous displacements of the collision interface has emerged as a characteristic feature of the ITHACA_SHIP Ice Interaction Model. Figure 4.1 illustrates the two surfaces defining the active zone of ship-ice

interaction. The upper boundary of the zone is given by a triangular element grid on the hull surface. It is dynamically sized and oriented to span the region of the ship's bow indented into the ice field. The lower boundary is shown as a coordinate mesh marking the excavated ice surface, which has been cumulatively developed by the motions of the bow into the ice body. Because of ship dynamics, the instantaneous grid elements and corresponding ice mesh coordinates will generally not coincide. The knowledge of the relative proximity and velocity of the individual elements of the two surfaces is used to determine the contact force, and makes possible a more realistic exploration of physical interaction mechanisms.

4.2 Ice Model Stage 1 - Projected Area of Indentation

The simplest relationship for determining the contact force assumes that the ice strength remains constant throughout the collision interaction. In this case, the contact force can be interpreted as an elastic reaction. Its components can be expressed in terms of the projections of the indented ice surface onto the vertical and horizontal planes respectively, as:

FIGURE 4.1 ICE INTERACTION MODEL

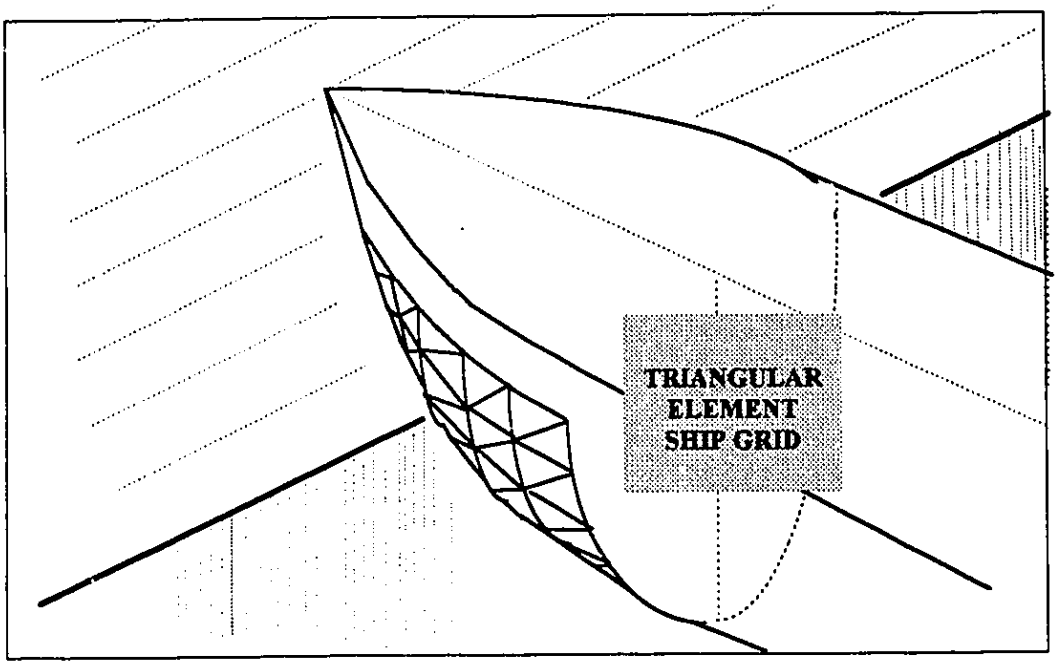

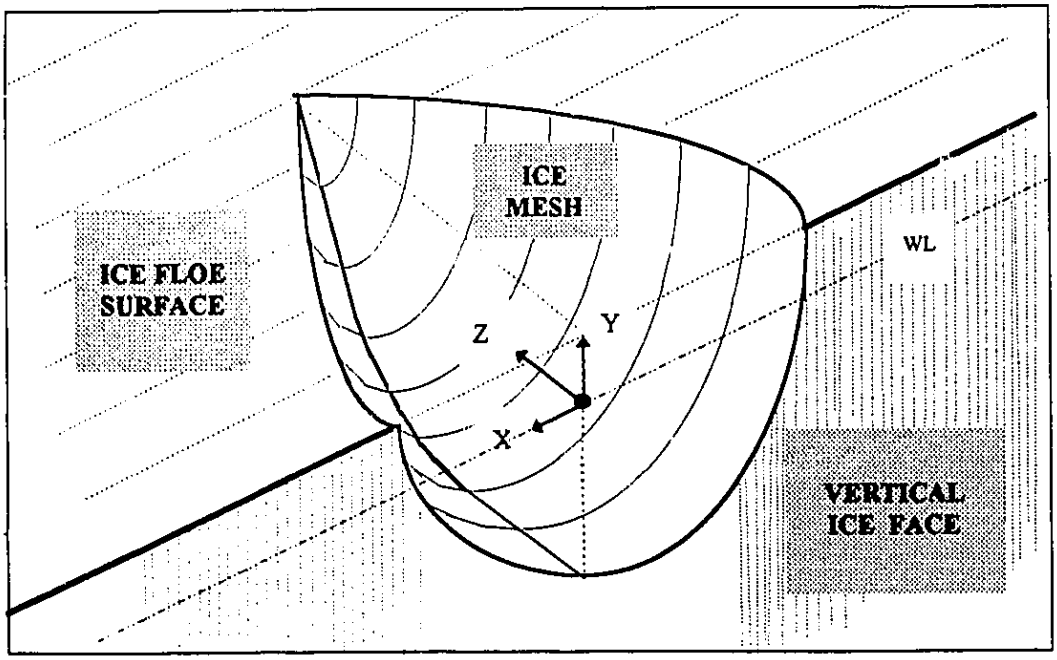

$$F_{CR_y} = \sigma_{CR} A_Y \tag{4.1a}$$

and

$$F_{CR_z} = \sigma_{CR} A_Z \tag{4.1b}$$

where σ_{CR} is the uniaxial crushing strength obtained from sample tests. White (1968) and Naegle (1980) have followed this method of representing the crushing stages of ramming and ice resistance interactions. But the continued application of these equations during the subsequent slide-up phase would lead to erroneous results.

In practice, equation (4.1) is seldom applied directly in describing an overall interaction. Rather, it has become more common to employ empirically based pressure-area relationships. These implicitly account for variations in contact pressure due to changing interaction mechanisms during the impact. An example is given by Daley and Phillips (1986). In comparing experimental time histories from the *MV Arctic* model tests to a numerical simulation they found that a good fit was given by a pressure-area relationship of the form:

$$p = 0.07 A_S^{-0.5} + 0.14 \tag{4.2}$$

where the average pressure, p, is in MPa; and A_S is the total geometric surface area in m^2. Such relationships are not being examined in the present research. Rather, a constant pressure relationship similar to equation (4.1) has been used as a basis for calculating

global loads and investigating the importance of different physical mechanisms by progressively varying components.

Figure 4.2 illustrates the basic components of the projected area model. The key step involves the kinematic description of the ship's bow profile with respect to the undisturbed ice face and surface. For the case of simple indentation, this involves only the determination of the coordinates defining the leading point and trailing edge of the ice notch. The profile view of the ship forebody in Figure 4.3 depicts the instantaneous displacement of the mathematical bow curve with respect to the boundaries of the ice body. The kinematic algorithms define the spatial orientation of the bow profile in terms of the surge, heave and pitch motions.

The endpoints of the indentation zone are expressed in ship-fixed coordinate, since the projected areas are based on section data from the Hull Design Model. The area projected into the vertical ice surface plane is determined by an integration of the half-breadths for the indented sections. A pitch angle correction is required in specifying the section depths and corresponding half-breadths since the indented ice surface generally will not lie on a vertical ship plane. The area in the horizontal plane depends on the depth of the indentation at the trailing ice edge. The areas for the stations nearest to the ice edge are first calculated, and these are then used in interpolating to the actual indentation distance. A trapezoidal integral approximation is employed.

A sliding ice force component is computed at each timestep as the resultant of the static moment balance between the gravitational weights and buoyancy force distribution.

The normal reaction is computed from the moment on the assumption that it acts at an angle, β; which is given in terms of the projected areas as:

$$\beta = \frac{\pi}{2} - \tan^{-1}\left(A_Z / A_Y\right) \qquad (4.3a)$$

The approximation is not based on the bow profile curve. This sliding force is used in defining the frictional forces, which are given by:

$$F_{f_z} = \left\{\frac{-v_t}{|v_t|}\right\} c_f N_Z \qquad (4.3b)$$

and

$$F_{f_{z_Y}} = \left\{\frac{-v_t}{|v_t|}\right\} c_f N_Y \qquad (4.3c)$$

where c_f is the coefficient of friction. The sign of the force will depend on the surge velocity. During the retreating motions of the slide-off phase, the static force components are used in place of the crushing force.

It should be remarked that a horizontal force due to iceknife indentation has been included that is distinct from the projected area integration. This is a redundant calculation since the section coordinates in the Hull Design data structure include the iceknife. However, it is retained to facilitate a comparison of different ice models.

FIGURE 4.2 PROJECTED AREA ICE MODELLING METHOD

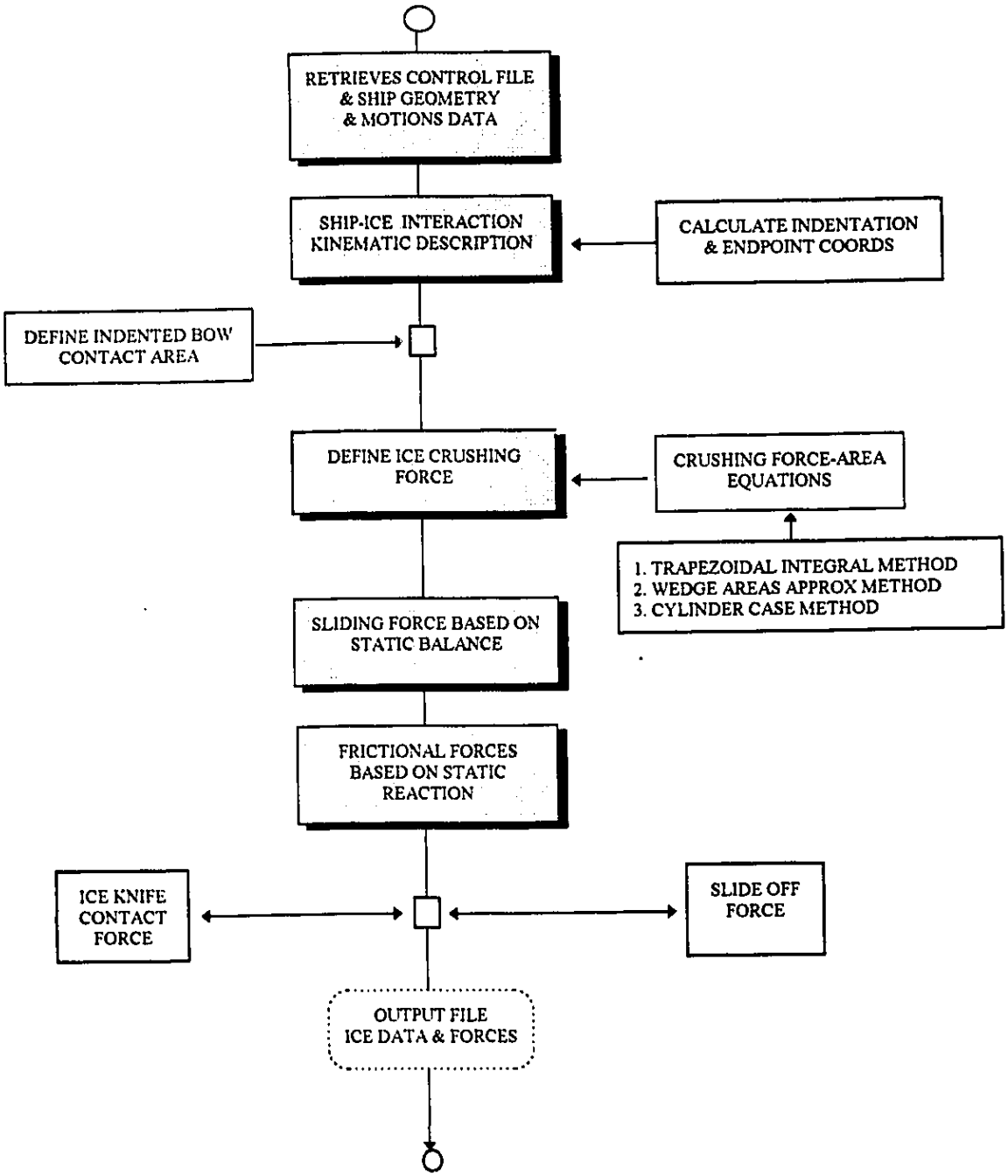

FIGURE 4.3 PROJECTED AREA COMPONENTS

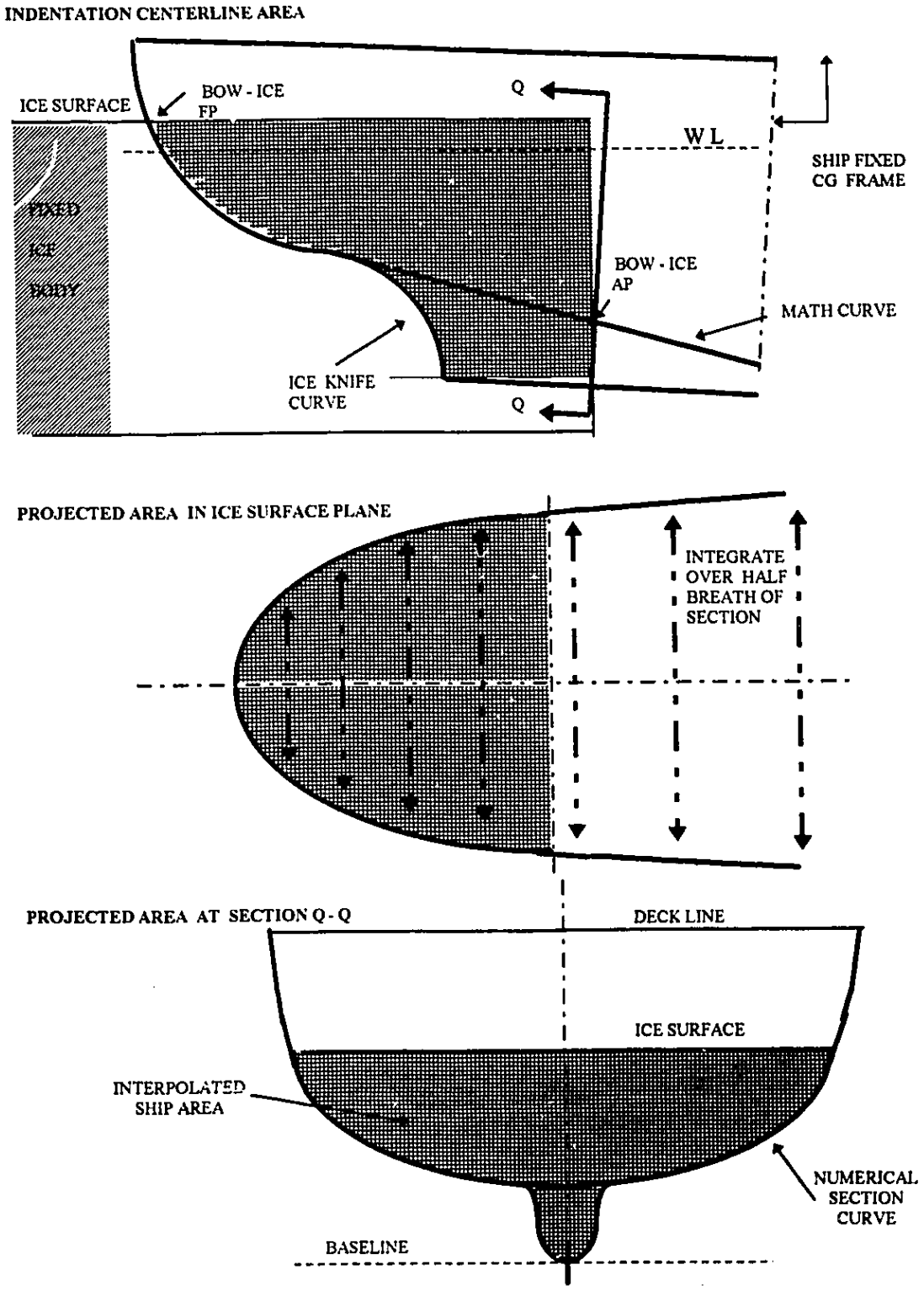

4.3 Ice Model Stage 2 - Dynamic Profile Contact Area

The concept of dynamic contact between the ship profile and the ice body arises naturally from considerations of two-body problems. The momentum of two colliding rigid bodies leads them to a bounce apart. A similar phenomena can be observed in physical modeling experiments. For example, it was observed in Riska's tests using a low density concrete as a substitute for ice. The bow of the *MV Arctic* model bounced repeatedly as it gouged a path upward onto the ice. Full scale force histories from the *Canmar Kigoriak* and *Robert Lemieux* reported by Ghoneim et al (1984) are indicative of the same process.

Figure 4.4 outlines the specific methodology developed to permit a practical implementation of this concept. It uses much of the same infrastructure as the projected area method for determining the instantaneous orientation of the ship with respect to the ice. But the kinematic description in the dynamic contact profile method is extended to correlate the relative displacements of two separate curves. One defines the instantaneous displacement of the ship profile. The other records the maximum extent of penetration of the bow into the ice body. Numerical algorithms of the ice interaction model check for the existence and location of intersection points between the two curves.

FIGURE 4. 4 DETAIL OF DYNAMIC PROFILE CONTACT AREA MODEL

UPDATE ICE_NOTCH PROFILE

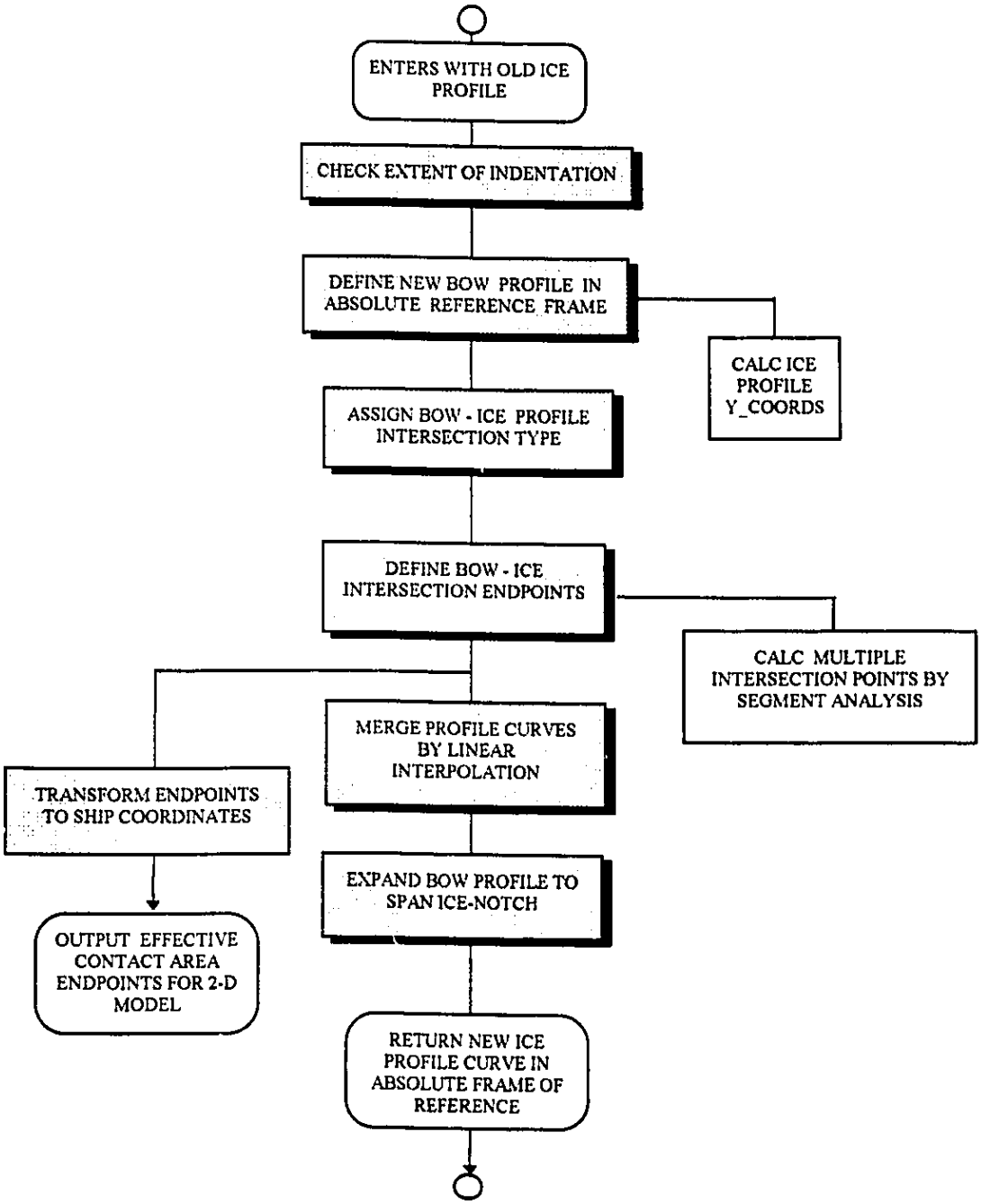

There are five possible states of intersection as illustrated in Figure 4.5. The most common condition involves a full range of penetration of the ice by the bow profile. This state is equivalent to the simple projected area model, since the full contact area is involved. The bouncing condition is indicated by the zero contact profile. There is no intersection between the curves, and consequently the contact area and corresponding forces are also zero. As the ship rises upward onto the ice along its bow profile, the bow curve may not remain in contact with the bottom boundary at the trailing ice edge. This results in an upper range of contact. Two other states are possible: mid range and lower range contact. These are most likely during the retreating phase of motion, but could also be associated with bouncing.

At each time-step a new set of bow profile coordinates is derived according to the kinematic algorithms. Figure 4.6 shows the formation of the ordinates of these points. Successive intersections of the displaced bow curve and vertical planes are obtained for equi-spaced abscissa values along the ice surface. The ice profile curve is defined with respect to an absolute frame of reference with its origin on the waterline at the ice face. In contrast, positions on the ship are referred to a ship-fixed origin located at the ship's centre of gravity. Coordinate transformations are given in terms of the surge, heave and pitch.

FIGURE 4.5 UPDATING ICE_ NOTCH PROFILE

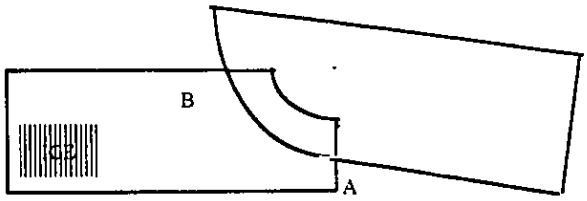

1. FULL CONTACT PROFILE

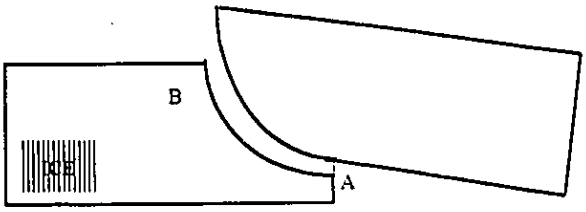

2. ZERO CONTACT PROFILE

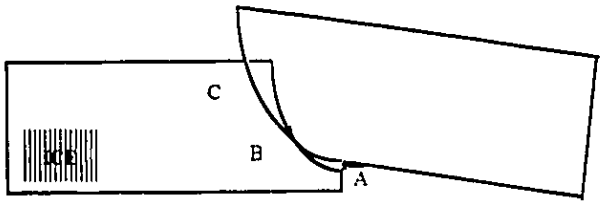

3. UPPER RANGE CONTACT

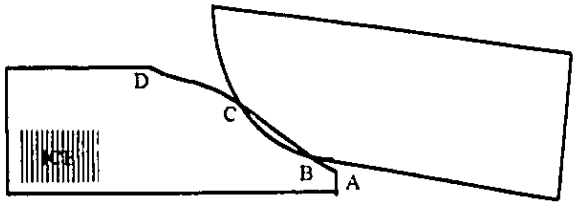

4. MID RANGE CONTACT

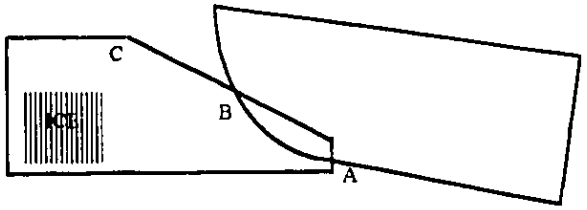

5. LOWER RANGE CONTACT

The intersection points on the ship, that are nearest to the forward and trailing ends, define the effective boundaries of ice contact. These coordinates are used to calculate the projected areas of the contact surface, which give the vector ice force components according to equation (4.1). It should be noted that the three dimensional Ice Interaction Model discussed in the next section does not use this effective area.

The bow profile curve is transformed into the absolute frame of reference, and its intersection points with the existing ice curve are determined. The ice profile is subsequently updated by means of the bow profile. This assumes that the set of intersection points is not empty, and that a further encroachment into the ice body has occurred. This merging involves a linear interpolation process since the curves generally are defined over different intervals. The new ice curve is stored for use in the next time-step.

FIGURE 4.6 DEFINING BOW PROFILE INTERSECTION POINTS

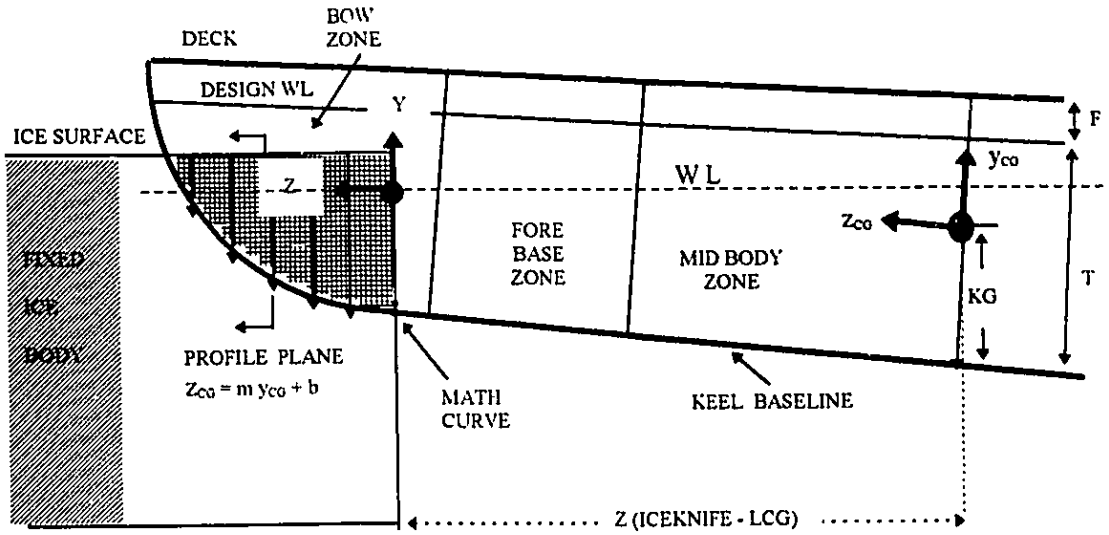

ABSOLUTE TO SHIPFIXED COORDINATE TRANSFORMATIONS

$$x_{CG} = X$$
$$y_{CG} = -(Z + \Delta Z)\sin\theta + (Y + \Delta Y)\cos\theta$$
$$z_{CG} = (Z + \Delta Z)\sin\theta + (Y + \Delta Y)\cos\theta$$

SHIPFIXED TO ABSOLUTE COORDINATE TRANSFORMATIONS

$$X = x_{CG}$$
$$Y = y_{CG}\cos\theta + z_{CG}\sin\theta - \Delta Y$$
$$Z = -y_{CG}\sin\theta + z_{CG}\cos\theta - \Delta Z$$

WHERE

ΔY = T - (KG + HEAVE)

ΔZ = Z (ICE EDGE - LCG) - SURGE

θ = PITCH

4.4 Ice Model Stage 3 - 3-D Icemesh Interface

The conceptualization of the full Ice Interaction Model involves two fundamental advances on the Dynamic Profile Contact Area method. The kinematic description of the interface is extended to three dimensions by algorithms which correlate the displacements of two control surfaces. One is comprised of triangular elements on the ship surface; the other is an ice mesh defining the maximum boundary of the volume excavated by the ship's penetration into the ice body. The second major change is the abandonment of the concept of projected area. It is replaced with the idea of a distributed interaction zone. Crushing is retained as one of several physical mechanism which may occur. In the previous method, only crushing and frictional forces were defined over the effective contact area. Anything outside of the intersection zone was ignored. In contrast, all of the volume between the two control surfaces contributes to the development of interaction forces in the three dimensional method.

Figure 4.7 shows the principal components of the ITHACA_SHIP Ice Interaction Model. Its main components can be roughly divided along two main paths. One sequence of program modules is primarily concerned with the kinematic control of the advancing ice interface. The second path is concerned with determining the ice interaction forces and energies. It contains algorithms for forming an instantaneous triangular element grid on the ship surface; calculating relative displacements and motions of the grid

elements with respect to the icemesh surface; and defining different interaction mechanisms.

The kinematic definition of displacements of curves in the ship centerline plane follow exactly the same procedures as have been described for the two dimensional case. This includes the development of the new bow profile and its transformation into absolute coordinate frame of reference; and the updating of the corresponding ice notch profile. In the three dimensional case, the profile intersection process is strictly for expanding the ice mesh, rather than for defining an effective contact zone.

The introduction of a triangular element grid is a key link in the development of the icemesh interface methodology. It is reconstructed at each time-step; spanning the portion of the hull surface immersed in the ice body. Figure 4.8a illustrates the basic characteristics of the grid. It is formed in the ship-fixed frame of reference. The leading point of the grid is given by the intersection of the undisturbed ice surface and oriented bow profile. The ice freeboard above the water is assigned by the user. The trailing edge is the corresponding intersection point at the ice edge. Because of pitch motions, the top line of the grid will be offset slightly from the actual ice zone. This is considered an insignificant discrepancy.

FIGURE 4.7 3-D ICEMESH INTERFACE

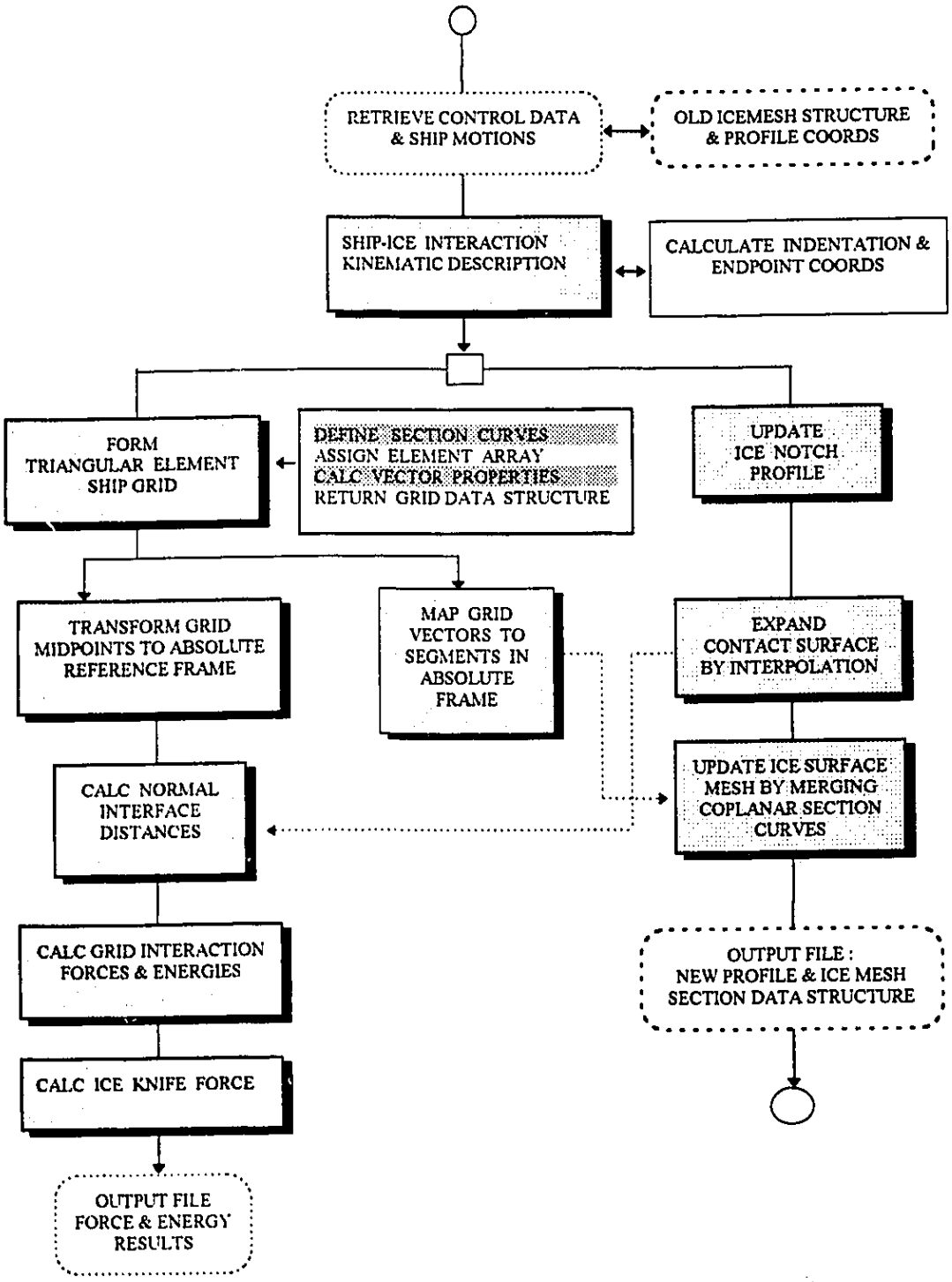

FIGURE 4.8 TRANSFORMING SHIP GRID

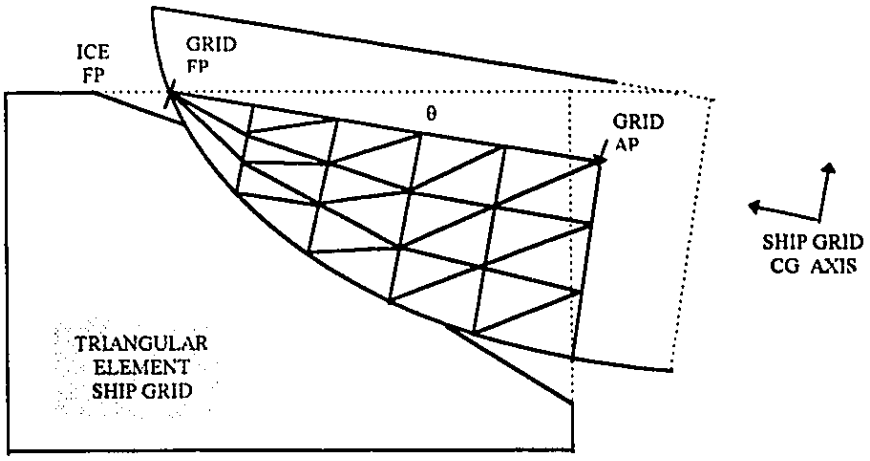

A. INSTANTANEOUS GRID ON INDENTED SURFACE OF SHIP

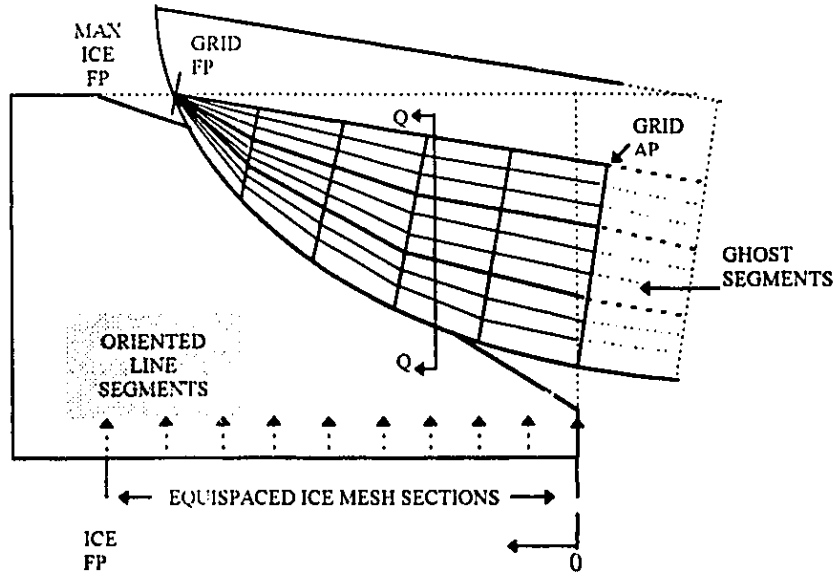

B. ORIENTED LINE SEGMENTS IN ABSOLUTE REFERENCE FRAME

The basic building blocks for the grid are coordinates located at equi-spaced sections between the leading point (or Grid FP) and trailing edge (or Grid AP) of the ice zone. These sections must be reconstituted at each instant by a process analogous to that in the Hull Design Model. Sets of row ordinates for each column coordinate are developed from the section curves by taking abscissa at equal intervals outward from the centerline to the maximum lateral value. The coordinates are systematically connected to form a set of triangular elements. An advantage of using triangular elements to discretize a three dimensional surface is that their vertices are coplanar. This greatly simplifies many of the vector properties. The grid depicted in Figure 4.8a is relatively coarse, having only 27 elements. The configuration most commonly used was a medium scale grid with 135 elements. Finer scaling only increases the computational effort and memory requirements without causing any significant change. The vector properties of each element are computed and assigned to an array for later use in calculating interaction forces. These include: element areas, midpoint coordinates, normal and tangential velocities, and corresponding unit vectors.

The process of expanding the ice interface is not trivial, since the grid and ice surfaces do not share a common frame of references, nor a common section spacing. The kinematic algorithms map both surfaces onto a common set of transverse planes in the absolute frame of reference. The old ice mesh data structure is first interpolated to form a modified set of ice sections along the ice profile curve between the Ice FP and the ice edge. It should be noted that the Ice FP and Grid FP will not be coincident, except for full

profile or upper range types of contact. In addition, the number of ice sections is greater than bow sections so that numerical precision in the interpolations in more readily maintained.

The mapping of the ship grid onto the same vertical planes as the ice mesh is accomplished in two steps. The vertices of the ship grid are first transformed into an array of line segments as illustrated in Figure 4.8b. An interpolation process is used to insert additional segments between the existing rows, to increase accuracy. The segments are then transformed from ship-fixed coordinates into the absolute reference frame. This permits extraction of vertical pseudo-grid curves by systematically searching the line segment array and determining the sets of intersection points corresponding to each of the icemesh planes. One additional set of ghost segments is tracked outside the ice zone, thereby circumventing problems when the pitch is negative.

Figure 4.9 shows the intersection and merging of a new, coplanar grid section and a modified, old ice section. Both have been interpolated to the new ice profile locations. It can be observed that the process for each section is analogous to the updating of the ice profile. A further parallel is found in the five possible types of ice mesh intersections that are illustrated in Figure 4.10. These consist of full range, zero range, upper range, middle range, and lower range interactions. The latter two types are only likely to occur during retreating motions. The updated data structure containing ice section records and the corresponding ice profile are stored for use in the next time-step.

FIGURE 4.9 EXPANDING ICE MESH SECTIONS

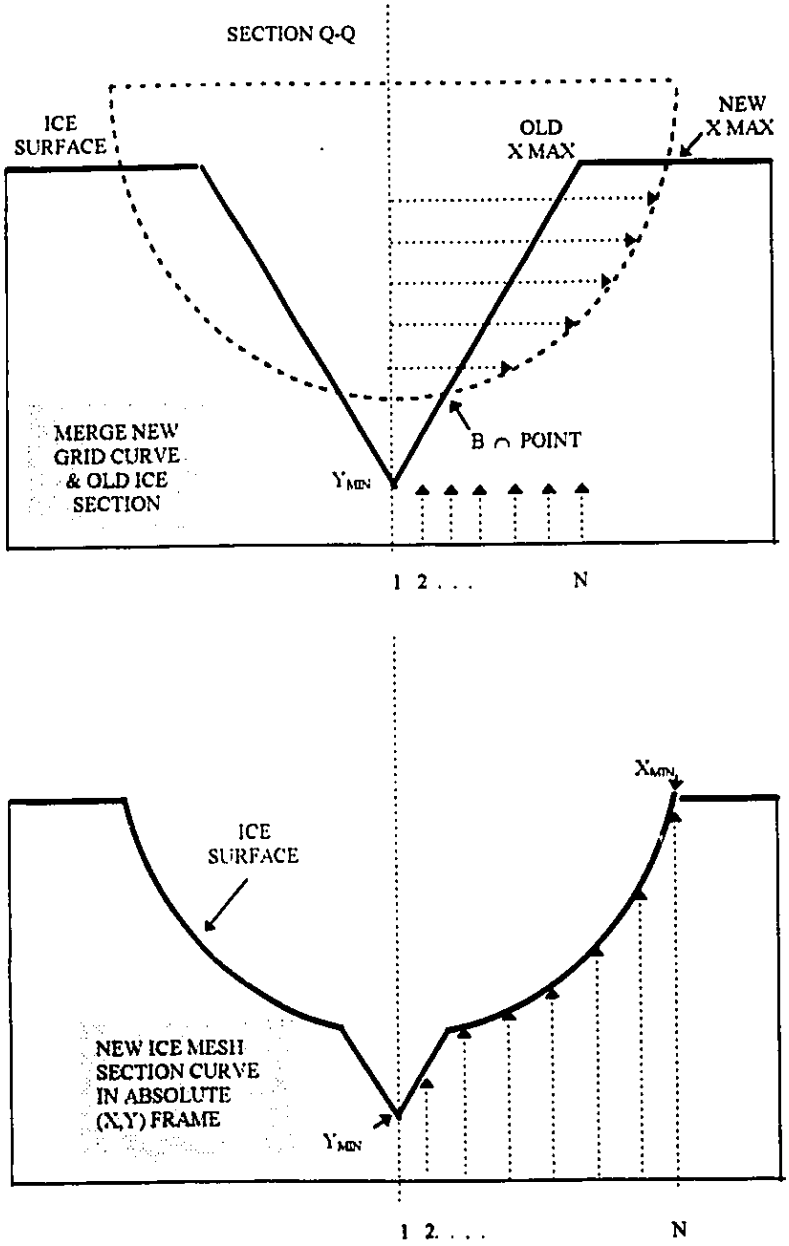

FIGURE 4.10 TYPES OF ICEMESH INTERSECTIONS

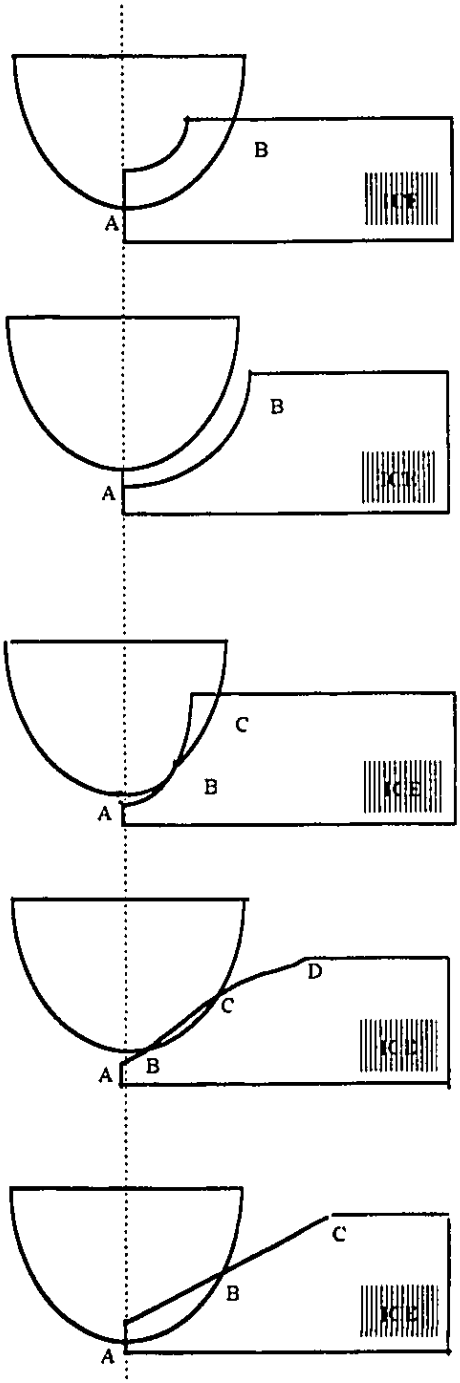

1. FULL RANGE INTERSECTION

PRIMARY FORCE MECHANISMS : CRUSHING AND FRICTION - PLUS EXTRUSION

2. ZERO RANGE INTERSECTION

SECONDARY MECHANISMS ONLY: FLUIDIZATION OR SUCTION

3. UPPER RANGE INTERSECTION

MIXED PRIMARY AND SECONDARY FORCE MECHANISMS

4. MID RANGE INTERSECTION

MIXED PRIMARY AND SECONDARY FORCE MECHANISMS

5. LOWER RANGE INTERSECTION

MIXED PRIMARY AND SECONDARY MECHANISMS

Generally speaking, the grid elements in a region where the ice interface is governed by a full range intersection will experience the primary interaction forces: crushing and friction. An extrusion force is also developed. For the zero range case, the only possible mechanisms are fluid pulverization or suction; depending on the sign of the normal velocity. The other types will be subject to mixture of primary and secondary force interactions.

The actual determination of the grid element interaction forces depends on the normal distance across the interface. A positive distance between the ship surface and ice mesh surface (from the previous time-step) means that no contact has occurred. In contrast, a negative distance implies that normal penetration of the ice surface by the element has occurred. The present model does not change the nominal crushing strength to account for gradations of the penetration state. Investigating strain rate behaviour on the basis of the local normal velocity would be a logical future research project. However, the secondary visco-elastic interaction effects (discussed in the next section) are dependent on normal velocities and relative displacements.

The process of computing the normal interface distances is shown in Figure 4.11. The first step involves transforming the midpoint coordinates of the triangular element grid into the absolute reference frame. A bracketing technique is then applied consecutively to the set of transformed midpoints. This extracts a pair of ice mesh sections and projects interpolated values onto a curve in the vertical plane defined by the element midpoint. The lateral and vertical intersection distances to the ice mesh curve are then

found. The perpendicular distance in this plane can then be easily determined. A similar process is followed in the ice surface plane, again giving a perpendicular distance. The normal interface distance is defined by the perpendicular from the midpoint to the line segment between the coordinates of the planar perpendiculars. It should be noted that the normal distance does not generally coincide with the unit normal vector for the element.

4.5 Modeling Interaction Forces

In an elasto-plastic or visco-elastic model, the averaged contact pressure exerted on an element of the hull surface would be determined on the basis of an analysis of three dimensional flow in the contact zone. This leads to a relaxed or nominal contact pressure as compared to the uniaxial compressive strength of the underlying, undisturbed ice body. Kheysin's (1966) model considered the contribution of viscous and inertial components to the contact pressure. In that analysis extrusion was represented by squeezing an incompressible material between two plates. The mathematical treatment involved using conservation of momentum and Reynold's equation for a thin layer. The latter expression:

$$\frac{\partial^2 v_x}{\partial y^2} = \frac{1}{\mu}\frac{\partial p}{\partial x} + \frac{\rho}{\mu} W_{cp} \qquad ; \; \frac{\partial p}{\partial y} = 0 \tag{4.4a}$$

introduces an average acceleration component, W_{cp}, which is given in terms of the thickness of the interface layer, ε, by an integral relationship:

$$W_{cp} = \frac{1}{\varepsilon}\int_0^{\varepsilon}\left(v_x \frac{\partial v_x}{\partial x} + v_y \frac{\partial v_y}{\partial y}\right)dy \tag{4.4b}$$

FIGURE 4.11 DEFINING NORMAL INTERACTION DISTANCES

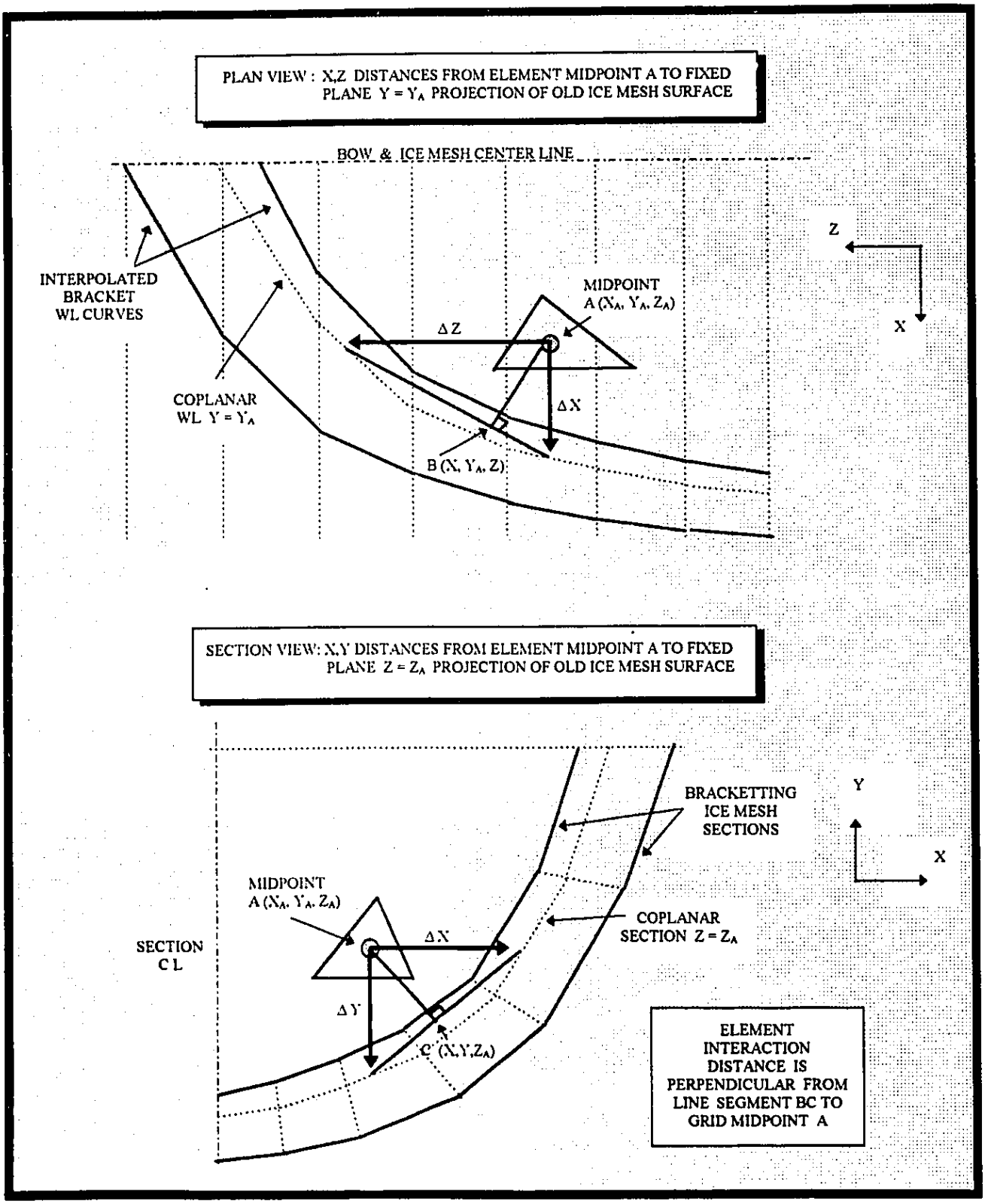

A relationship is determined for the distribution of the contact pressure in terms of location and normal velocity. This takes the general form:

$$p(y) = k(\varepsilon)\, v_n \left(\frac{c^2}{4} - y^2 \right) \tag{4.5}$$

where the coefficient, k(ε) exhibits an inverse cubed dependence on the interface depth. The squared coefficient, c, accounts for the geometry and dimensions of the indentor. For the thin layer approximation, the inertial terms are quadratic in the interface depth, and are neglected. Nevertheless, it was predicted that the liquid lubrication effect alone would reduce the contact pressure by a factor of four. In subsequent papers, a number of minor modifications were introduced which changed the precise exponents on various factors and permitted an analytic solution for certain simple shapes. But in practice, the application of the theory remained dependent on a determination of experimental coefficients.

Kheysin et al (1973) verified the elastoplastic modeling assumptions by comparing the analytical predictions to experimental findings (reported by Liknomanov and Kheysin, 1971) from drop tests of a hemispherical steel body. These tests also showed a direct proportionality between a nominal contact pressure and specific breakup energy. In this instance, the nominal pressure was the maximum pressure during the interaction, averaged over the contact area. The specific breakup energy was defined as the ratio of the impacting kinetic energy to the total crushed volume.

The development of more general models based on these theoretical formulations has been hampered by concern about scale effects. The empirical coefficients derived from small scale testing have not been accepted as representing the properties of the contact zone for prototype ship collisions. The ice interaction forces included in the present model are shown in Table 4.1 listed in order of their expected relative magnitudes. A number of simplifications have been introduced, in lieu of applying a full elastoplastic analysis. In particular, the contributions to the contact pressure from areas of direct contact are divided into a mean component and secondary variations. In compensation, the model has been extended to consider non-contact interaction effects.

4.5.1 Crushing Force Mechanism

The crushing interaction is considered the primary force mechanism. Its occurrence is limited to the direct contact region of the interaction interface; that is to those grid elements which have penetrated into the ice surface. While closely related to the compressive strength, this force should not be interpreted simply as an elastic reaction. Rather, the crushing strength is an empirical parameter; representing the nominal contact pressure associated with all elasto-plastic phenomena. It was defined by calibrating the numerical model such that simulated indentations corresponded with measured *MV Arctic* indentations at a 4 knot collision speed. This was equivalent to the method used to define the physical model ice strength. The nominal strength was found to be approximately one-third that of the uniaxial compressive strength of the underlying, elastic ice body.

TABLE 4.1

ICE INTERACTION MECHANISMS

ICE INTERACTION MECHANISMS			
MECHANISM	**TYPE**	**APPLICATION AREA**	**DESCRIPTION**
CRUSHING	ELASTIC	GRID ELEMENTS	EMPIRICAL MEAN CONTACT PRESSURE BASED ON COMPRESSIVE STRENGTH
FRICTION	SHEAR	GRID ELEMENTS	FRICTION FORCE COMPONENTS PROPORTIONAL TO NORMAL CRUSHING FORCE
EXTRUSION 1	PLASTIC	CIRCULAR REGION EQUIVALENT TO TOTAL CONTACT AREA	MOMENTUM CONTRIBUTION TO CONTACT FORCE
EXTRUSION 2	VISCOUS	CIRCULAR REGION EQUIVALENT TO TOTAL CONTACT AREA	VISCOUS ENERGY CONTRIBUTION TO CONTACT FORCE
FLUID EXPULSION	PLASTIC	GRID ELEMENTS	NON-CONTACT MOMENTUM OPPOSING DOWNWARD MOTIONS
FLUID SUCTION	PLASTIC	GRID ELEMENTS	NON-CONTACT MOMENTUM OPPOSING UPWARD MOTIONS

The frictional force components are directly determined from the corresponding crushing forces. A constant frictional coefficient of 0.10 has been adopted. Oksanen (1983) has presented results from a theoretical calculation of this coefficient which indicates somewhat lower values. But their extrapolation into regions of high normal loads is uncertain. The traditional coefficient value has therefore been used. This value is also consistant with measurements for physical model ice materials reported by Howard et al (1989).

4.5.2 Contact Extrusion Mechanisms

The viscous and inertial contributions to the contact force are calculated independently and added to the mean crushing component. The individual contribution from each grid element is not considered separately. Rather, an equivalent circular control volume is constructed by a summation of the individual elements which are within the direct contact region. The total surface area, A_s, and volume, V, are preserved. The average penetration distance gives the characteristic depth of the region. For the purpose of analysis the control volume is treated as if it was flat cylinder. It is further assumed that the velocity profile is uniform at all points originating on its surface.

The inertia component can be approximated by impulse theory. The rate of momentum transfer outward from the periphery of the region is related to the impulse according to Newton's law as:

$$F\Delta t = \Delta m v_{mean} \tag{4.6}$$

The mean radial velocity remains a constant at all radial distances outward from the centre. It is uniquely defined by the total volume, V, which must be extruded through the circumferential area, A_{cir} during a time-step. In determining the mass of the volume of ice extruded, the density is assumed equal to water at zero degrees Celcius. This gives an expression for the inertial contribution to the contact force of the form:

$$F_{Inertia} = \frac{1}{2}\frac{\varepsilon \rho}{\Delta t^2}\frac{A_s^{3/2}}{\pi^{1/2}} \tag{4.7}$$

where the exponent on the total surface area in the direct contact zone, A_s, indicates a gradual confinement effect.

The viscous contribution is also determined using a circular cylinder approximation. In this case the force is determined from the corresponding energy losses due to shear within the volume. The mean radial velocity is again a constant depending on the volume flow rate of extrusion. It is further assumed that the velocity profile along any radial segment exhibits a linear gradient between its base in the undisturbed ice surface and its maximum velocity at the penetrating body. A triangular profile would have given no-slip conditions at the two bounding surfaces; but a skewing of the profile towards the top of the zone seemed to better represent a system in which the effective viscosity might increase with depth. In fact, the extrusion of the crushed ice from the contact interface could possibly be modeled as a non-Newtonian flow. Bratanow and De Grande (1982) have described a formulation for a mush-ice flow considered as a Reiner-Rivlin fluid. In the present case, however, a Newtonian fluid approximation has been made. It is based on the simple shear relationship:

$$\tau = \mu \frac{dv}{dy} \tag{4.8}$$

where μ is the dynamic viscosity, which must be specified by the user. Since there is little experimental data concerning ice zone viscosity, the value for water is provided as a default. For a linear gradient, the shear becomes:

$$\tau = 2\mu \frac{v_{mean}}{\varepsilon} \quad . \tag{4.9}$$

The corresponding energy density over the surface is found by integrating the product of the shear and its corresponding displacement. The latter is taken from the linear velocity profile, such that:

$$\delta E_\tau = \int_0^\varepsilon \tau(y)\, y(x)\, dx \quad \text{for} \quad y(x) = \frac{2v_{mean}\Delta t}{\varepsilon} x \tag{4.10}$$

The total shear energy is found by integrating over the circular area. The viscous force is then obtained by dividing the total energy by the characteristic depth through which the contact area has traveled. This can be expressed:

$$F_{Viscous} = \frac{1}{\varepsilon} \int_{A_s} \delta E_\tau \, dA \tag{4.11}$$

Its solution gives the total viscous force component for the direct contact surface area as:

$$F_{Viscous} = \frac{\mu}{4\pi} \frac{A_s^2}{\varepsilon \Delta t} \tag{4.12}$$

where the squared area term, A_s again indicates possible confinement effects. Because of

the characteristic depth in the denominator, it is necessary to constrain the maximum viscous force to the friction force in the limit as $\varepsilon \rightarrow 0$. The force would be increased by a factor of 2 by introduction of a triangular velocity profile.

4.5.3 Non-contact Interaction Forces

The grid elements which are not in direct contact with the ice surface are treated in a somewhat analogous manner to the contact inertial forces. Except that each of the grid elements of non-contact type is considered separately as an equivalent circular region. The characteristic depth of each circular region is modified to account for the normal distance, ε, of the element to the ice surface and its direction of motion. The impulse-momentum relationship is again applied, giving the non-contact force component for the element as:

$$\delta F_{Non-contact} = \frac{\pm 1}{\left(\varepsilon + |v_n| \Delta t\right)} \left\{ \frac{1}{2} \rho v_n^2 \right\} \left(\frac{A_s}{\pi} \right)^{3/2} \quad . \tag{4.13}$$

A negative sign corresponds to suction effects, and positive to fluid expulsion. The separation distance term in the denominator for the suction case has an minimum absolute value of $v_n \Delta t$. This avoids occurrences of singular behaviour which might be caused if the distance was to approach zero. The total contribution of these two non-contact force is given by a summation over each element type.

4.6 Comparison of Ice Models and Interaction Energies

Figure 4.12 shows qualitatively why it is important for the ice interactions to be defined in terms of a dynamic mapping of the kinematic displacements. It shows a comparison of vertical force time-histories resulting from a series of rigid body motion simulations. A projected area model was first applied, and then a dynamic profile contact area method. Three increasing values of ice strength were tested at a constant impact velocity of 4 knots. These numerical results were derived using only steady-state, i.e. Bernoulli dynamic pressures, rather than the complete hydrodynamic model.

It may be observed that the projected area model produces a force time history which greatly exaggerates the dynamics of the ice crushing process. The overall system responds at about 0.67 Hz in a wetted heave/pitch mode. It is effectively acting as a beam on a spring foundation, with the ice interaction included as an additional, time-varying spring. With increasing ice strength, the dynamic effect becomes progressively larger. It should be remarked that the maximum surge occurs at about 8 seconds; but the same crushing force relationship is applied throughout the following interaction process. In practice, a sliding or slide-off constraint is generally applied to limit the magnitude during this phase of the interaction.

In contrast, the dynamic profile contact model shows a marked decrease in the amount of dynamic content. A damping component has been introduced as a result of the improved kinematic representation. The relative displacement of the hull profile and the underlying ice centerline allows for a non-contact condition during which the force goes to

zero. This condition is associated with rebounding motions, which occur at progressively earlier times as the ice strength is increased.

Figure 4.13 shows corresponding force histories for the three-dimensional Ice Interaction Model. In this case the extraneous dynamic content has been effectively eliminated. The rebounding mechanism is moderated by the kinematic capacity of each triangular grid element to interact individually with the underlying ice surface. This produces a ragged, but continuous curve; rather than a discontinuous bouncing. The magnitude of the initial contact peak is equivalent to that of the other methods, but the force is substantially reduced during the remainder of the interaction period. It will be shown in Chapter 6 that the force history for 1.5 MPa ice is in good agreement with measured *MV Arctic* 1984 Trials data.

A second set of force time-histories is also presented in Figure 4.13, showing the trend at 18 knots. Despite the high impact velocity, the dynamic content remains well damped. In contrast, the simpler methods would fail for this condition. These icemesh force histories exhibit well-defined first dynamic peaks, approaching the maximums reached later. A second peak also becomes more dominant with increased ice strength. The magnitude of peak force for 1.5 MPa ice increases from approximately 13 MN at 4 knots to 80 MN at 18 knots. (Substantially larger peaks for higher ice strengths after 5 seconds are extraneous spikes arising from reduced damping in the simplistic, steady-state hydrodynamic model employed in this test.) Similar magnitudes and dynamic trends are observed in physical model test data. However, it should be cautioned that the rigid body forces should not be compared directly to hydroelastic forces.

The relative magnitudes of the components of the ice interaction force and their corresponding energies are shown in Figure 4.14 and 4.15 respectively. The energy components associated with the interaction forces are determined as an output from the three dimensional ice model. In the case of crushing and friction, the corresponding energies for each grid element are accumulated on the basis of the known displacements at each point. Energies from contact inertial forces are based on a collective approximation to the kinetic energy for the circular region. For non-contact elements the inertial energies are calculated individually. The viscous contact energies were determined as a step in defining the effective viscous force by integrating the shear and displacement over the zone depth.

It can be observed from both the force and energy plots that the crushing is the primary mechanism contributing to the overall contact pressure. Of the secondary force mechanisms, only extrusion gives a measurable component. It attains a value approximating the magnitude of the friction force at the highest impact speeds. At low speeds it is an order of magnitude smaller. The insignificant secondary components are not unexpected, since a viscosity equivalent to water has been assigned to the fluidized material in the interface zone. So these energies are largely experimental at this stage. But the description of the ice interaction process in terms of energy losses will, in Chapter 5, provide a useful measure in quantifying the influence of hydrodynamic phenomena.

FIGURE 4.12
Comparing Ice Modelling Methods

A. Projected Area Model B. Dynamic Contact Profile Model
Steady-State Dynamic Pressure Foundation. mpact Velocity = 4 knots

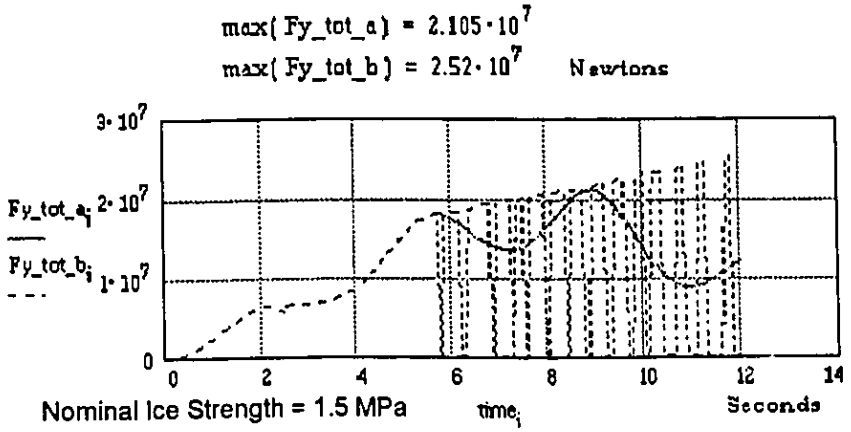

Nominal Ice Strength = 1.5 MPa

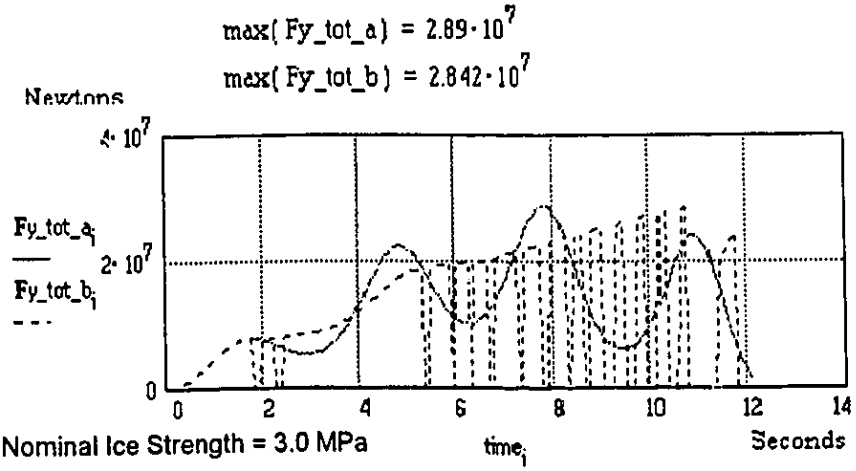

Nominal Ice Strength = 3.0 MPa

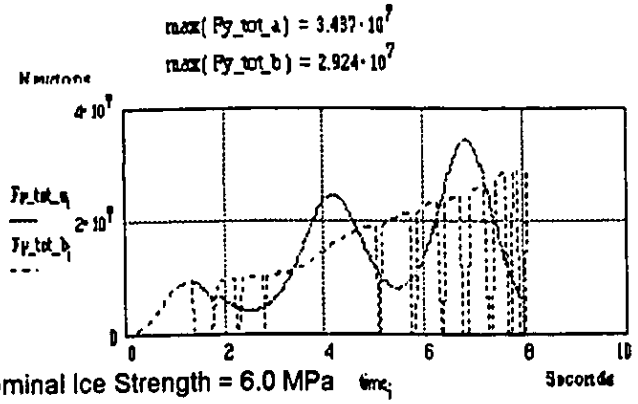

Nominal Ice Strength = 6.0 MPa

FIGURE 4.13
3-D ICEMESH VERTICAL FORCE TIME-HISTORIES

Runs for MV Arctic using Steady-State Dynamic Pressures
and Ice Strengths: #1= 1.5, #2= 3.0 , #3= 6.0 MPa

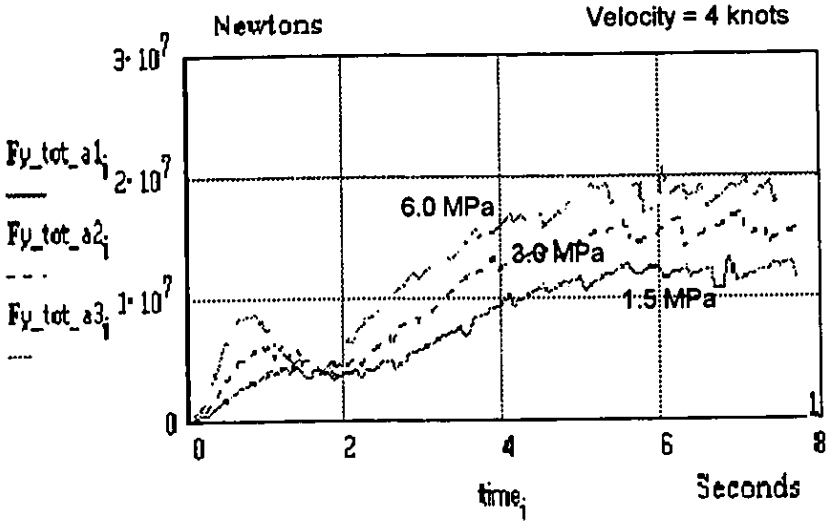

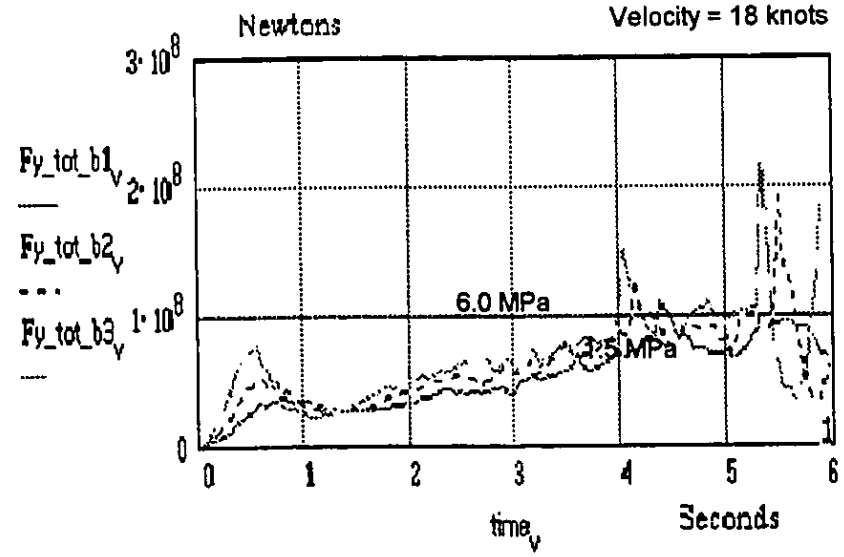

FIGURE 4.14
SAMPLE OF 3-D ICE INTERACTION FORCES

USING 3-D ICEMESH MODEL
Nominal Ice Strength = 1.5 MPa

BEM NUMERICAL WAVETANK MODEL
Primary Interactions : Crushing & Friction
Secondary Effects: Extrusion, Fuidization & Suction
IMPACT SPEED = 18 Knots

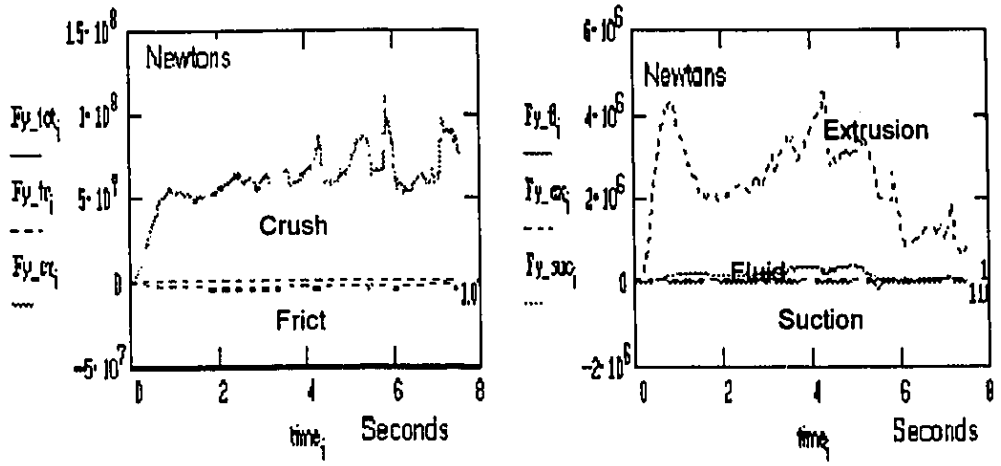

INTERACTION FORCE COMPONENTS for IMPACT SPEED = 4 Knots

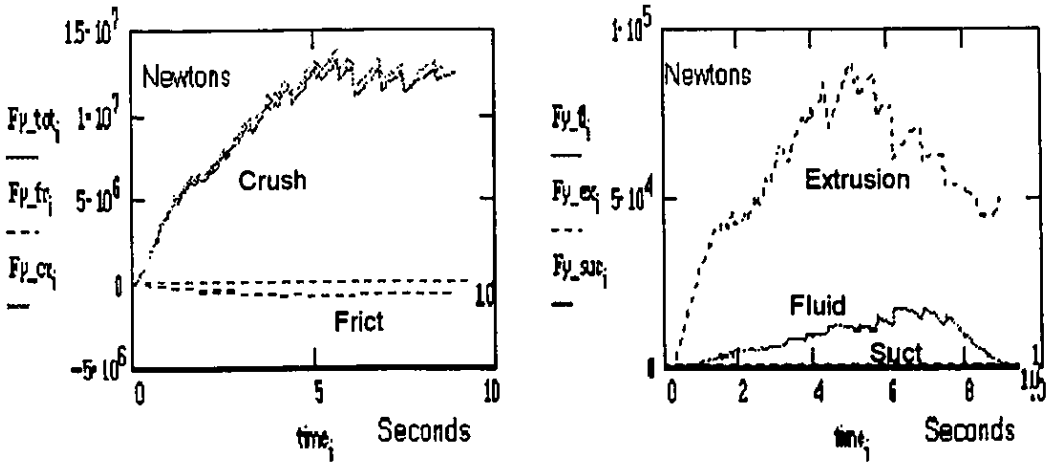

FIGURE 4.15
SAMPLE OF 3-D ICE INTERACTION ENERGIES

USING 3-D ICEMESH MODEL
Nominal Ice Strength = 1.5 MPa

BEM NUMERICAL WAVETANK MODEL
Primary Interactions : Crushing & Friction
Secondary Effects: Extrusion, Fuidization & Suction
Rigid Body IMPACT SPEED = 18 Knots

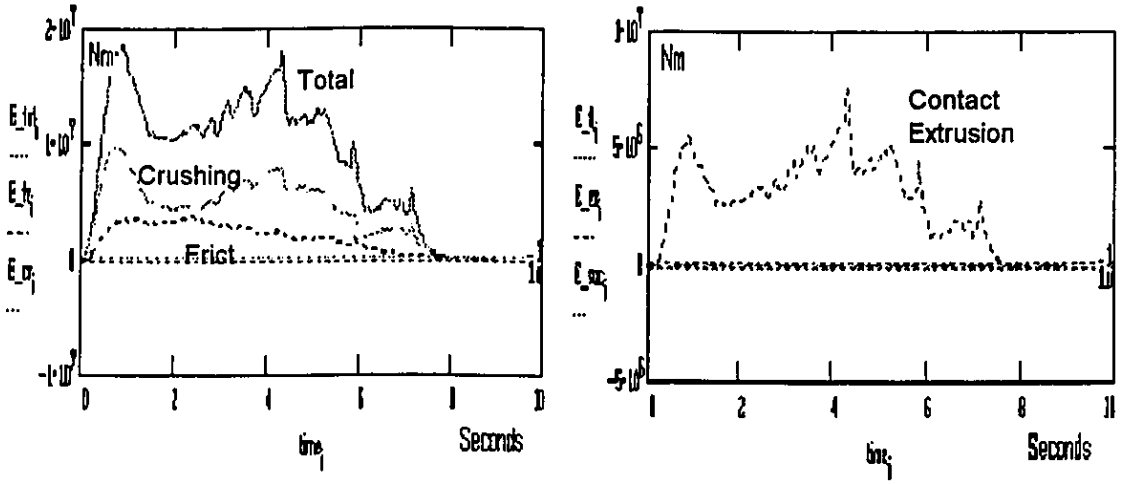

ENERGY COMPONENTS for Rigid Body IMPACT SPEED = 4 Knots

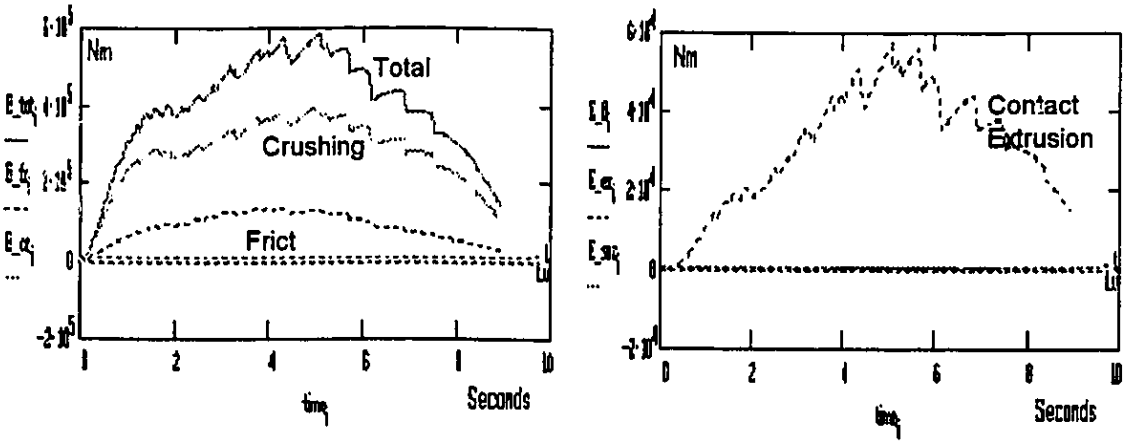

Chapter 5 Modeling Transient Hydrodynamic Forces

Hydrodynamic forces in the ITHACA_SHIP Model are computed by means of a strip representation using a boundary element (or boundary integral equation) method; abbreviated as BEM or BIEM. The present chapter discusses the principal assumptions and theory underlying the application of this approach to calculating time-domain hydrodynamic forces in the transient ship motions problem. The numerical algorithms which have been implemented for this purpose are referred to collectively as the BEM Numerical Wavetank. It defines a set of independent, two-dimensional sectional wavetanks, which are linked through the ship motions program. The method was first tested with a single sectional wavetank configured as a piston wavemaker; and then as a circular cylinder oscillating in forced periodic heave. The setup was then modified to investigate transient motions. Subsequently, the configuration was generalized to a multiple strip representation of three-dimensional hullforms. Specific descriptions are given of characteristic features, such as scaling at individual ship sections and the method of determining the unsteady pressures. Finally, comparative data showing the relative magnitudes of different hydrodynamic components is presented, which demonstrates the importance of modeling the transient effects.

5.1 Unsteady Hydrodynamic Phenomena

It could be said that the modern mathematical treatment of hydrodynamics originates from Stokes' Fundamental Theorem of multivariate calculus. Spivak (1965) describes the first statement of Stokes' Theorem in 1950 as appearing in a postscript to a letter between Lord Kelvin (Sir William Thompson) and Stokes. In its most general form, Stoke's Theorem encompasses both the Divergence Theorem and several variants of Green's Theorem as corollaries. In mathematical physics these theorems initially found application in the treatment of elastostatics, electromagnetism and gravitational theory where it defined the flow of an invisible aether. It could be shown that the mass of a body moving through the aether was increased by the presence of the field. In hydrodynamics this led to the concept of added mass.

The basic assumptions of classical hydrodynamics are those which are consistent with representing a fluid as a potential field. It is assumed to be inviscid, isotropic, homogeneous, incompressible and irrotational. This leads to a general form of differential equation known in potential theory as Laplace's equation. Its non-equilibrium counterpart is Poisson's equation. A systematic treatment of problems governed by Laplace's equation is given by Kellogg (1953). So central is the role played in hydrodynamics by the Stokes' Theorem corollaries, that many problems are identified collectively as Green's Function formulations. Their solutions generally make use of methods from the theory of integral equations, developed by Volterra and Fredholm. A monograph by Tricomi (1985) describes many of these methods.

Figure 5.1 illustrates the complexity of fluid phenomena for the steady state motions of a ship approaching an ice floe. After impact occurs, the fluid representation becomes yet more complicated. The steady state flow is characterized by a free surface wave along the ship's centerline profile and a wake behind the stern. The wave pattern shown depicts the classical results of a Thin Ship solution of Michell's Theory. Wehausen and Laitone (1960) have documented the mathematical methods for solving a ship's steady state wavemaking resistance, and for formulating the initial value problem. Early theoretical treatments of the transient flow problem were given by Finkelstein (1957),. Cummins (1962) and Wehausen (1967) using time dependent Green's functions. Following this tradition, Wang (1986) and Korsmeyer (1988) have developed methods based on second order, transient velocity potentials.

Numerical solutions of wave radiation problems have generally avoided the complexity of time-dependent Green's function representation. Longuet-Higgins and Cokelet (1976) introduced a Lagrangian formulation, which was solved by a boundary method transformed into complex domain. This boundary integral approach was computationally more effective than finite difference or finite element methods, since it has one less dimension than grid methods. A number of researchers have implemented variants of this numerical approach, but using boundary element methods. Lau (1985), Chan (1987), Cointe (1989) and Sen et al (1989) have provided the immediate background for the present work. In general, these authors have differed in only inessential ways, except for their treatment of the motion of particles on the free surface boundary.

Seakeeping analysis provided many of the mathematical and numerical techniques that have been adapted to transient motions problems. The practical solution of ship motion problems in seakeeping has for many years depended on strip theory methods. These theories generally use added mass and damping coefficients which have been extracted from a numerical solution of the integral equations. Newman (1977) describes mathematical transformations of a ship's sectional shape to determine its added mass and damping. This representation is commonly referred to as a Lewis transformation, in deference to Lewis' (1929) introduction of techniques for mapping arbitrary section shapes into equivalent circular cylinders. It was, however, Ursell (1949,1953) who developed techniques for representing the velocity potential of a periodically heaving cylinder as the sum of an infinite set of multipoles. A number of variations on this approach have since emerged. For example, Gerritsma and Beukelman (1968) used an eleven parameter expansion. Frank and Salvesen (1970) based their strip theory on the Frank Close-fit Method (Frank, 1967), which directly represents an arbitrary hull section by a distribution of sources.

FIGURE 5.1 WAVE PATTERN OF SHIP

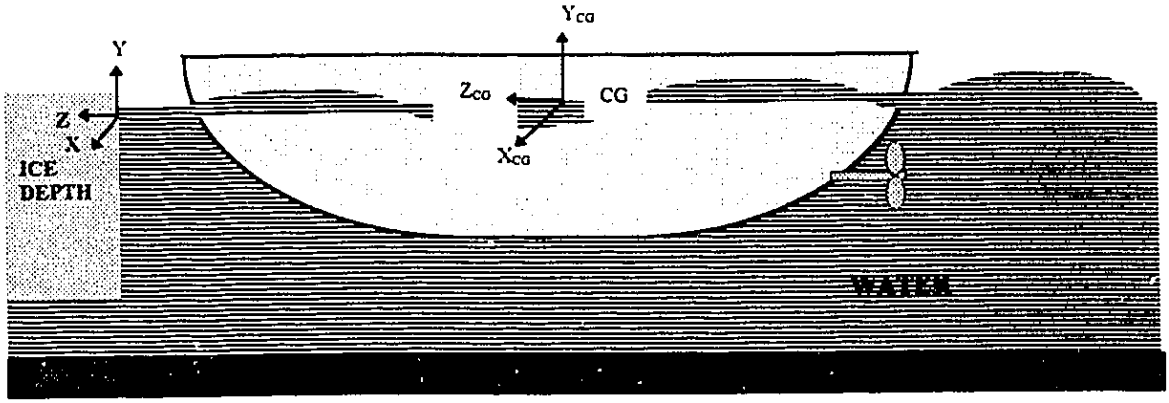

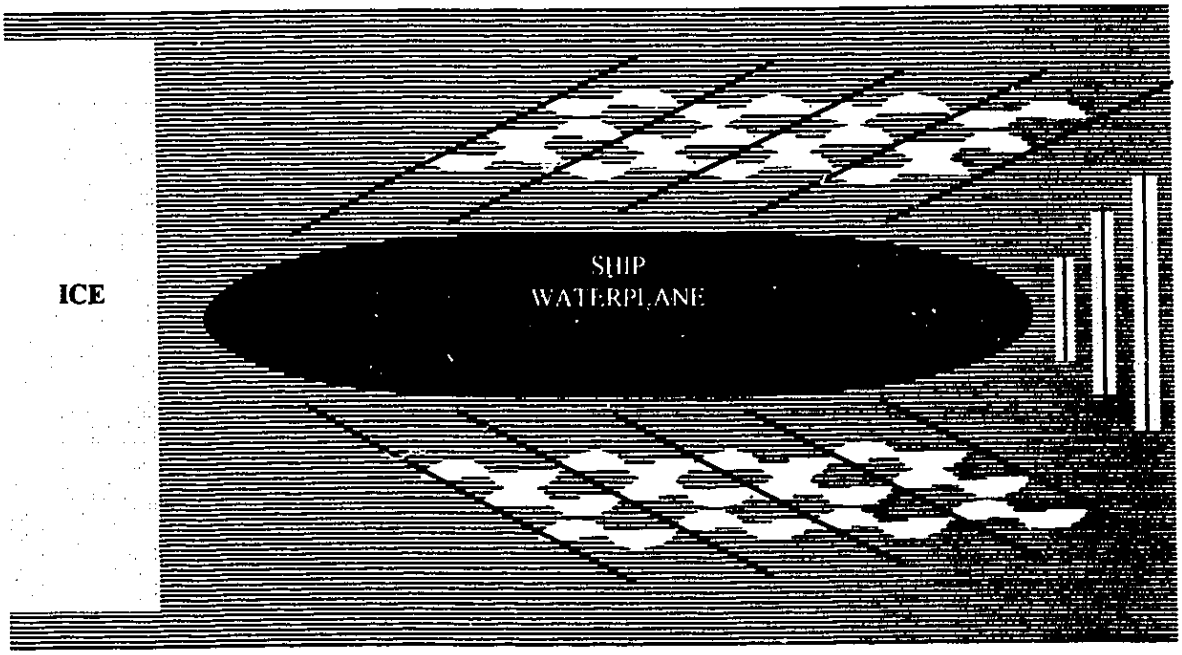

Betts et al (1977) departed from traditional strip methods by formulating equations of motion with the hydrodynamic coefficients expressed as a generalized force in the Lagrangian sense. The fluid force density at a section was derived from an expression given by Gerritsma and Beukelman (1964) for pitching and heaving of ships in still water. The force corresponding to a relative displacement, Y(x,t), was expressed in terms of the local section breadth, B(x), added mass, m(x), and damping N(x). This had the form:

$$F(z,t) = -\left\{ \frac{D}{Dt}\left[m(z) + \frac{i}{\omega_e} N(x) \right] \frac{DY(z,t)}{Dt} + \rho g B(z) Y(z,t) \right\} \qquad (5.1)$$

where ω_e is the radian frequency of wave encounter. A total or material derivative is assumed. Betts later added a frequency dependence to the hydrodynamic coefficients in this equation.

Figure 5.2 shows the strip representation for transient fluid forces, as implemented in the ITHACA_SHIP Hydrodynamic Model. It emulates the reasoning of Betts' generalized fluid force approach, but introduces time-domain solutions from the BEM Numerical Wavetank in place of frequency based hydrodynamic coefficients. The influence of the initial wave pattern is ignored in determining the collision forces and a flat waterline is assumed. This simplification was justified by experimental measurements (Phillips and Daley, 1986) showing that rapid stopping of a flexible MV Arctic model did not introduce observable levels of bending stress. It should be noted that only the hydrostatic component of the section hydrodynamic force is corrected for pitch angle.

FIGURE 5.2 BEM STRIP REPRESENTATION OF HYDRODYNAMIC FORCE

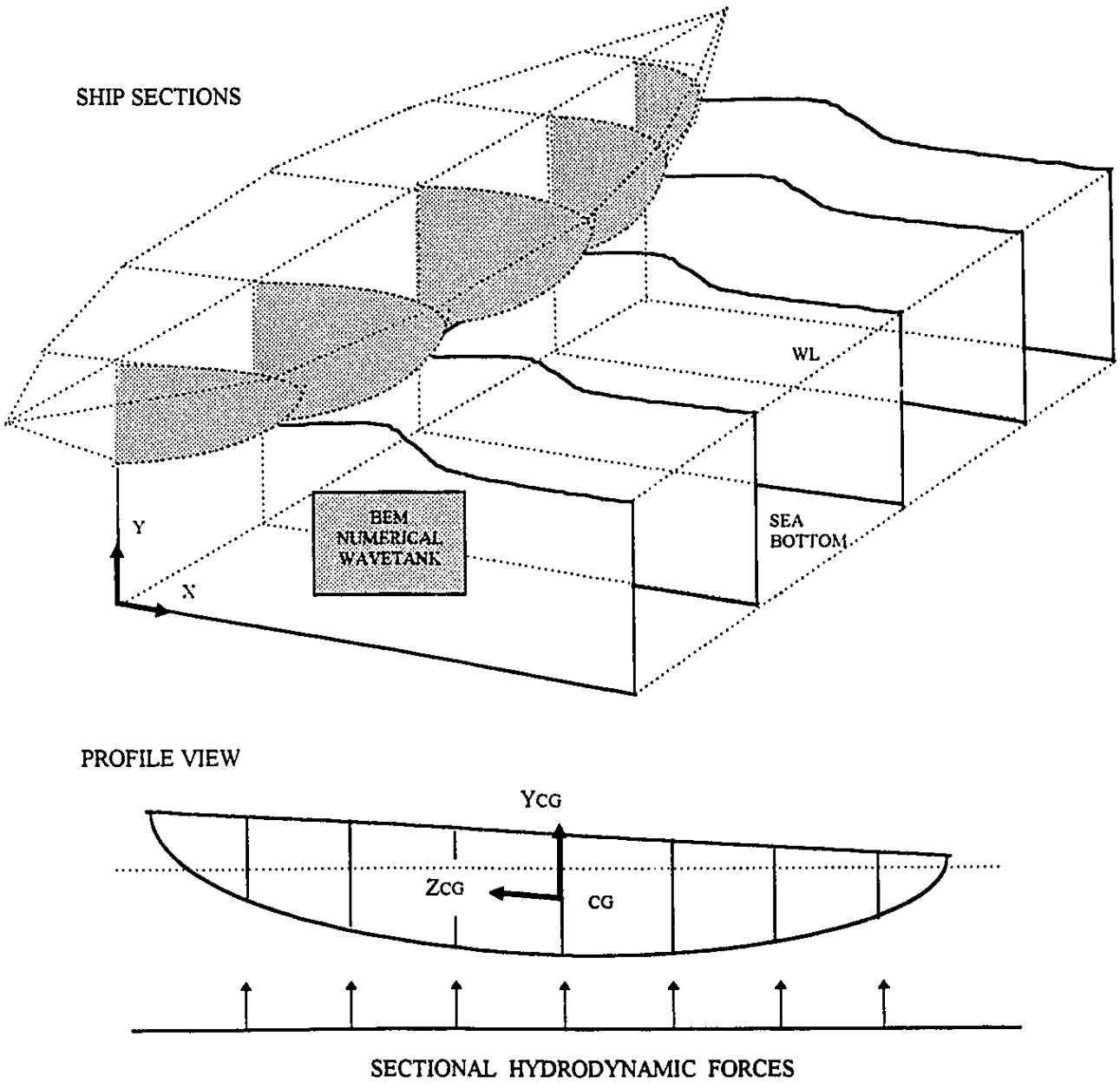

5.2 Mathematical Formulation

Wehausen and Laitone (1962) give a detailed development of the unsteady motions problem for a ship floating on an inviscid, incompressible and irrotational fluid. It is formulated in terms of Laplace's equation and requires six exact boundary conditions in its most general form. Following Longuet-Higgin and Cokelet's (1976) treatment of the two-dimensional wave flow, the problem can be somewhat reduced . In indicial notation the Laplace equation can be written:

$$\phi_{,ii} = \nabla^2 \phi = 0 \tag{5.2}$$

Its first boundary condition is a dynamic constraint existing on the hull surface:

$$\frac{p}{\rho} = c\phi_{,z} - \frac{1}{2}(\nabla^2 \phi) - gy \tag{5.3}$$

assuming a reference system where z gives displacements along the direction of motion, and y is vertical with respect to the waterline. There is a corresponding hull kinematic condition:

$$\phi_{,n} = \vec{v} \bullet \vec{n} = 0 \tag{5.4}$$

which ensures that no fluid can move normally across its impermeable boundary. The finite depth condition and the downstream wall condition also represent impermeable boundaries; and so must satisfy equation (5.4). The vertical plane directly below the keel is equivalent to a rigid boundary since it is a plane of symmetry. On the free surface, the

kinematic condition is expressed in a Lagrangian form (in the sense of following fluid particles) as:

$$\frac{Dx}{Dt} = \phi_{,x} \ , \ \frac{Dy}{Dt} = \phi_{,y} \tag{5.5a}$$

where the material or total derivative is:

$$\frac{D}{Dt} = \frac{\partial}{\partial t} + \nabla\phi \bullet \nabla \tag{5.5b}$$

In addition, there is a dynamic free surface condition corresponding to Bernoulli's equation which is given by:

$$\frac{D\phi}{Dt} = -p_s - gy + \frac{1}{2}\left(\nabla^2\phi\right) \tag{5.6}$$

where p_s is the applied pressure, which can generally be set to zero. Following Chan (1987), the separate kinematic and dynamic free surface conditions are recast into a combined form as:

$$\frac{D^2\phi}{Dt^2} - \frac{1}{2}\frac{D}{Dt}\left(\nabla^2\phi\right) + g\phi_{,y} = 0 \ \ at \ y = \eta \tag{5.7}$$

which must be satisfied on the surface profile, η. Subsequently Chan extracted the vertical velocity from the dot product of the gradient and the unit normal components on the free surface. This rearrangement gives the free surface condition:

$$\phi_{,n} = \phi_{,x} n_x + \frac{1}{g}\left(\frac{1}{2}\frac{D}{Dt}\left(\nabla^2\phi\right) - \frac{D^2\phi}{Dt^2}\right) n_y \tag{5.8}$$

which is well suited to a BEM treatment, since it expresses the normal velocity in terms of

the velocity potential. At this juncture, Chan effects a solution by introducing a finite difference approximation for the quadratic material derivative term of the form:

$$\frac{D^2\phi}{Dt^2} = \frac{2\phi^0 - 5\phi^{-1} + 4\phi^{-2} - \phi^{-3}}{\Delta t^2} \tag{5.9}$$

This leads to a nonlinear (or alternatively a linearized) expression with both the potential and normal velocity as unknowns. But the relationship between them is specified in terms of the potentials at three previous time-steps, denoted by use of negative integer superscripts.

The present method solves explicitly for the potential. In the linearized case, the Bernoulli equation (5.6) is recast in terms of a material derivative, giving:

$$\frac{D\phi}{Dt} = -g\eta - \frac{1}{2}(\nabla^2\phi) \tag{5.10}$$

which is then directly integrated by a 4th order Runge-Kutta technique to give the potential. The final potential at an element midpoint is a linear combination of the results of the four mini-steps, according to the relationship:

$$\phi_{new} = \phi_1 + 2\phi_2 + [2\phi_3 + \phi_4]/6 \tag{5.11}$$

For nonlinear motions, a finite difference scheme similar to Chan's is introduced; but a mixed BEM formulation is not used. The unknown ϕ^0 values are directly extrapolated at the predicted new midpoint coordinates. The Runge-Kutta technique is again employed.

5.3 Boundary Integral Equation Methods

The general problem in potential theory involves solving Laplace's equation or Poisson's equation subject to given boundary conditions. A Dirichlet condition prescribes the potential at points on the boundary. In the case of a Neumann condition, the normal velocity is specified. Alternatively, a mixed formulation prescribing the relationship between the potential and normal velocity can be imposed.

Standard treatments of boundary element theory are readily available, so only a brief description of its salient features will be included. The present approach is directly based on the methodology and kernel algorithms reported by Tan (1987). He describes two essential steps in the solution of the BEM problem. A simple principal solution is first found. Then, a reciprocal relationship is introduced which expresses the potential and normal velocities (or tractions) at any two arbitrary points on the boundary. This mathematical transformation is similar to theoretical Green's function methods in its use of Green's theorem identities; and in the integral form of the resulting equations.

In the BEM Numerical Wavetank model, the boundary is discretized into a finite number of segments. Zeroth order or constant elements are used, on which the potential takes the same value over a segment as at its midpoint. Lau (1985) and Sen et al (1989) have discussed the advantages and disadvantages of employing higher order elements. But the use of simpler elements avoids possible problems with discontinuities at the

Figure 5.3 illustrates the subdivision of the exterior boundary of the fluid domain into five regions, which vary with the instantaneous motions of the solid body and radiated waves. The sizing of element segments has been selected to minimize the total number of elements, and therefore the computational effort. It should be observed that the problem size increases as the square of the number of elements, since the Green's integral contribution of each element with respect to all others must be determined. In the present case, this consideration sets an upper limit of approximately 80 for the maximum number of elements. The majority of elements are distributed over the free surface and the body contour. A smaller number are assigned to the centreplane, bottom and wall boundaries.

5.4 Free Surface Multiple Path Regridding Concept

From physical considerations it is evident that a minimum of four points per wave period are required to preserve the frequency content of waves formed on the nonlinear free surface. This limitation is recognized by assigning a gradual increase in element size with distance away from the body. The condensing of points close to the body gives a more accurate representation of the formation of the transient waves. The larger segment sizes farther away introduce an effective damping and dispersion of the waves. The downstream boundary is prescribed as an impermeable wall, rather than a radiation condition; since wave reflection is not generally a significant consideration in transient problems.

FIGURE 5.3 BEM NUMERICAL WAVETANK ELEMENTS

LINEAR FREE SURFACE

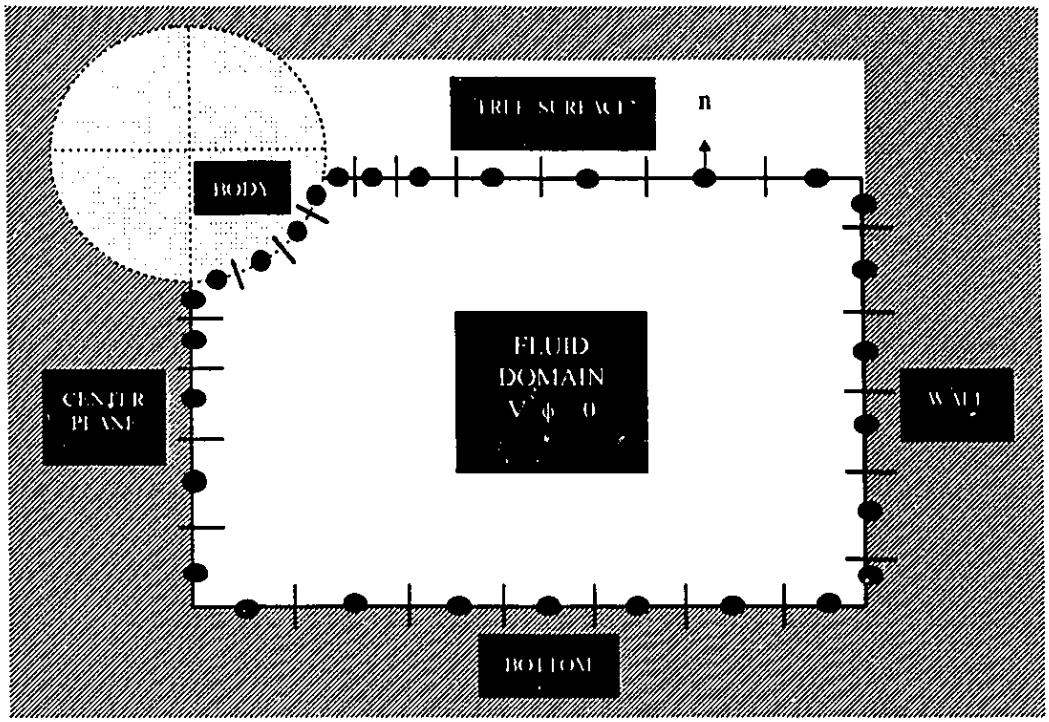

NONLINEAR SURFACE INTERSECTION POINT

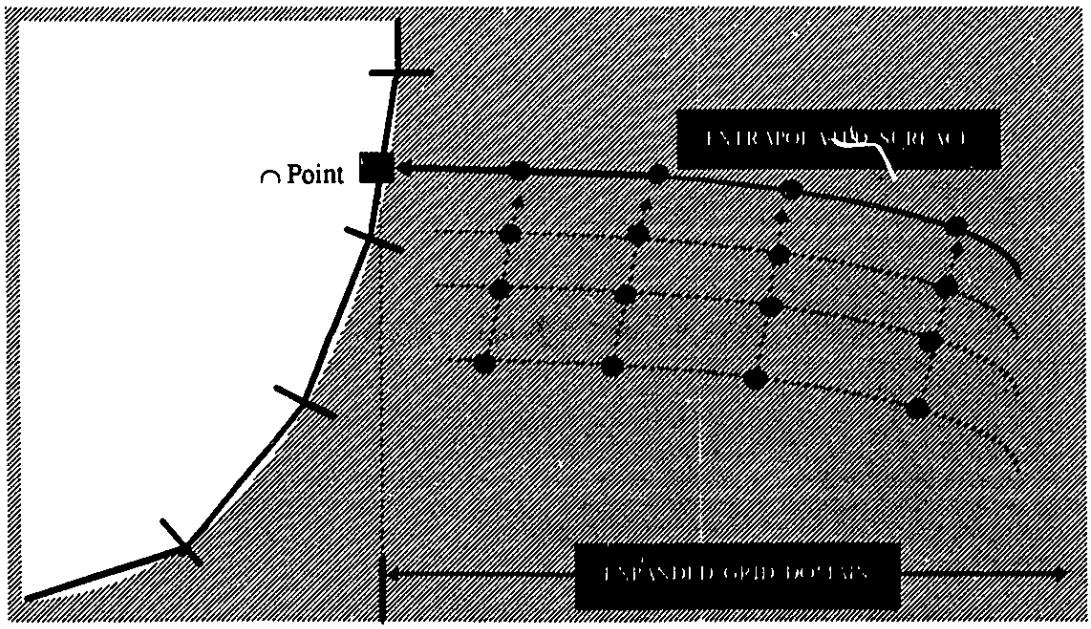

The sizing of the n_{max} surface elements is achieved by assigning segment endpoints based on a one-sided Chebyshev spacing, according to the expression:

$$X(n) = X_1 + \Delta X\left\{1+(1-\frac{k}{n_{\max}})^2\right\}\left[1-\cos(\frac{\pi k}{2n_{\max}})\right] \qquad (5.12)$$

where k=$(0,n_{max})$ and ΔX is the total distance along the surface. The element location, n=(NTOT+1)-k is counted counter-clockwise around the entire boundary starting from the body-surface intersection. And NTOT is the total number of elements. A spreading factor is included which doubles the size of surface elements near the body, so avoiding unacceptably small segments.

The abscissa range of the body contour is similarly subdivided, but utilizes a two-sided Chebyshev formula. The ordinates of the centerplane contour are subdivided according to a one-sided formula with the smallest elements being nearest to the body. The bottom abscissa and wall ordinates are equi-spaced. This selection of element sizes gives a finer scale element definition in the regions bordering the slope discontinuity at the body intersections points.

In the linearized case, the instantaneous abscissa range along the free surface is determined by the intersection of the moving body contour and the undisturbed waterline. The lower diagram in Figure 5.3 depicts the process of defining the nonlinear wave-body intersection point. The new displacements of the wave boundary are not yet known. So an extrapolation of predicted midpoint coordinates based on previous time step data is required; and then a linear intersection between the nearest two surface midpoints and the body curve.

The instantaneous kinematic description of the nonlinear free surface contour and the wave-body intersection point is dependent upon multiple path regridding algorithms which have been incorporated in the BEM Numerical Wavetank. The free surface boundary elements are re-sized and new midpoint abscissas are assigned at each instant in accordance with equation (5.12). This is fixed scheme, depending only on the horizontal distance between the body intersection point and the wall. The initial fluid particles are not being continuously followed in a strictly Lagrangian sense. It is expected that this would lead to a complicated movement of grid points away from the boundary or into it. Instead, a multiple path interpolation scheme has been devised which preserves the Lagrangian context by a continuous transfer of the essential data from older onto new paths. Each path is followed for three consecutive steps and is then abandoned. The oldest path contains sufficient information regarding the fluid displacements, velocities and potentials, allowing extrapolation of the new wave surface.

Figure 5.4 illustrates the transfer of data between these paths for each of a number of ship sections. It should be remarked that in the linear free surface problem there is no horizontal translation of the fluid points, and therefore only a subset of the algorithms are required. This requires a simpler interpolation of previous midpoint data to the new element midpoints on the expandable surface grid.

There is also storage of coordinate and velocity potential data for the body elements. However, in this case it involves only a single path, and a limited amount of information from one previous step.

FIGURE 5.4 NONLINEAR WAVE SURFACE DATA FLOW

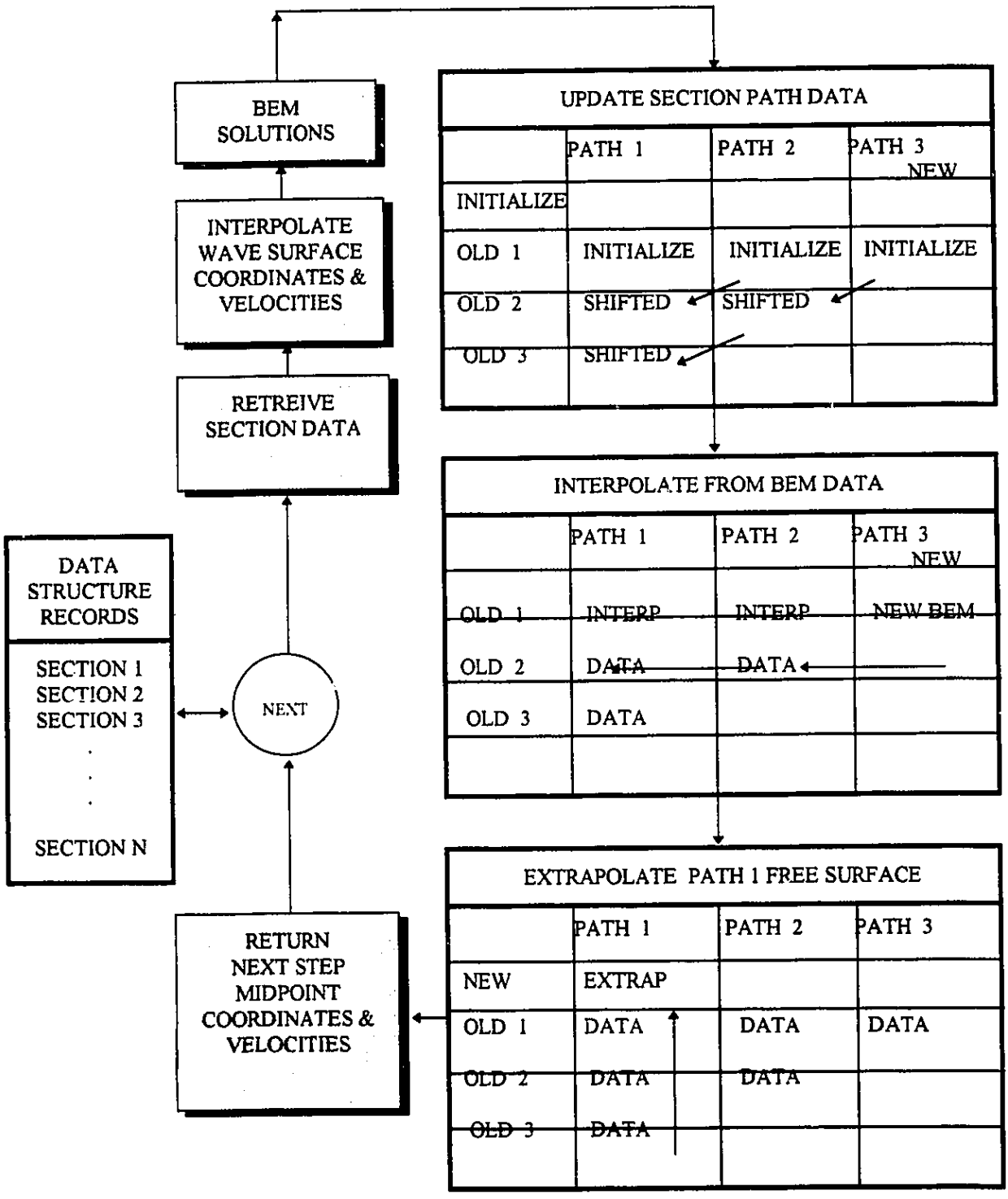

5.5 *Transient Hydrodynamic Pressures on the Body Contour*

The unsteady Bernoulli equation (5.6) permits a computation of the hydrodynamic pressure components on the elements of the body contour. Because the body is moving and the element midpoints are also redistributed at each instant, it is not convenient to determine the material time derivative of the velocity potential directly. Instead, the Bernoulli equation is written in its Eulerian form:

$$\frac{p}{\rho} = -\{gy + \frac{\partial \phi}{\partial t} + \frac{1}{2}(\nabla^2 \phi)\} \qquad (5.13)$$

where the material derivative has been rendered into its corresponding partial derivative and spatial gradients. A second order Taylor expansion is used to map the velocity potentials stored from two previous time-step onto the coordinates occupied by corresponding new set of element midpoints. This permits a parabolic extrapolation of the partial derivative, $\partial\phi/\partial t$, at the current instant. All of the gradient information is easily determined from potential and coordinate data on the current body profile.

Figure 5.5 shows the principal steps in the calculation of sectional hydrodynamic forces. Normal velocities are prescribed as body boundary conditions at the element midpoints. The corresponding tangent velocities are derived from the velocity potentials which are given as output from the BEM solution. The limited midpoint data is interpolated onto a finer scale grid for discretizing the components. A parabolic

interpolation scheme is used to extract the gradient of the potential along the contour, and a five point Hamming smoothing technique is applied to reduce numerical noise.

The first and second order derivatives required for the Taylor expansion of the velocity potential are based on the normal and tangential velocities at the midpoints. These vectors are again transformed onto a fine scale grid and smoothed to increase precision in the calculations. The Cartesian velocity components are given by:

$$v_x = \phi_{,x} = \phi_{,t} \cos\theta - \phi_{,n} \sin\theta \qquad (5.14a)$$

$$v_y = \phi_{,y} = \phi_{,t} \sin\theta + \phi_{,n} \cos\theta \qquad (5.14b)$$

where

$$\theta = \tan^{-1}\left(\frac{dy}{dx}\right) \qquad (5.14c)$$

The second derivatives are approximated by the direct variation of the velocity components with respect the corresponding coordinate axis. The mixed derivative term is taken as the mean of the two possible combinations, dv_y/dx and dv_x/dy.

Three component terms from the Bernoulli equation are assembled as separate vectors. The hydrostatic term accounts for buoyancy effects and depends only on the relative displacement of the element midpoint from the free surface. In the nonlinear case, there is a wave component due to the increase in hydrostatic pressure caused by displacement of the body-surface intersection point. The unsteady component consists of a dynamic pressure term based on the tangential velocity, and the transient potential term. In general, it is observed that the latter will be most important. Each of these pressure

vectors is then integrated over the wetted surface to give a corresponding hydrodynamic force term acting vertically. A fine grid trapezoidal integration with respect to the horizontal axis is employed for ship forms. This is modified to a vertical axis integration for cylinders, since the wetted displacements may include the upper quadrants.

5.6 Piston Wavemaker and Forced Cylinder Heave Oscillations

Figure 5.6 shows three stages in the development of the BEM Numerical Wavetank algorithms. Following Chan (1987), the wavetank was initially configured as a piston-type wavemaker. It was tested for a range of piston amplitudes. The wavetank length was varied from 50 to 200 metres. Its depths was typically 5 meters. Using 80 elements, of which approximately 40 were on the free surface; it was possible to generate stable linearized waves comparable in period and amplitude to those reported by Chan and satisfying wave dispersion theory. Figure 5.7 provides an example of a typical numerical simulation for sinusoidal oscillation at a frequency of 0.10 hertz; showing the progressive growth and propagation of a typical wave profile.

FIGURE 5.5 BERNOULLI PRESSURE CALCULATION

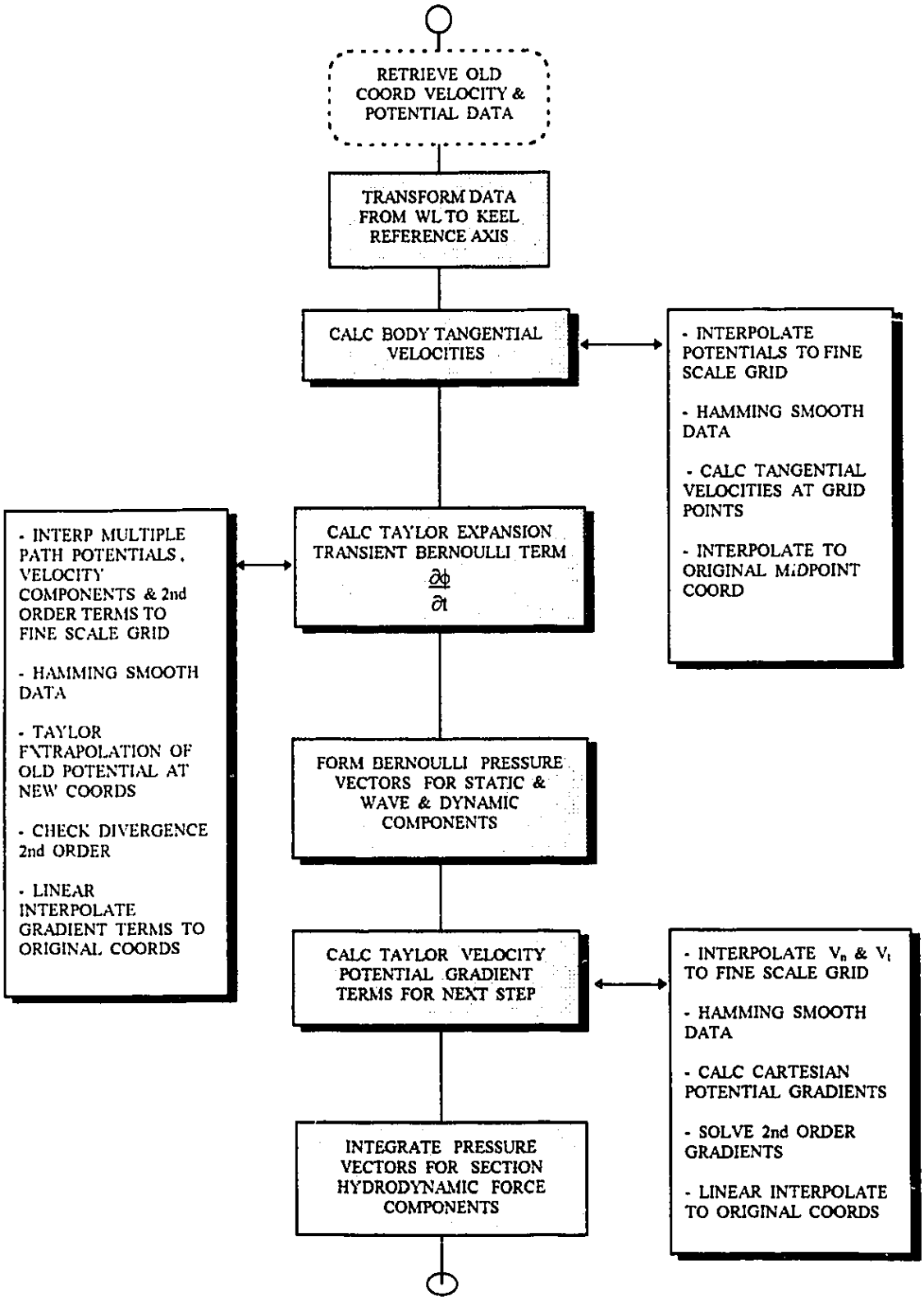

Chan had reported the development of numerical instability in attempting to investigate nonlinear wave phenomenon. He used 450 elements on the free surface. An attempt to replicate this work was precluded by system memory limitations. At the much smaller number of elements available to the present wavetank sections it was not possible to entirely resolve numerical instabilities in the nonlinear model. The linear free surface model was therefore used as the default condition in the BEM Numerical Wavetank.

The forced periodic oscillation of a circular cylinder was next examined. Figure 5.8 presents selected hydrodynamic force histories for a cylinder having a 10 metre radius. It was subjected to periodic oscillation at a frequency of 0.1 hertz, and at a range of amplitudes. The relative influence of the unsteady hydrodynamic terms can be observed to increase significantly with amplitude and frequency.

The heave oscillation tests demonstrated the importance of properly assigning the wavetank dimensions and the number of elements on the free surface in accordance with the physical scaling the problem. For example, the wave period is scaled by Froude's relationship, not geometrically. Carelessness in matching these conditions might leave insufficient elements to represent the wave potential variation along the wavetank. An assessment of the scale and a warning are incorporated into the program setup.

FIGURE 5.6 STAGES OF BEM NUMERICAL WAVETANK IMPLEMENTATION

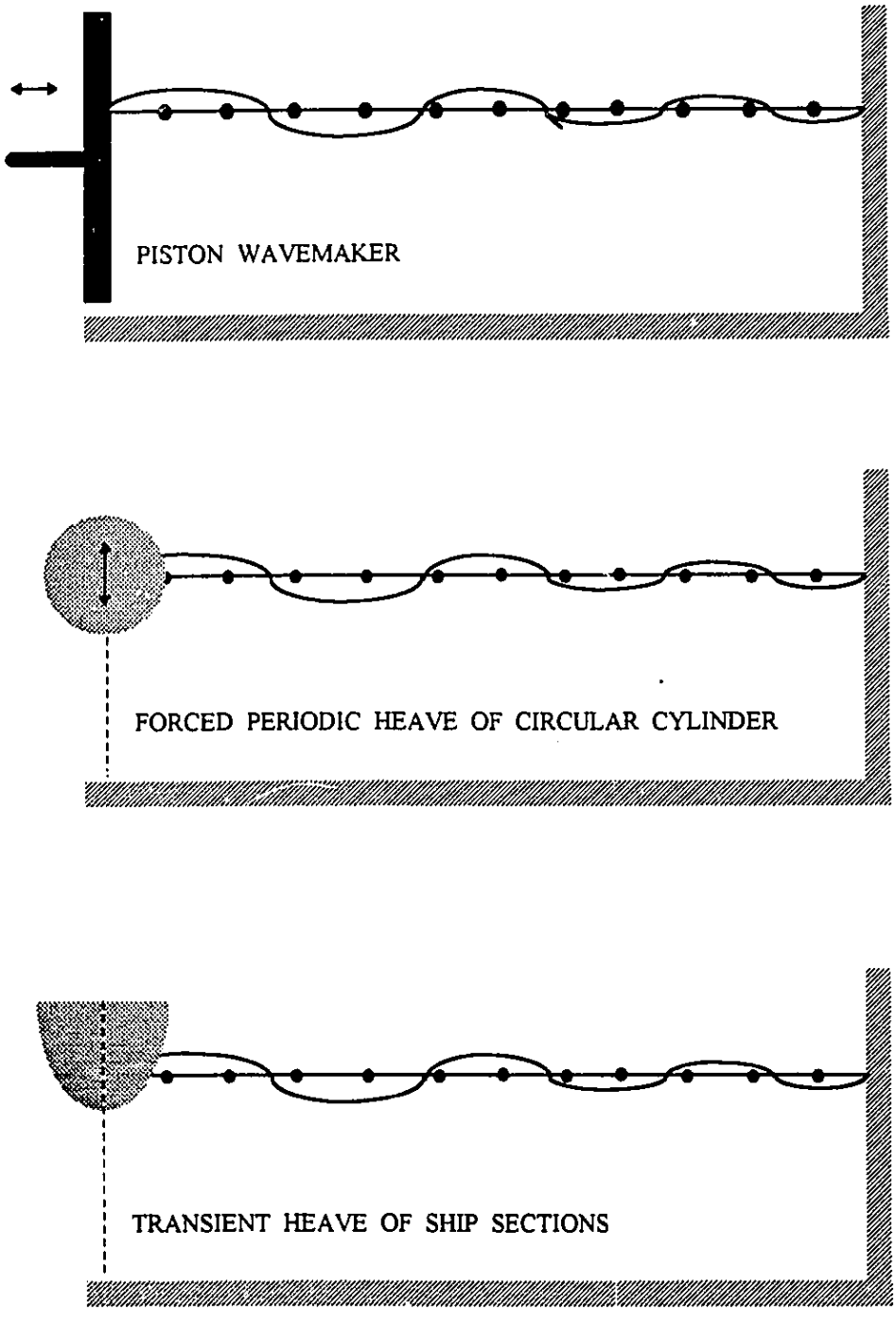

FIGURE 5.7
SAMPLE OF WAVE PROPAGATION BY CYLINDER

radius= 10 m draft = 7.5 ampl = 2 m. freq = 0.158 hz
depth = 40 m. tank =200 m

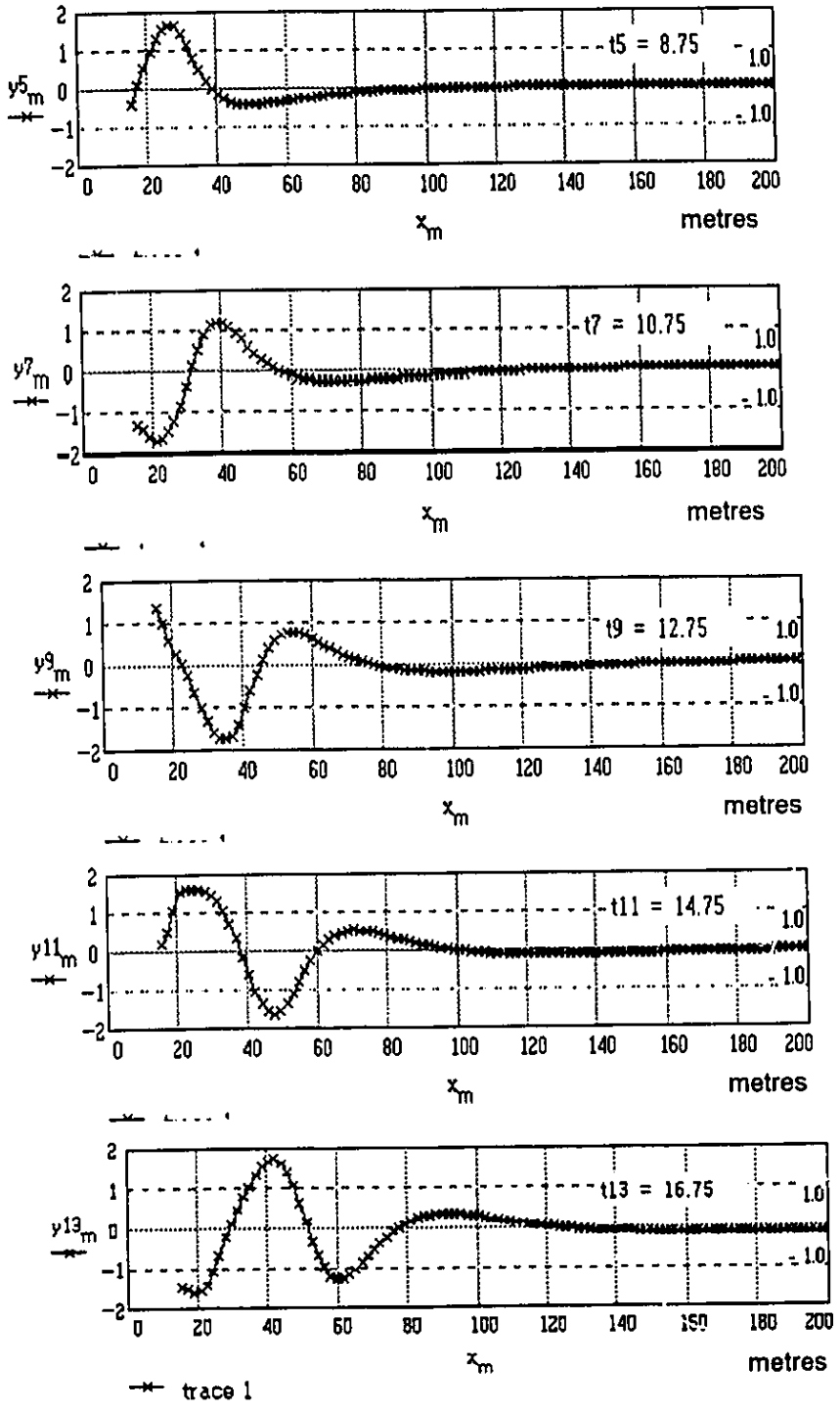

FIGURE 5.8
CYLINDER HYDRODYNAMIC FORCE TIME-HISTORIES

radius= 10 m draft = 7.5 ampl = 2 m. freq = 0.158 hz
depth = 40 m. tank =200 m (Test Run Big3*.prn)

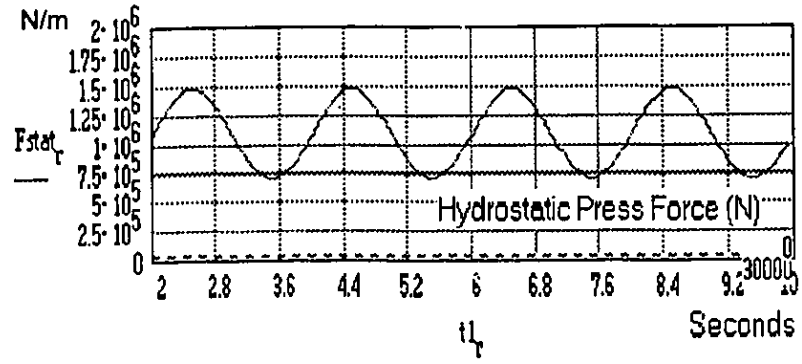

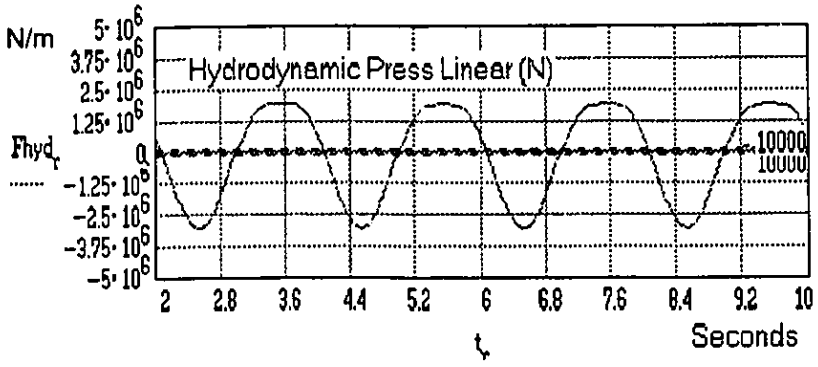

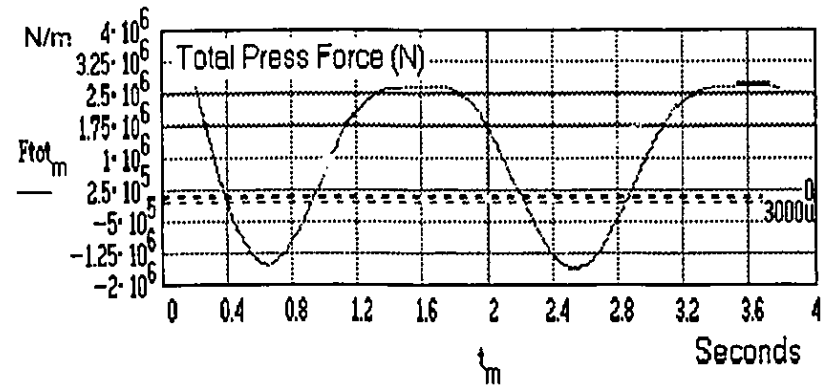

5.7 Strip Representation of Ship

The final stage in the development of the BEM Numerical Wavetank involved its generalization to handle arbitrary numerical section geometries and transient motions. Figure 5.9 shows the basic flow of data in of the general method. The program starts by assessing the kinematic description of the particular ship section. If the section falls within the wetted length of the ship, then it is accepted for analysis. Possible conditions of submergence beyond the deck level are also considered.

Memory is dynamically allocated to hold the multiple path data structures containing information for this section from previous time-steps. The main data bank storing the collected information concerning all of the ship sections is retained in core memory (RAM). But each section adds nearly 0.25 megabytes of storage memory above a base amount of approximately eight megabytes. For 28 ship sections, the dynamic runtime memory associated with the BEM Numerical Wavetank would be in excess of 12 megabytes. Continuous transfers of data to a hard disk would be detrimental to the efficiency of the program. As a reasonable compromise, the data structures are stored in floating point format. Only the dynamic memory specifically allocated for the sectional wavetank calculations is double precision, allowing for greater accuracy in critical, repetitive computations.

The procedures for scaling the sectional wavetanks are illustrated in Figure 5.10. The total section area below the main deck is transformed into an equivalent circular area.

The beam and total depth at the midship section define the maximum area. The dimensions of the wavetank are scaled in accordance with the ratio of the radii of the equivalent sectional circle and the maximum area circle. A freeboard correction factor is included to ensure that the dimension scaling precludes bottoming out. There is an additional constraint limiting the minimum wetted depth that will be considered. Otherwise there would be an unacceptable discrepancy in size between elements on the body boundary, as compared to other regions.

Once the coordinates of element nodes and midpoints on the boundaries have been defined (as previously discussed) a fourth order Runge-Kutta technique is used to advance the velocity potential in time. This entails four repetitions of the BEM solution process, and a subsequent extrapolation of a revised free surface velocity potential. On the basis of the normal velocities resulting from the BEM solution, it is possible to determine the distribution of hydrodynamic pressure on the section, and its integrated force components. The final steps in the sectional wavetank data path involve the updating of the multiple path data records.

5. 8 *Influence of Transient Hydrodynamic Phenomena*

The dissipation of energy through wave radiation offers the fluid foundation a mechanism for moderating the buoyancy restoring forces. Otherwise the large amplitude, transient motions of the ship would contribute only undamped, elastic forces. In the undisturbed free surface, the buoyancy force is in equilibrium with the gravitational weight

of the ship. The overall effect of the ship's motion in the fluid is defined by Bernoulli's equation. Difference in the instantaneous buoyancy from equilibrium due to motions is referred to as the hydrostatic component of the fluid force. The remainder is defined as the unsteady or hydrodynamic component, which consists of the steady-state dynamic pressure and the transient term.

As might be expected, the hydrodynamic component plays a minor role at lower impacts speeds. Figure 5.11 shows a series of snapshots of the fluid force distribution along the ship. At an impact speed of 4 knots, the buoyancy forces are clearly dominant at all of the time-steps which are presented.

For the 18 knot impact shown in Figure 5.12, the situation is markedly different. The hydrodynamic force contribution represents a significant portion of the total fluid reaction. In general, the largest values occur nearest to the bow, and at the stern. Its relative influence is greatest during the initial phase of the interaction. Therefore, a comparison in Figure 5.13 of the relative contributions of the hydrodynamic and hydrostatic components gives a clearer indication of the significance of the hydrodynamic term at higher impact speeds.

Figure 5.14 and 5.15 provide a more detailed analysis of the relative contributions of the two fluid components. At both low and high speeds there is a common trend. It is observed that the hydrodynamic term is the dominant component during the initial period. It determines the vertical force and the fluid moment during this initial time frame, and may be coupled to the corresponding initial ice force peak. The ratios of the two fluid components are seen to balance after about 2 seconds; and thereafter the hydrostatic

contribution remains larger. (The hydrodynamic component may again become larger during slide-off, but that process has not been analyzed in the present study.) Whereas the magnitude of this initial hydrodynamic effect at low speeds is insignificant, at high speeds it becomes the primary factor.

The relative influence of the hydrodynamic force can be quantified by analyzing the variation in ice interaction forces and moments which are caused by progressively introducing each of the Bernoulli equation terms. The steady-state condition includes the dynamic pressure and hydrostatic component. This is compared to the output from the BEM Numerical Wavetank, which computes both dynamic and transient terms, as well as the hydrostatic contribution. Figure 5.16 and 5.17 illustrate the results of this process for a range of the impact speeds. In these tests the ice strength was held constant at 1.5 MPa. The most striking effect is the augmentation and leveling of the magnitude of the 18 knot vertical ice force time-history.

During the crushing phase the transient pressure raises the initial steady-state peak and trough from a mean of 35 MN to about 55 MN. For the case of dynamic pressures only, the sliding phase exhibits a maximum of about 90 MN, but is confused with dynamic content which give some higher extraneous peaks. This was reduced by 50 percent to about 60 MN in the transient case. The trough at 1 second into the steady-state force data is raised from 25 to 60 MN in the transient model. A similar trend is observed in the horizontal force data.

Figure 5.18 shows the variation in each of the ice interaction energies which is caused by including the transient pressure term. This effect shifts the energy pattern to

give maximum energy losses during the initial phases of the interaction, and less during the subsequent sliding-up phase. The average energy dissipated at each instant of the crushing phase is nearly doubled.

This increased dissipative trend, associated with the transient term, shows the importance of a direct time-domain modeling of the total unsteady hydrodynamic force. In its turn, the fluid damping constrains the dynamic content of the ice interaction forces, resulting in a greater stability for the iceforce data obtained during later stages.

FIGURE 5.9 BEM NUMERICAL WAVETANK DATA FLOW

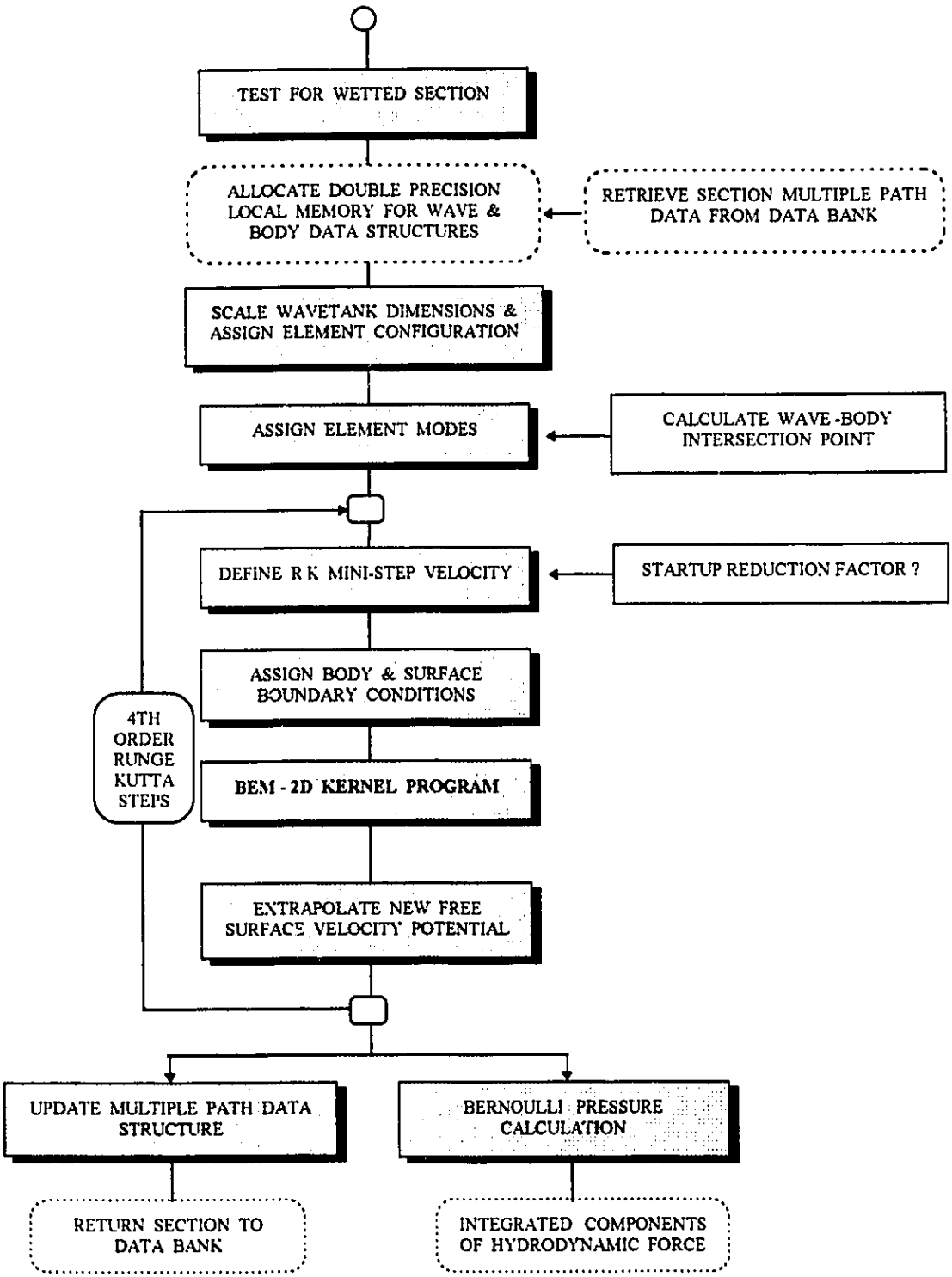

FIGURE 5.10 EQUIVALENT AREA SCALING OF TANK DIMENSIONS

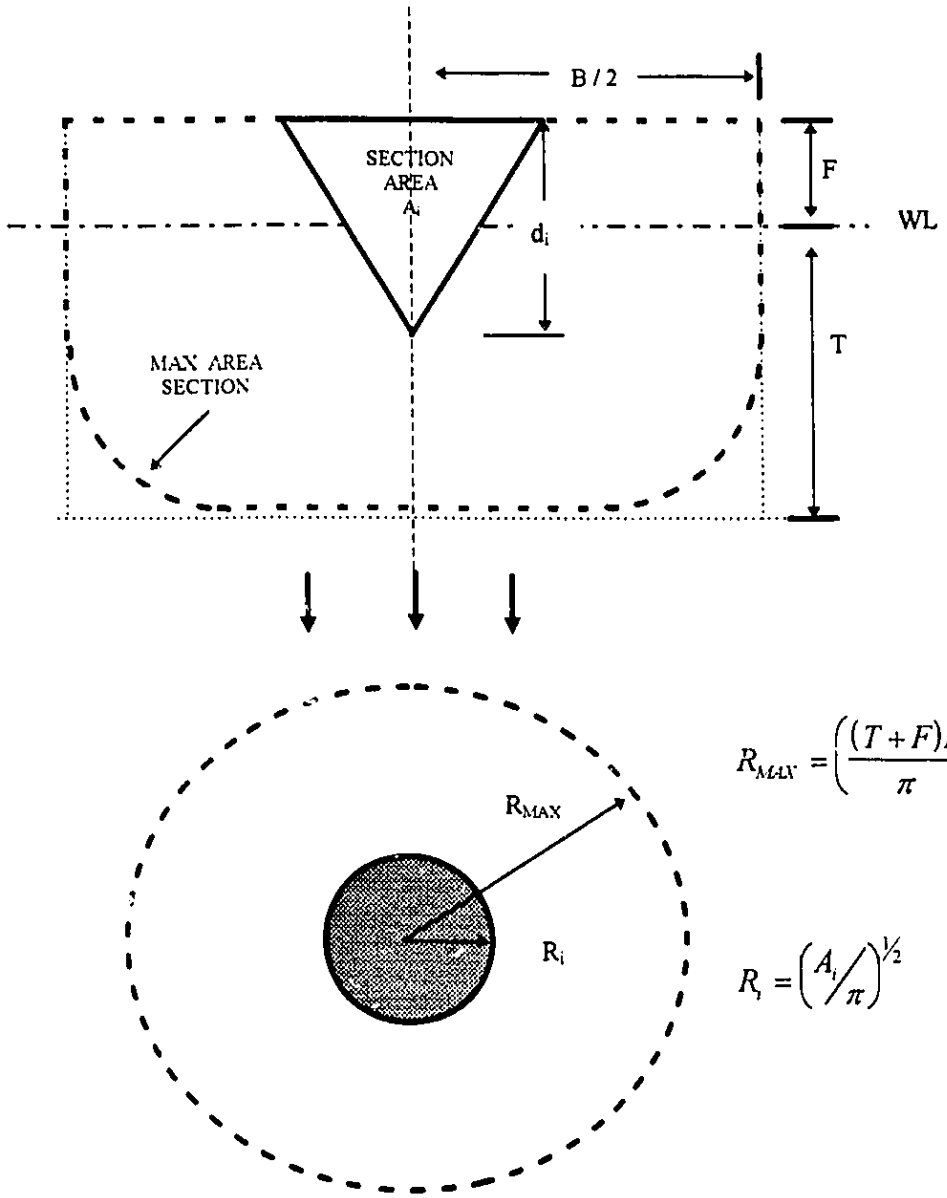

$$R_{MAX} = \left(\frac{(T+F)B}{\pi}\right)^{1/2}$$

$$R_i = \left(A_i/\pi\right)^{1/2}$$

$$SCALE = \left(R_i/R_{MAX}\right)CF$$

Where a freeboard factor:

$$C_F = \left(\frac{d_i + F/2}{T+F}\right)^{1/2}$$

Is included to avoid bottoming at maximum section immersion

FIGURE 5.11
HYDRODYNAMIC FORCE DISTRIBUTION AT LOW SPEED

BEM Numerical Wavetank & 3-D ICEMESH MODEL
Rigid Body IMPACT SPEED = 4 Knots

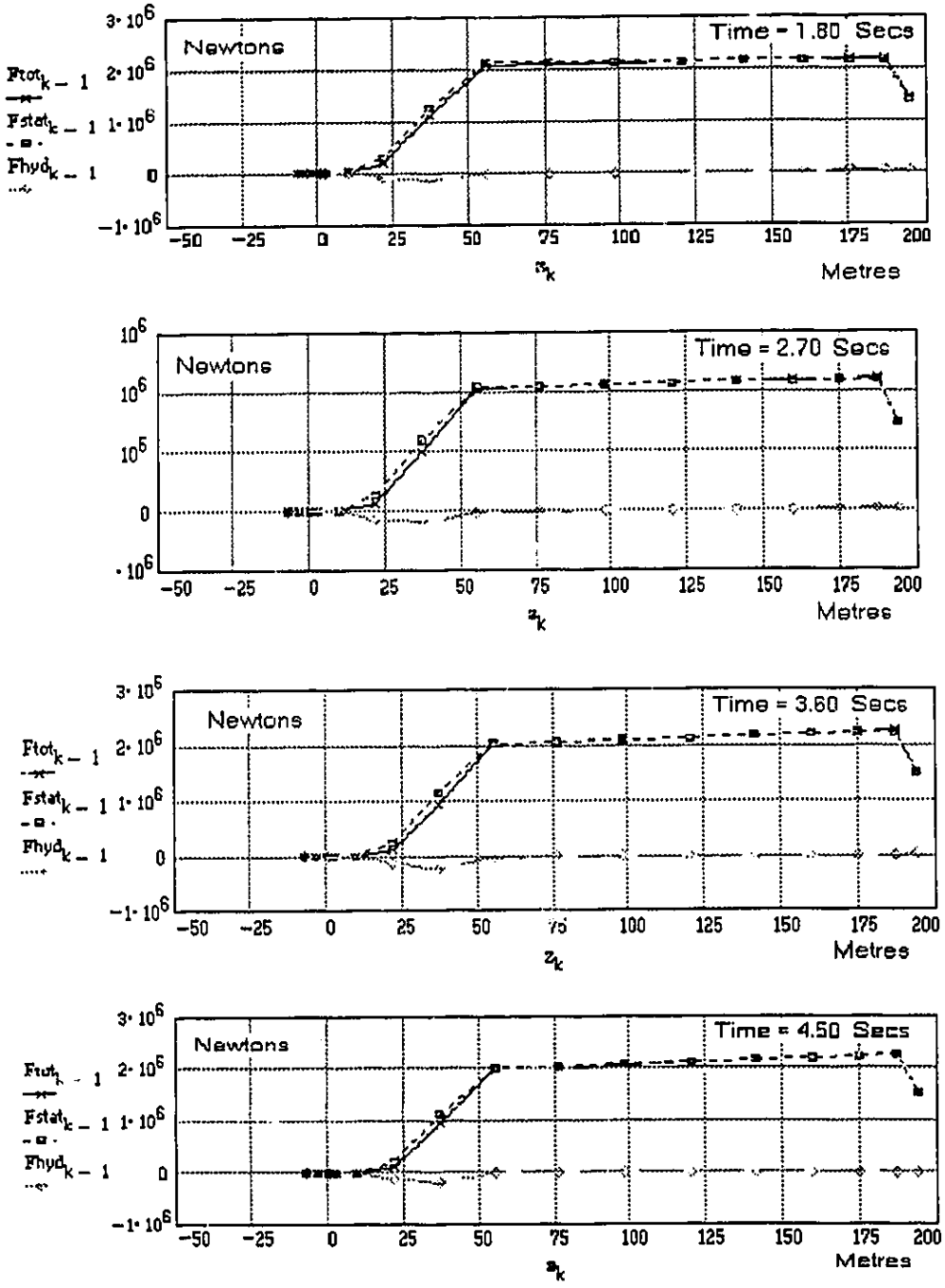

Note: Static Force includes total of buoyancy effects

FIGURE 5.12
HYDRODYNAMIC FORCE DISTRIBUTION AT HIGH SPEED

BEM Numerical Wavetank & 3-D ICEMESH MODEL
Rigid Body IMPACT SPEED = 18 Knots

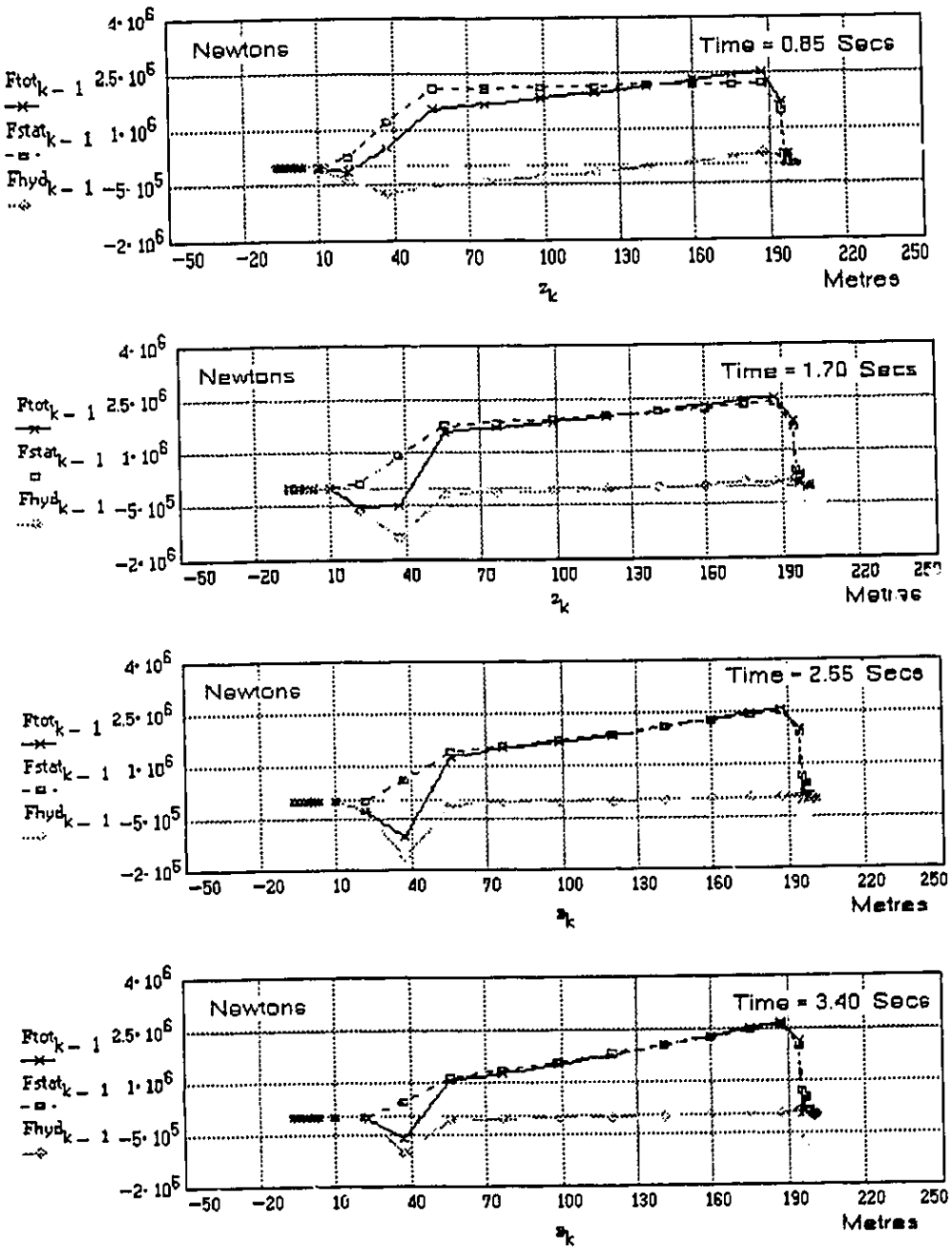

FIGURE 5.13
COMPARING HYDRODYNAMIC VS. HYDROSTATIC TERMS

BEM Numerical Wavetank & 3-D ICEMESH MODEL
Rigid Body IMPACT SPEED = 18 Knots

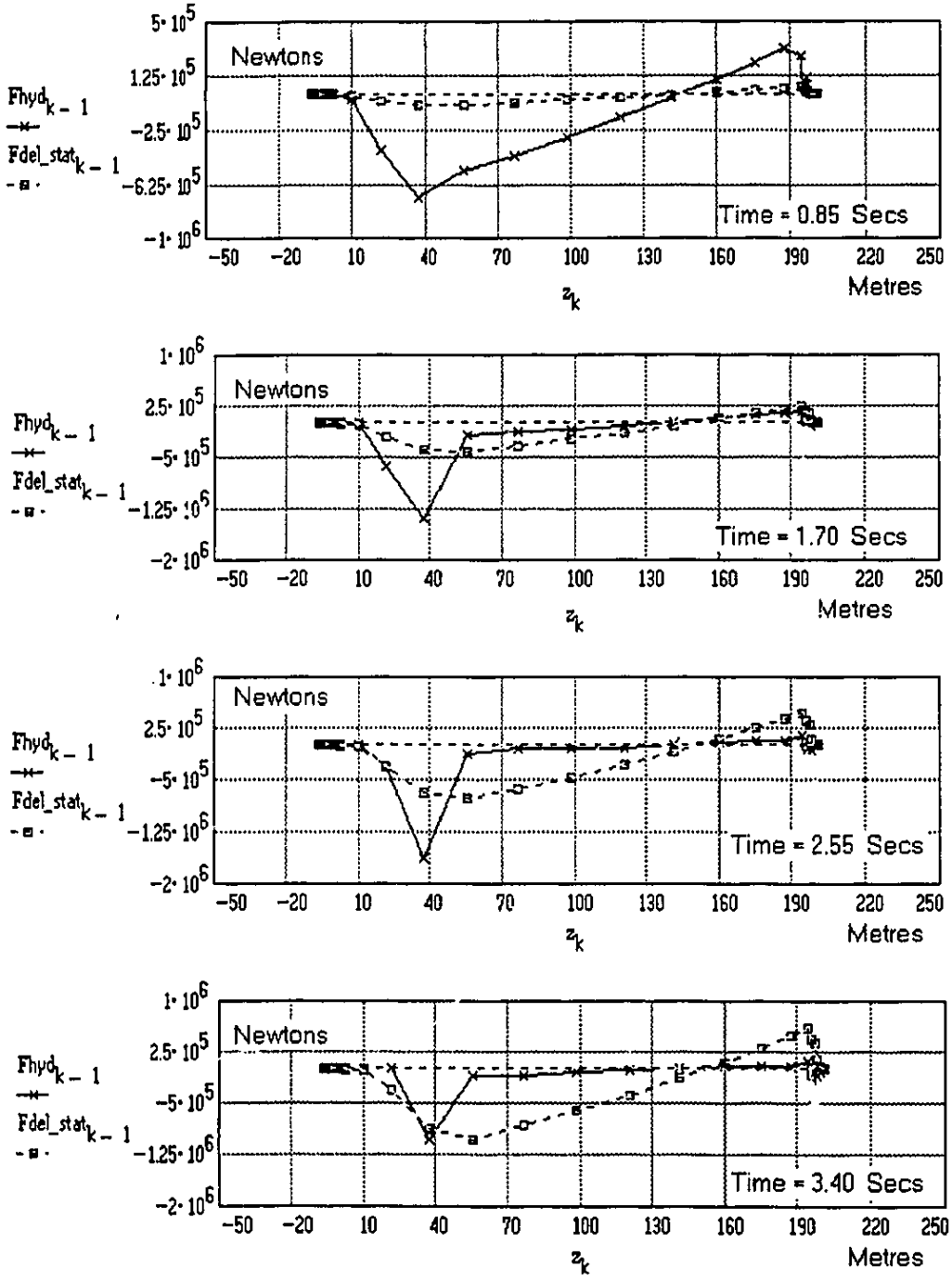

Note: Hydrostatic Force is difference in buoyancy term from equilibrium

FIGURE 5.14
COMPARISON OF FLUID EFFECTS AT LOW SPEEDS

BEM Numerical Wavetank & 3-D ICEMESH MODEL
Rigid Body IMPACT SPEED = 4 Knots
Nominal Ice Strength = 1.5 MPa

TOTAL VERTICAL FORCE = b + c Terms
b = Hydrostatic , c = Hydrodynamic

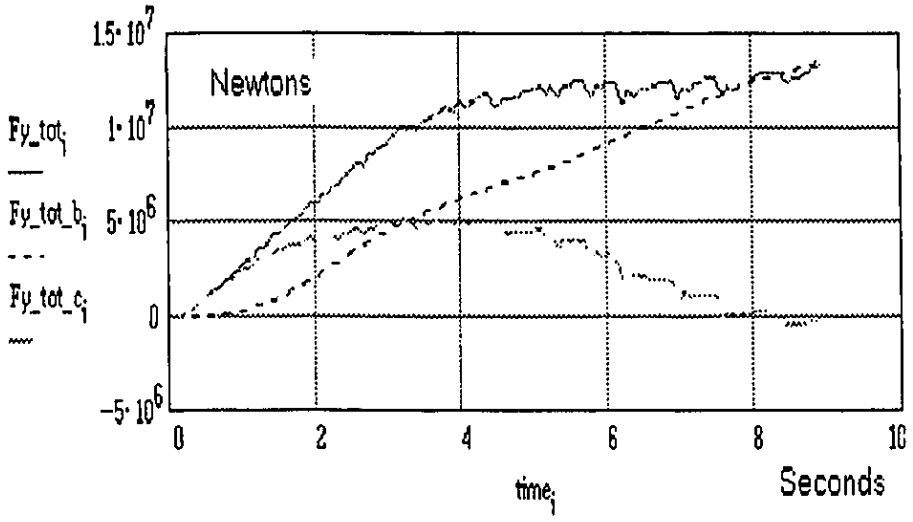

RATIOS OF FLUID FORCE COMPONENTS wrt TOTAL
b = Hydrostatic , c = Hydrodynamic

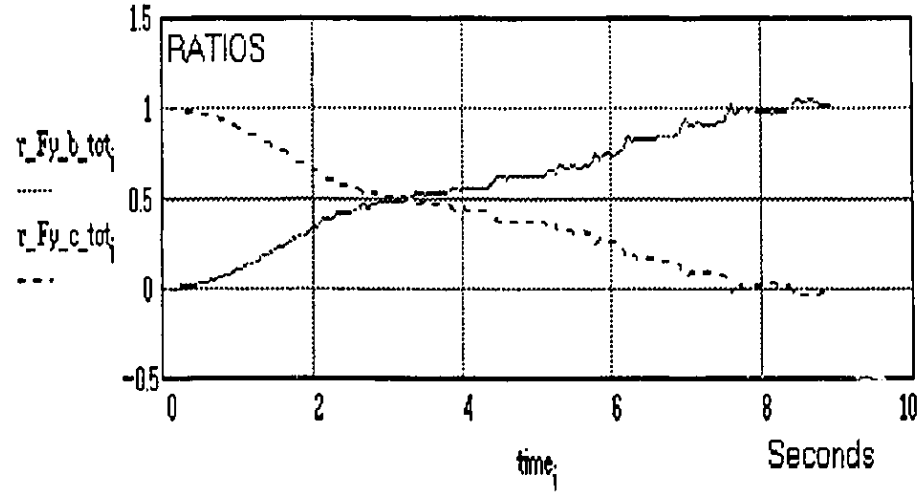

FIGURE 5.15
COMPARISON OF FLUID EFFECTS AT HIGH SPEEDS

BEM Numerical Wavetank & 3-D ICEMESH MODEL
Rigid Body IMPACT SPEED = 18 Knots
Nominal Ice Strength = 1.5 MPa

TOTAL VERTICAL FORCE = b + c Terms
b = Hydrostatic , c = Hydrodynamic

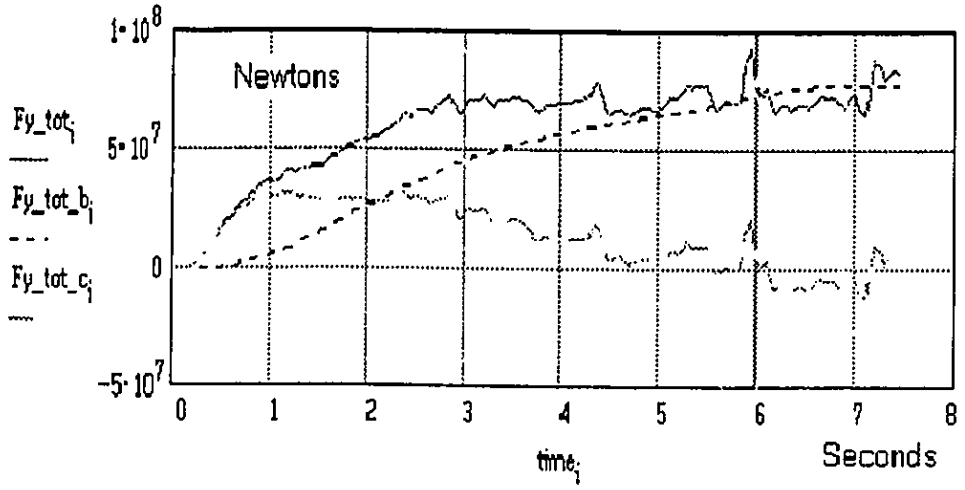

RATIOS OF FLUID FORCE COMPONENTS wrt TOTAL
b = Hydrostatic , c = Hydrodynamic

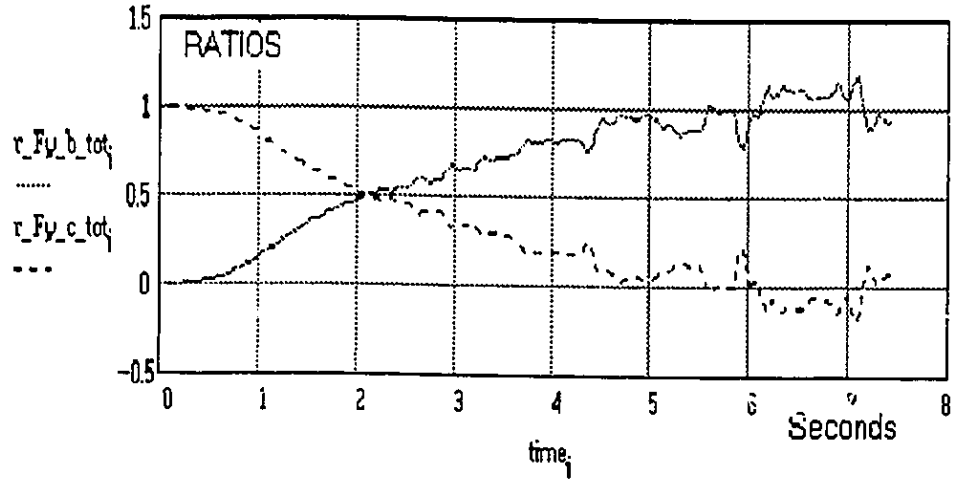

FIGURE 5.16
EFFECT OF FLUID MODEL ON VERTICAL ICE FORCE

USING 3-D ICEMESH MODEL
Nominal Ice Strength = 1.5 MPa

STEADY-STATE Dynamic Pressures
Total Force, Crushing & Friction
Rigid Body IMPACT SPEED = 18 Knots

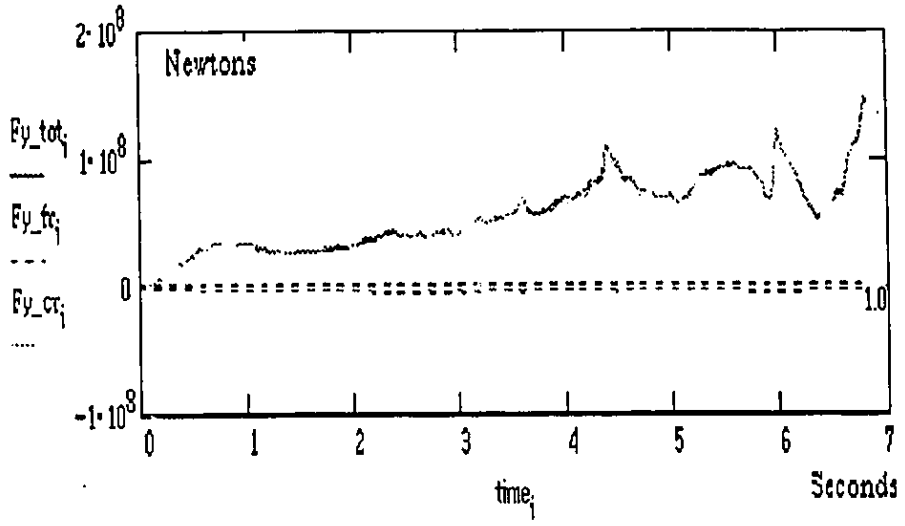

BEM NUMERICAL WAVETANK MODEL
Total Force, Crushing & Friction
Secondary Interaction Forces Not Shownl
Rigid Body IMPACT SPEED = 18 Knots

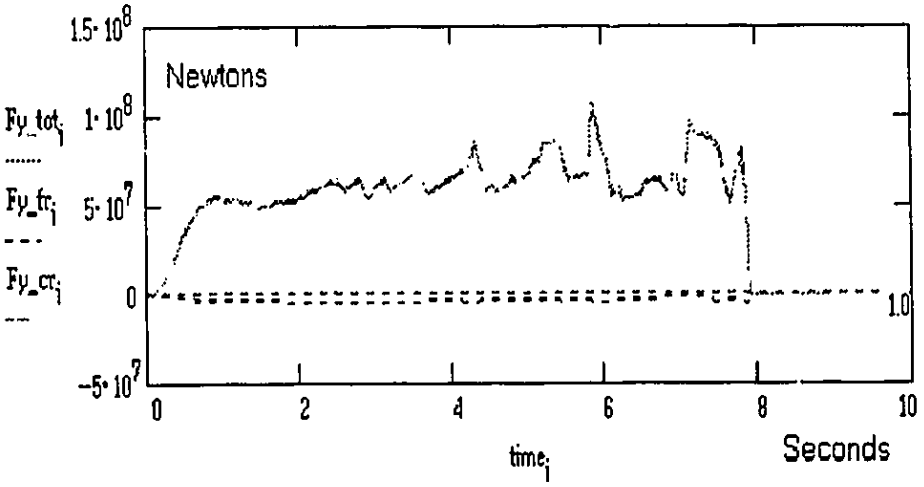

FIGURE 5.17
EFFECT OF FLUID MODEL ON HORIZONTAL ICE FORCE

USING 3-D ICEMESH MODEL
Nominal Ice Strength = 1.5 MPa

STEADY-STATE DYNAMIC PRESSURES
Total Force, Crushing & Friction
Secondary Interaction Forces Not Shown.
Rigid Body IMPACT SPEED = 18 Knots

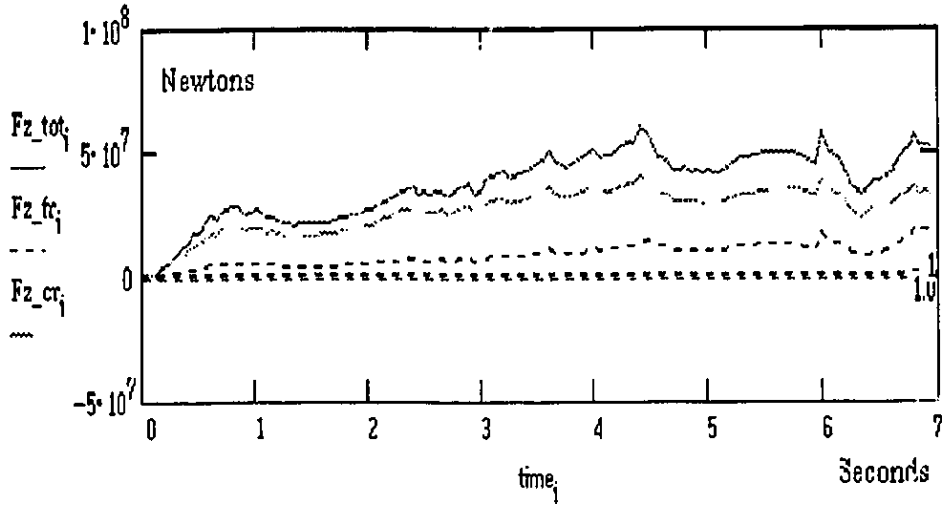

BEM NUMERICAL WAVETANK MODEL
Total Force, Crushing & Friction
Secondary Interaction Forces Not Shown.
Rigid Body IMPACT SPEED = 18 Knots

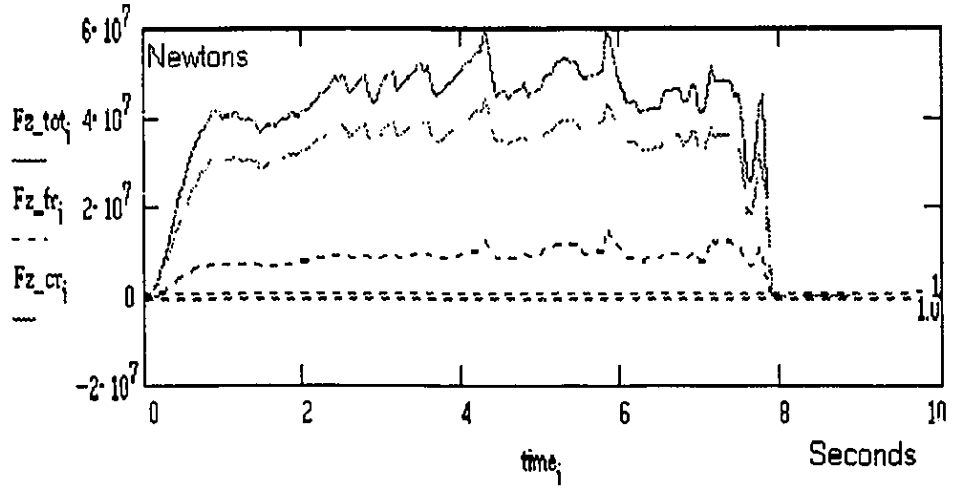

FIGURE 5.18
EFFECT OF TRANSIENT PRESSURES ON ICE ENERGIES

USING 3-D ICEMESH MODEL
Nominal Ice Strength = 1.5 MPa

STEADY-STATE DYNAMIC PRESSURES
Total Ice Energy, Crushing & Friction
Secondary Interaction Terms Not Shown.
Rigid Body IMPACT SPEED = 18 Knots

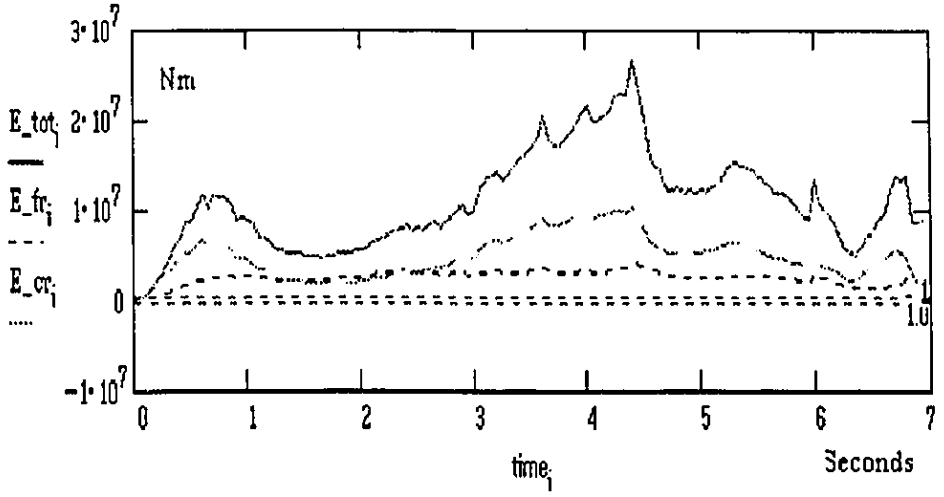

BEM NUMERICAL WAVETANK MODEL
Total Ice Energy, Crushing & Friction
Secondary Interaction Terms Not Shown.
Rigid Body IMPACT SPEED = 18 Knots

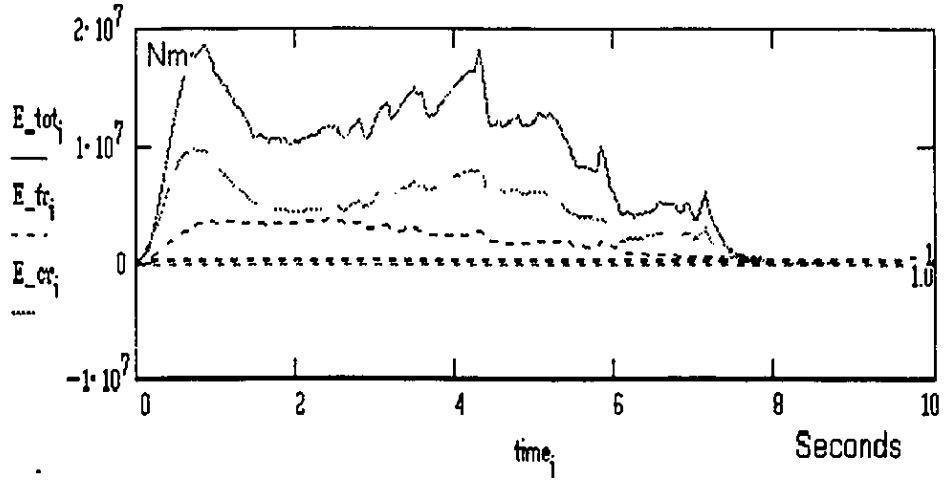

Chapter 6 Case Study: *MV Arctic* Hullgirder Stresses

The development of the ITHACA_SHIP model has profited from a wealth of practical experience gained from a decade of physical model testing and dedicated full scale trials involving the *MV Arctic*. The principal particulars and structural properties of this ship have been described in Chapters 2 and 3 respectively. Visual observations of these tests and analysis of their experimental data have helped identify pertinent physical mechanisms which have been idealized in the numerical model.

Previous chapters have described certain elements of the concept exploration model and its relation to the *MV Arctic* test program. For example, in Chapter 3 the importance of kinematic displacements in mapping the ice interface was demonstrated. It was similarly shown in Chapter 5 that transient hydrodynamic phenomena becomes a significant factor at higher collision speeds. As a further demonstration of the method, numerical predictions of hullgirder stress variation with impact velocity will now be examined. The resulting trends are compared to the physical model and 1984 Trials data. This analysis provides a means of assessing the current model's effectiveness in replicating known data, of extrapolating to new test configurations, and of illustrating its inherent limitations.

6.1 Reference Data from Trials and Model Tests

Data from full scale ramming trials for the *MV Arctic* has provided a common reference point for physical model studies and for the current numerical computations. Melville/VTT (1982) has reported on the structural properties and modal characteristics of the prototype; based on exciter testing. Dedicated multi-year ice ramming trials were subsequently carried out in 1984. Canarctic/NS&E have described the ice properties and notch measurements for the tests. An analysis of the test results is given by German and Milne/VTT (1984).

The ice indentation measurements were taken in two ways. One method involved a determination based on the ship's surge and pitch motions with respect to the ice edge. A second estimate of the indentation was obtained by physically measuring the notch dimensions. This included an attempt at correcting the measurements to account for the breaking away of portions of the edge. From an analysis of this data, Daley and Phillips (1985) estimated that a mean indentation of 5.8 metres would occur for an impact speed of 4 knots. As a note on possible error limits, it should be remarked that the ship motions method suggested a value closer to 7.2 meters.

The prototype vertical force time-histories were extracted from strains which were measured along the *MV Arctic* hullgirder. A finite element model, including fluid elements, was used to transform these strains into corresponding bow forces.

The flexural model tests (Daley and Phillips, 1985, and Phillips et al, 1986) started from the reference indentation as a basis for a dynamic (or Froude) scaling of the overall

collision process. The model ice material was scaled to achieve this indentation for a 4 knot collision. This resulted in a material scale defined in terms of the geometric scale factor, λ=40, and the diameter, d=25 mm, of cylinders used for testing model ice strength. The standard cylinder diameter is d_o=100 mm. Following a regression analysis of the first series of ice impact tests it was found that the ice scaling relation took the form:

$$\sigma_{MS}=(\sigma_{CR}\ \lambda^{-1})\ f(\lambda,d) \qquad (6.1a)$$

where

$$f(\lambda,d)=(\ (\lambda d/d_o)^{-0.98} \qquad . \qquad (6.1b)$$

The full scale uniaxial compressive strength of the multi-year ice was estimated to have been 4.8 MPa at a strain rate of 10^{-1}/sec. On this basis the model scale ice was required to be 10.5 kPa. In practice the material exhibited a range of strengths, with a preponderance of values about 30 kPa. But the scale value only has meaning in providing a consistent reference strength corresponding to the reference indentation.

The model scale collision testing was carried out at these ice strengths and converted to the reference condition using a 1/7 power relationship between ice strength and force. While this correction showed that the peak forces have a very slow variation with ice strength, it should be noted that the first peak dynamics of the force are strongly modified. This was found in the model tests, and was equally observed in the numerical computations of ice forces in Chapter 4. The experimental modeling was completed by verifying that the measured vertical ice force agreed with the prototype value of 22.2 MN

at a 4 knot impact. The corresponding midship deck bending moment was derived and the stress estimated using a section modulus of 14.2 m^3.

On the basis of this scaling procedure, it was possible to extend the experimental test range to higher velocities. Global loading and deck stresses were obtained for impact speeds ranging up to about 14 knots. Because of dynamics in the collision process, the peak forces and stresses did not follow a simple, monotonously increasing trend with speed. Rather, there was an oscillatory pattern about the mean. The vertical ice force was expressed by a regression relationship:

$$F_V = 5.233\ V^{0.976} \tag{6.2}$$

where the velocity, V, is in knots and the force has the units of MN. A corresponding expression for the midship deck stresses in MPa is:

$$\sigma_6 = 8.382\ V^{0.981} \tag{6.3}$$

and the maximum deck stress is given by modifying the constant in this equation to 9.640. Table 6.1 gives the mean predicted values of vertical force and deck stress indicated by the regression curves.

Table 6.1 Extracted Model Test Data

Speed [Kts]	F_V [MN]	σ_6 [MPa]	σ_{Max} [MPa]
4	20.3	32.7	37.6
6	30.1	48.6	55.9
8	39.8	64.5	74.1
10	49.5	80.2	92.3
12	59.2	95.9	110.3
14	68.8	111.6	128.4
16	78.3	127.2	146.3
18	87.9	142.8	164.2

6.2 Calibration of Nominal Ice Strength

Prior to initiating a concept exploration study and collision analysis for the *MV Arctic*, it was necessary to define a nominal ice strength for the Ice Interaction Model. This was established on the basis of calculated indentations. Preliminary numerical simulations using the Rigid Motions Model were carried out for the *MV Arctic* using the quicker dynamic pressure model. Indentation data was obtained for a range of uniaxial compressive strengths as shown in Figure 6.1. The nominal ice strength was selected by interpolation from this data. It gave 1.5 MPa; corresponding to the Trial's indentation of 5.8 meters. This procedure neglects the secondary ice mechanisms and transient hydrodynamic effects, which are insignificant at 4 knots. The translation of a uniaxial ice strength of 4.8 MPa into a nominal pressure of 1.5 MPa gives a linear proportionality factor of 0.31.

This is a simple relationship for defining the effective ice strength; but it is reasonable considering the 1/7th power relationship between ice force and strength, and in view of the present emphasis on kinematic displacements, rather than ice properties.

6.3 *Time-domain Predictions of Stresses*

The Rigid Body Model simulation has been carried out using the procedures outlined in Section 2.6. A numerical ship with 15 stations located at Chebyshev intervals between perpendiculars was developed. This gives 23 sections in total. Options were specified so as to include both the 3-D Ice Interaction Model and the BEM Numerical Wavetank. A time-step of 0.05 seconds was assigned. Ice freeboard was set at 1.0 metre. The simulation continued until such time as negative surge velocities were encountered. It should be remarked that a 10 second real-time simulation requires approximately 15 hours of CPU time on an IBM 486/66 system. This assumes that the BEM model uses only 80 elements per ship section.

Figure 6.2 and 6.3 show time-histories of the vertical and horizontal forces respectively. The peak values of the rigid body vertical force throughout the speed range are somewhat smaller than the physical model's hydroelastic forces. While a direct comparison cannot be made, the lower values for the rigid forces are in the direction expected. A vertical force of approximately 80 MN is predicted at 18 knots. The dynamic trends appear to agree well with the model test results.

FIGURE 6.1
ITHACA Rigid Indentation Data

Preliminary Model Calibration Runs for MV Arctic with:
Steady-State Berrnoulli Dynamic Pressures and
3-D IceMesh at Strengths: #1= 1.5, #2= 3.0 , #3= 6.0 MPa

TESTS AT VELOCITY = 4 KNOTS

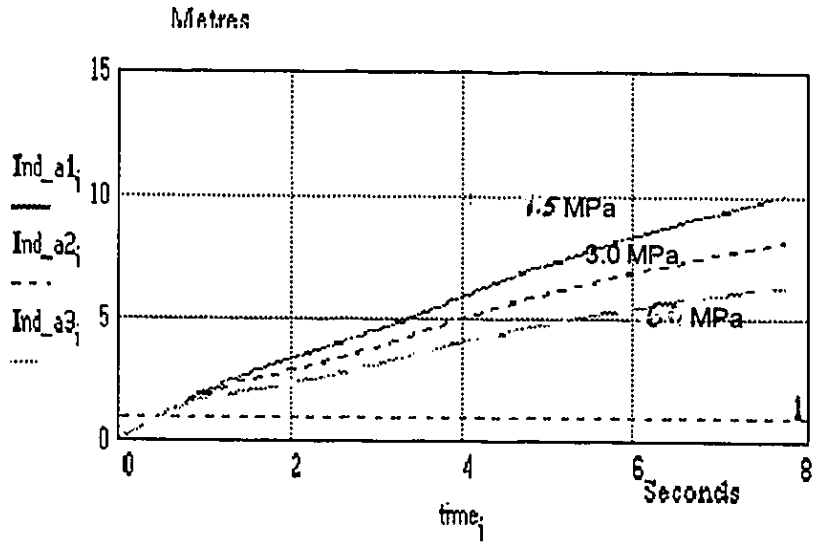

TESTS AT VELOCITY = 18 KNOTS

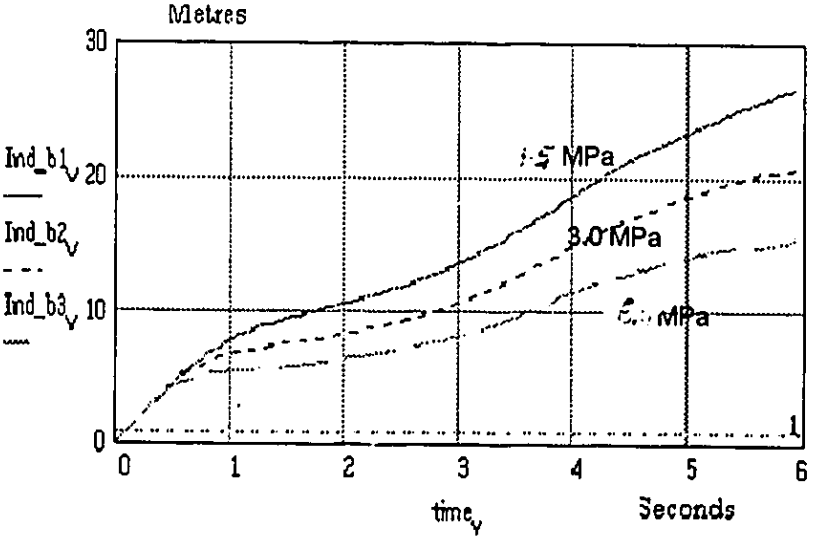

FIGURE 6.2
ITHACA RIGID VERTICAL ICE FORCE TIME-HISTORIES

USING BEM WAVETANK & 3-D ICEMESH MODEL
Nominal Ice Strength = 1.5 MPa

4 Knots

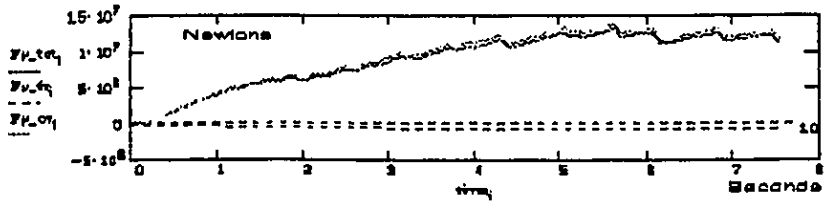

6 Knots

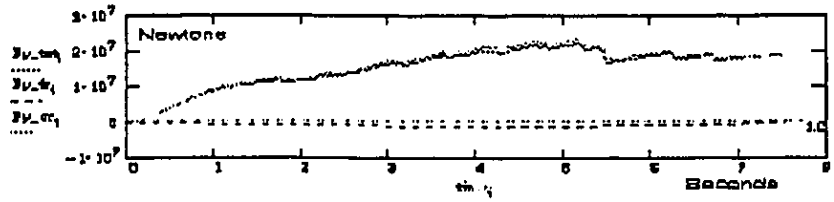

9 Knots

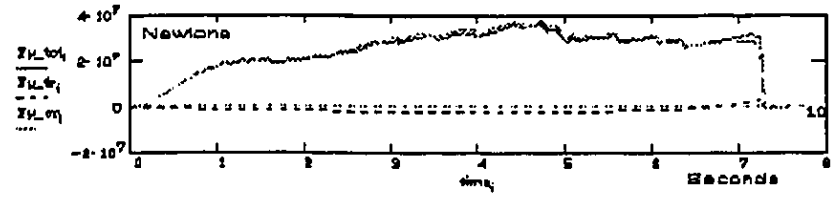

12 Knots

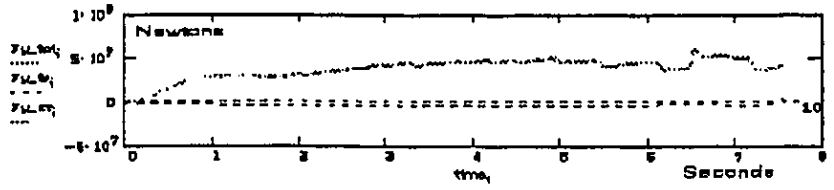

15 Knots

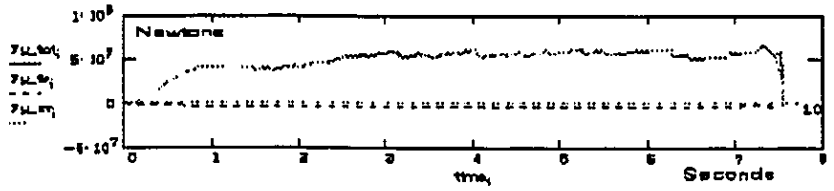

18 Knots

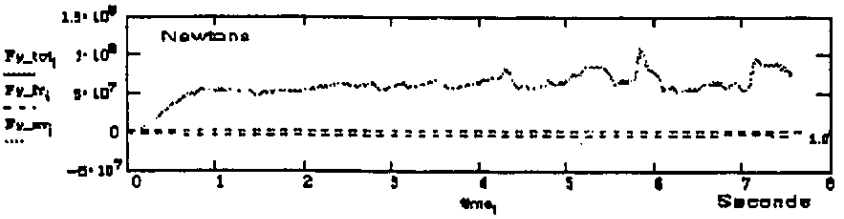

21 Knots

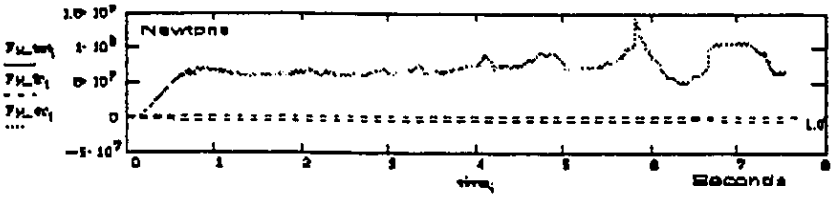

FIGURE 6.3
ITHACA RIGID HORIZ ICE FORCE TIME-HISTORIES

USING BEM WAVETANK & 3-D ICEMESH MODEL
Nominal Ice Strength = 1.5 MPa

4 Knots

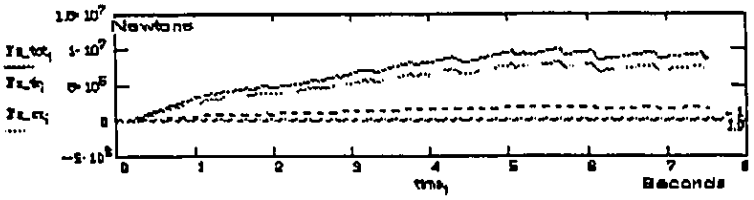

6 Knots

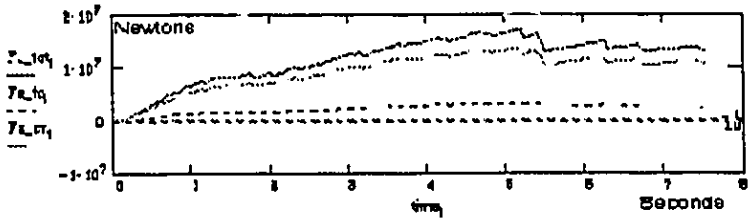

9 Knots

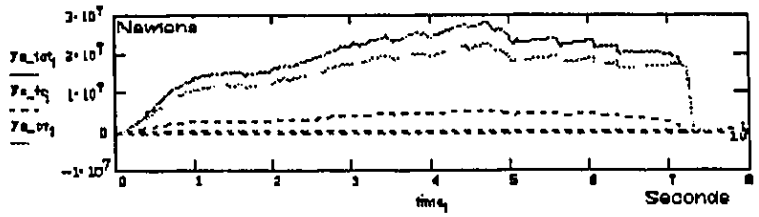

12 Knots

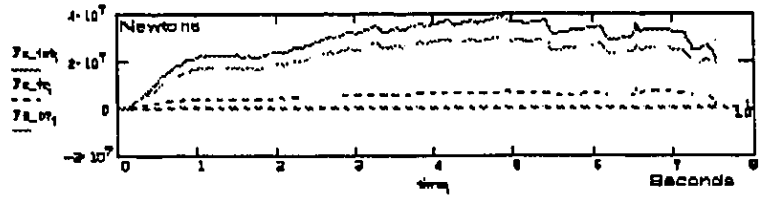

15 Knots

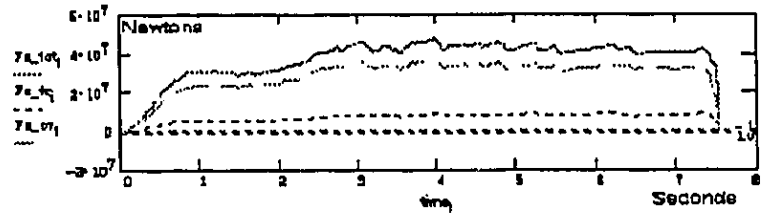

18 Knots

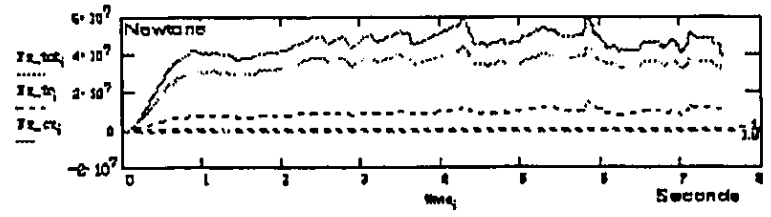

21 Knots

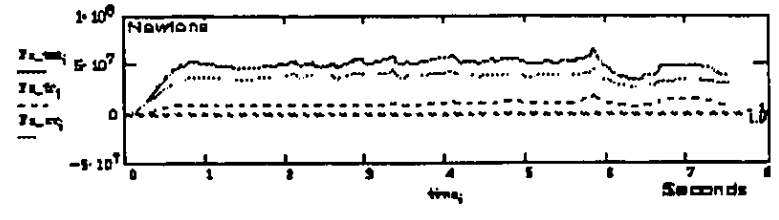

The second step in the simulation process involved the Hydroelastic Model. It uses the ice and hydrodynamic force data obtained from the Rigid Body Model as input. The section modulus at the midship is assigned a value of 14.2 m^3 in agreement with the prototype and model test condition. Figure 6.4 provides a sampling of snapshots of the resulting stress distribution along the ship at various instants during the collision interaction. It is observed that the stress typically reaches a maximum near the midship section. This tendency increases with higher impact speeds. Midship peak stress data for a range of impact velocities is shown in Figure 6.5. Similar data is given in Figure 6.6 for the maximum peaks of stress in the time-histories.

At 4 knots the peak midship stress is 30.7 MPa and the maximum deck stress is 37.8 MPa. These results are in excellent agreement with the physical model values of 32.7 MPa and 37.6 MPa respectively; and with the Trial's data. Just as the correlation with the Trial's force data provided a verification for the physical modeling methods; so too the agreement of the ITHACA_SHIP results with the prototype stress data serves a similar function.

Figure 6.7 plots the variation of simulated midship stress with velocity together with the corresponding data from model tests. It can be observed that the predictions are nearly identical over the lower and medium range of impact speeds. But for simulations at speeds beyond the physical model test range, significant dynamic content enters the numerical stress data. This causes a trend towards higher numerical stress predictions than expected from regression curves based the model test data. For example, at 18 knots

a maximum of approximately 200 MPa occurs at the midship section. This is accompanied by springing of the hullgirder at a frequency of 1.25 Hz; which is well above the 0.95 Hz first wetted mode frequency, as defined in the full scale exciter tests. It should be noted that the normal mode algorithms assign a Rayleigh proportional damping, based on the assumption that the structural component of the damping is 2 percent of critical for the lowest flexural mode.

FIGURE 6.4
SAMPLE OF ITHACA FLEXURAL STRESS TIME-HISTORIES

USING BEM WAVETANK & 3-D ICEMESH MODEL
Nominal Ice Strength = 1.5 MPa

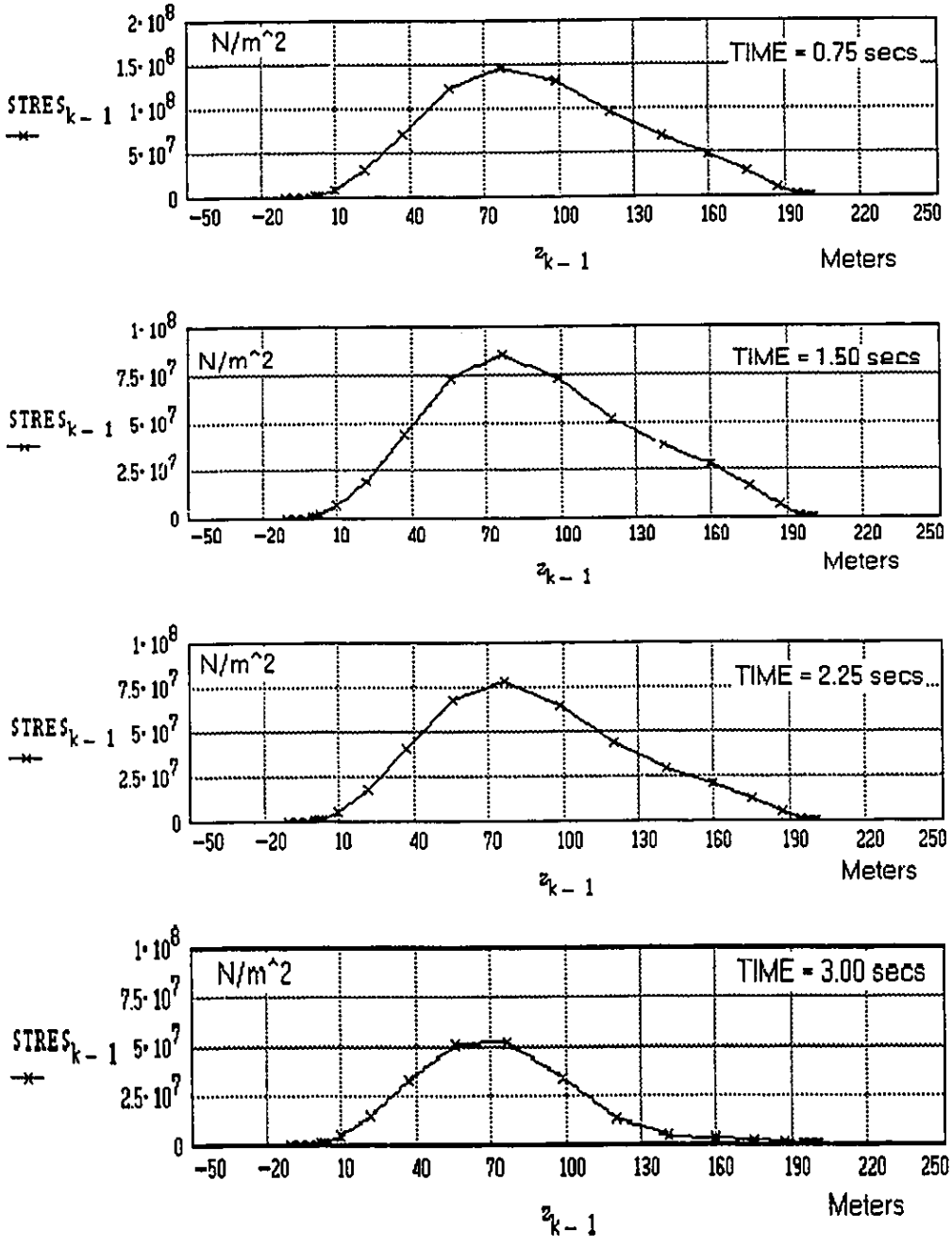

FIGURE 6.5
MIDSHIP FLEXURAL STRESSES

BEM Numerical Wavetank & 3-D ICEMESH MODEL
Sect_mod = 14.2 m3 Shapefuncs = 16 Modes = 5

SPEED 4 KNOTS

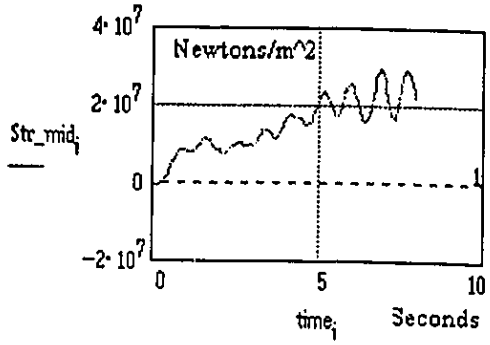

SPEED 6 KNOTS

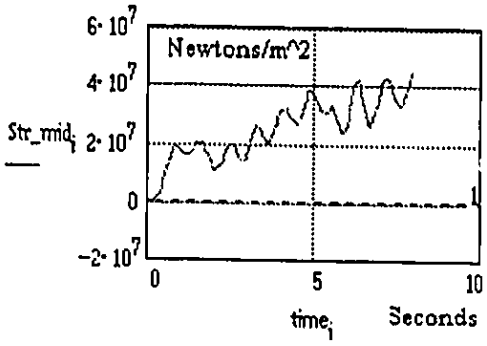

SPEED 9 KNOTS

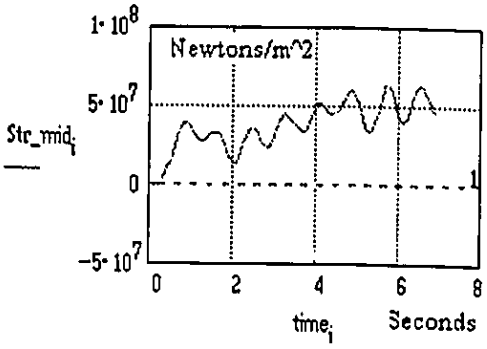

SPEED 12 KNOTS

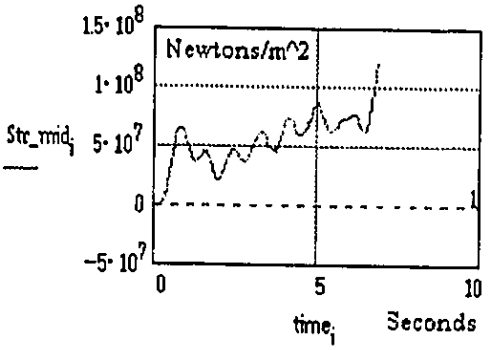

SPEED 15 KNOTS

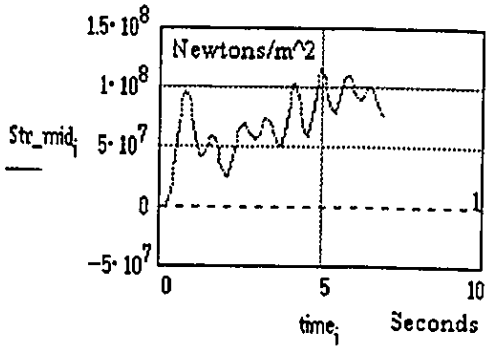

SPEED 18 KNOTS

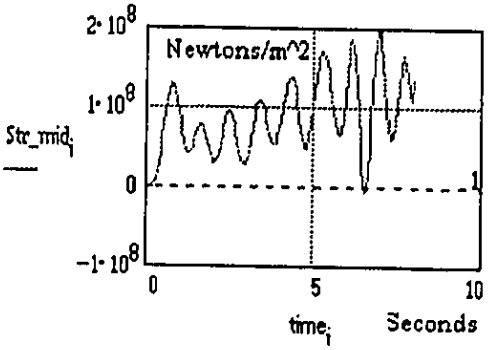

FIGURE 6.6
MAXIMUM FLEXURAL STRESSES

BEM Numerical Wavetank & 3-D ICEMESH MODEL
Sect_mod = 14.2 m3 Shapefuncs = 16 Modes = 5

SPEED 4 KNOTS

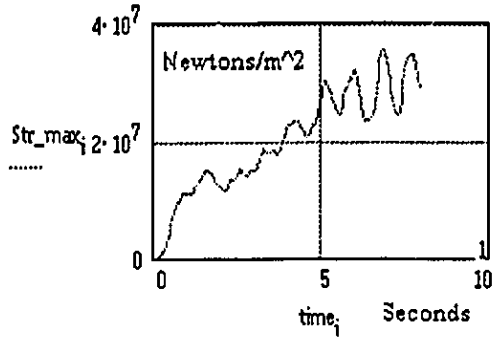

SPEED 6 KNOTS

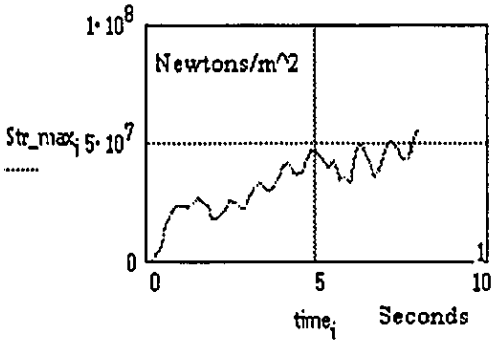

SPEED 9 KNOTS

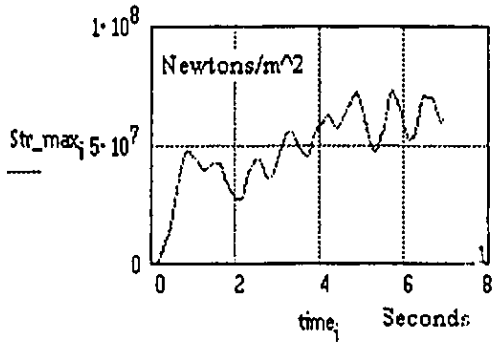

SPEED 12 KNOTS

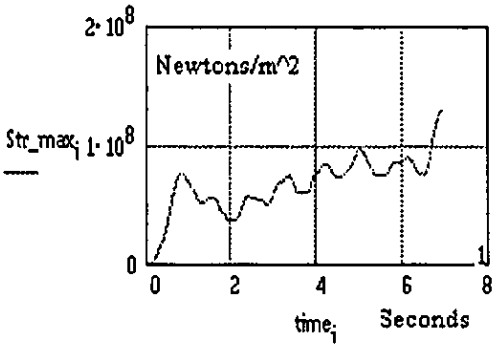

SPEED 15 KNOTS

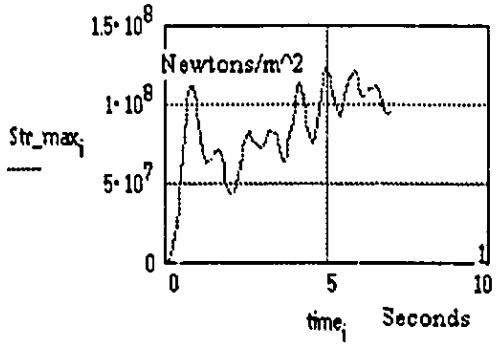

SPEED 18 KNOTS

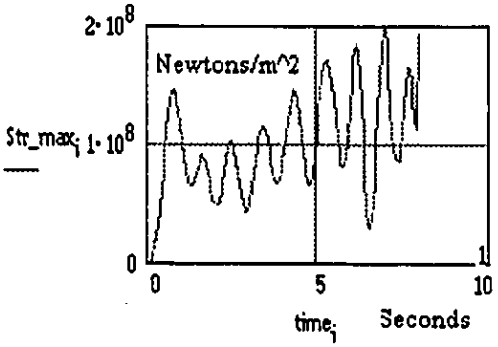

FIGURE 6.7

Comparison of ITHACA Midship Stress to Model Test

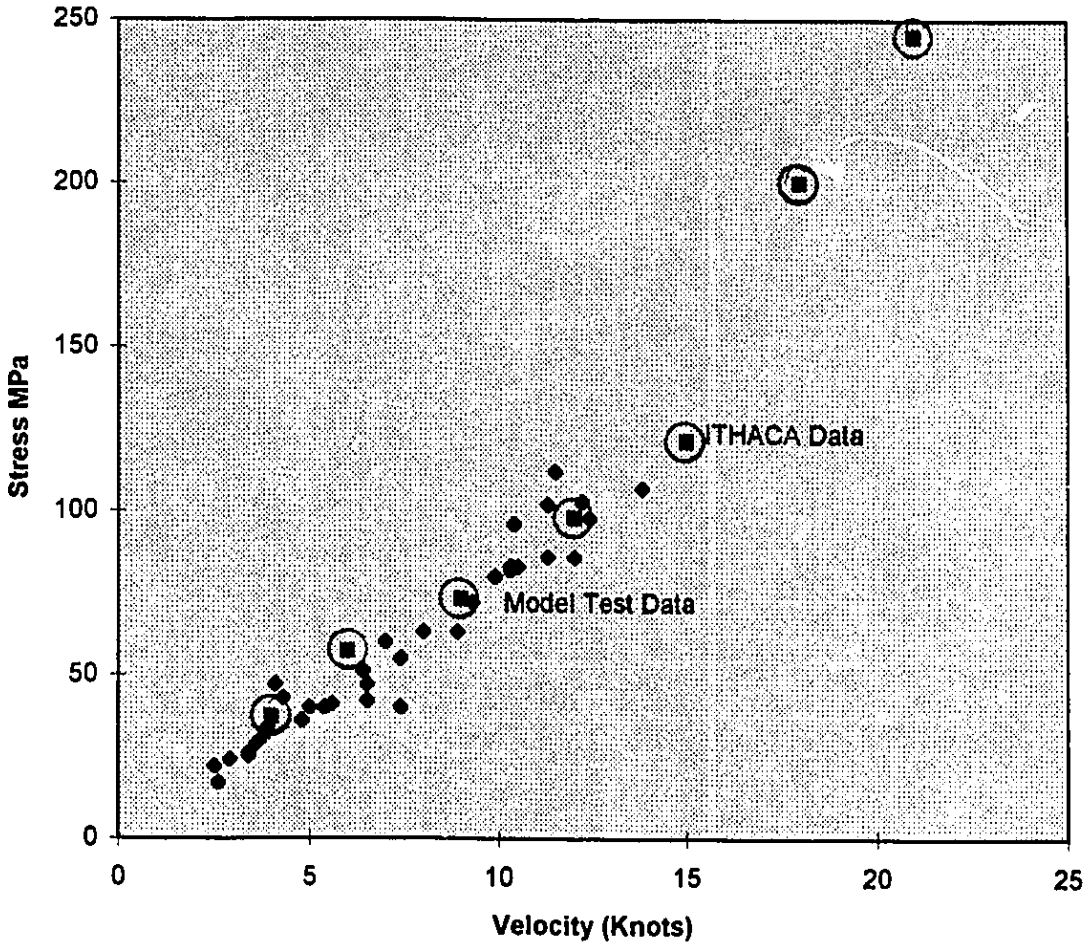

CHAPTER 7 SUMMARY AND CONCLUSIONS

The objective of the present research has been the development of numerical procedures for predicting hydroelastic stresses in the hullgirder of icebreaking ships during collisions with multi-year ice. The essential modeling problem has involved the formulation of an appropriate mathematical and computational representation for each of the significant physical mechanisms governing the ship response. Earlier models had reported only limited success in replicating the collision dynamics since an insufficient degree of complexity was retained in defining hydrodynamic and ice interaction forces. A nonlinear dynamics methodology has therefore been introduced - permitting a straightforward, time-domain computation of the structural dynamics - which simultaneously incorporates ship-ice and fluid-structure interaction forces from more complex models. These nonlinear forces are coupled through the ship dynamics.

The numerical procedures governing the collision interaction have been implemented as a concept exploration model, ITHACA_SHIP. It includes software modules for interactive design of a basic hull geometry and its corresponding structural properties. Hydroelastic stresses are determined according to a two step modeling process; whereby flexural response depends on global ice force and hydrodynamic force histories derived from a prior rigid body collision simulation. These features are intended to facilitate the application of the model to parametric analysis.

The hydrodynamic forces associated with transient, large amplitude motions of a body floating within a three dimensional free surface have been modeled using a strip formulation. A series of two dimensional cross-sections through the ship and the surrounding fluid body are taken. The fluid pressure acting on each of these slices is separately calculated in a numerical wavetank which solves the flow problem by a mixed Euler-Lagrange approach using boundary integral equation methods.

The concept of a numerical wavetank based on integral methods had been previously developed by researchers studying wave radiation. However, the application of the approach to the transient ship response case has necessitated a number of specific technical developments. For example, a multiple path regridding scheme for tracking points on the free surface (in a Lagrangian sense). This procedure eliminates the problem of relative movement of fluid elements near to a solid boundary; avoiding end points separating from, or alternatively, collapsing into the intersection point. A Chebyshev sizing of boundary elements along the free surface and body segments of the fluid boundary was also introduced to minimize the size of the computational problem at each ship cross-section. This gives smaller elements and therefore greater accuracy close to the body-wave intersection point.

Another innovation was the kinematic algorithms used to compute the transient pressure term in the unsteady Bernoulli expression. In that case, a Taylor series expansion of the velocity potential is used in conjunction with a scheme for redistributing elements on the moving body boundary.

It was found that the time-domain BEM computation of hydrodynamic forces significantly affected the simulated rigid body motions and hydroelastic stress results. At higher impact speeds the unsteady hydrodynamic effects nearly doubled the dissipation of ice energies, as compared to a spring foundation representation. This affected the magnitude of the initial crushing force peak, and gave a more stable sliding phase.

The transient hydrodynamic term was identified as the dominant pressure component over the initial phase of the collision. The characteristics of the resultant force time history, and its instantaneous distribution along the hull, were shown to be non-periodic and inconsistent with traditional interpretations of hydrodynamic phenomena in terms of linearized added mass and damping coefficients.

A rigorous, three-dimensional kinematic description of the ice interface displacements was identified as the most critical factor in modeling the ship-ice collision interaction. This observation oriented the ITHACA_SHIP Ice Interaction Model towards rigorously defining the instantaneous displacements of the ice boundary relative to the indented hull surface. The three-dimensional kinematic approach permitted abandonment of projected area methods which had proved unsatisfactory. It closely reflected the dynamics of comparable physical data - naturally introducing damping into the collision process without requiring artificial constraints, such as ice springs or virtual coefficients.

The ice force was principally defined in terms of a nominal crushing strength for the individual grid elements on the indented hull surface. But the interface formulation of the ice model facilitates introduction of more complex representations of the mechanical

ice properties. In the present investigation the simplified elasto-plastic terms constituted a negligible contribution, except for extrusion effects at the highest impact speeds.

A significant coupling between the ice and fluid interaction forces has been clearly demonstrated, justifying the nonlinear dynamics treatment of the collision problem. The magnitude and dynamic character of the ice force time histories are subtantially altered by the introduction of transient hydrodynamic modeling. Similarly, the sectional hydrodynamic forces are strongly affected by the ice force via the ship motions.

The methodology represented by the ITHACA_SHIP model was verified by comparisons with hydroelastic stress data from *MV Arctic* physical model tests and full scale trials. The nominal ice strength in the numerical model was defined in a manner consistent with the physical model test calibrations, such that predicted ramming indentations those measured in the full scale trials for a 4 knot impact. Subsequent simulations showed an excellent correlation of numerical stress predictions to comparable physical model test results.

The simulations also indicated a significant shift in the trend at higher impact speeds, giving peak stresses much greater than predicted by the physical model tests. This trend is closely associated with the emergence in the time-histories of whipping. A peak midship stress of approximately 200 MPa. was predicted at 18 knots. For longer ships or stronger ice the dynamic amplification associated with whipping might give stresses exceeding the elastic limit of hullgirder elements, especially if stress concentrations are considered.

There remain, of course, a number of limitations in the ITHACA_SHIP model. For example, the nonlinear free surface hydrodynamic model is unstable for the largest number of boundary elements which are currently feasible, so the present applications have been limited to the linearized free surface model. In the ice modeling, it is possible that the accuracy of stress predictions at higher impact speeds is degraded by the two step modeling process, since the flexural response contributions are not represented in the interaction forces. This suggests that would be useful to compare stress results predicted by a direct hydroelastic solution with those given by the present two step approach.

The development of the kinematic approach has rationalized the computation of ice forces, allowing confidence that the numerical mechanisms replicate the physical mechanisms of crushing - at least for a particular type of model ice which is a relatively homogenous and isotropic material. In contrast, the mechanical properties of multi-year ice and its failure mechanisms under different environmental and loading conditions remain poorly understood.

In summary, the ITHACA_SHIP model has permitted testing of a number of suppositions concerning the collision process. After nearly two decades of steady progress towards safer and more environmentally sound icebreaking ships; many questions affecting structural design criteria remain unresolved due to the complexity of the physical mechanisms. The present research has attempted to establish a more integrated conceptual framework for handling these problems, as well as developing specific techniques which can be applied in designing or analyzing specific ship forms.

REFERENCES

Andronov, A.A., Vitt, A.A., Kaikin, S.E. (1966)
"Theory of Oscillators". Dover Publications Inc.

Atkins, A.G. (1973)
"Scaling in Ice Fracture Mechanics : Non-Proportionately Scaled & Non-Linear Behavior". Ice Technology Proceedings of the First International Conference. Cambridge, Mass.

Atlar, M. (1982)
"A Study of the Frank Close-Fit Method; Theory, Application and Comparison with Other Methods". University of Glasgow, Department of Naval Architecture & Ocean Engineering.

Archtarides, T.A. (1979)
Wave Excited Two-Node Vertical Resonant Vibration (Springing) of Flexible Ships". Marine Technology '79 International Conference and Exhibition. October 10-12, 1979. New Orleans, La., USA.

Bathe, K-J. (1982)
"Finite Element Procedures in Engineering Analysis". Prentice-Hall Inc.

Betts, C.V., Bishop, R. E. D., Price, W. G. (1977)
"The Symmetric Generalised Fluid Forces Applied to a Ship in a Seaway". The Royal Institution of Naval Architects.

Beukelman, W. (1980)
"Bottom Impact Pressures Due to Forced Oscillations". Delft University of Technology, Ship Hydromechanics Laboratory, Delft, Netherlands.

Bishop, R. E. D., Price, W. G. (1976)
"On Model Analysis of Ship Distortions in Still Water". The Royal Institution of Naval Architects.

Bishop, R. E. D., Price, W. G., Tam, P. K. Y. (1978)
"The Representation of Hull Sections and its Effects on Estimated Hydrodynamic Actions and Wave Responses". The Royal Institution of Naval Architects.

Bishop, R. E. D., Price, W. G., Tam, P. K. Y. (1978)
"Hydrodynamic Coefficients of Some Heaving Cylinders of Arbitrary Shape". International Journal for Numerical Methods in Engineering. Vol 13 , pg 17-33.

Bishop, R. E. D., Price, W. G. (1979)
"Hydroelasticity of Ships". Cambridge University Press.

Bottema, O., Roth, B. (1979)
"Theoretical Kinematics". Dover Publications Inc.

Bratanow, T., DeGrande, G., (1982)
"A Non-Newtonian Model of the Flow of Mush-Ice". Applied Math Modeling. Vol 6.

Canadian Marine Drilling. (1985)
"*Kigorak* and *Robert LeMeur* 1983 Ice Impact Tests. Refinement of Model Ship/Ice Interaction Energies". CANMAR for the Canadian Coast Guard - Northern, TP6813E

Canarctic / NS&E (1984)
"Test Ice for Dedicated Tests, *MV ARCTIC*, 1984, Vol 1 & 2". Transport Canada TP6270E, by Norland Science and Engineering Ltd.

Chan, J. L-K. (1987)
"Numerical Procedure for Potential Flow Problems with a Free Surface". The University of British Columbia.

Comstock, J. P. (1967)
"Principles of Naval Architecture". The Society of Naval Architects & Marine Engineers.

Cointe, R. (1989)
"Non-Linear Simulation of Transient Free Surface Flows". Fifth International Conference on Numerical Ship Hydrodynamics. Hiroshima, Japan.

Craig, R. R. (1981)
"Structural Dynamics. An Introduction to Computer Methods". John Wiley & Sons

Croasdale, K.R., Morgenstern, N.R., Nuttall, J.B. (1977)
"Indentation Tests to Navigate Ice Pressures on Vertical Piers". Journal of Glaciology. Vol 19, No 81.

Cummings, W.E. (1962)
"The Impulse Response & Ship Motions". Schiffstecnik 9, pg 101-109.

Daley, C. G. (1992)
"Aspects of Ship-Ice Interaction in a Natural Ice Cover". Report from Finnish-Canadian Joint Research Project No. 5. Otaniemi 1992/m-120. Helsinki University of Technology.

Daley, C. G. (1991)
"Ice Edge Contact. A Brittle Failure Process Model". ACTA Polytechnica Scandinavica. Mechanical Engineering Series No. 100.

Daley, C. G., Phillips, L. D. (1986)
"Dynamic Ship Ice Impact - Results of Parametric Model Testing ". Ice Technology Proceedings of the First International Conference. Cambridge, Mass.

Daley, C. G., Phillips, L. D. (1985)
"Parametric Model Study of *M. V. Arctic* Hydroelastic Response During Multi Year Ice Impacts". Volume 1: Methodology and Results. Arctec Canada Ltd. Transport Canada Report TP536E.

Daley, C. (1984)
"Baffin - A Dynamic Ship/Ice Interaction Model". The Society of Naval Architects & Marine Engineers. Ice Tech '84.

Daley, C., St.John, J. W., Seibold, F., Bayly, I. (1984)
"Analysis of Extreme Ice Loads Measured on USCGC *Polar Sea*". The Society of Naval Architects & Marine Engineers, No 92.

Dand, I. W. (1976)
"Hydrodynamic Aspects of Shallow Water Collisions". The Royal Institution of Naval Architects, pg 323-346.

Dean, R.G., Dalyrymple, R.A. (1984)
"Water and Wave Mechanics for Engineers and Scientists". Prentis-Hall Inc.

Eames, M. C., Drummond, T. G. (1976)
"Concept Exploration - An Approach to Small Warship Design". The Royal Institution of Naval Architects, Paper No 2.

Edwards, R. Y., Major, R. A., Kim, J. K., German, J. G., Lewis, J. W., Miller, D. R. (1976)
"Influence of Major Characteristics of Icebreaker Hulls on their Powering Requirements and Maneuverability in Ice". The Society of Naval Architects & Marine Engineers, No.12.

Edwards, R.Y., Dunne, M.A., Comfort, G., Bulat, V., Johnson, B. (1981)
"Results of Full Scale Trials in Ice of CCGS *Pierre Radisson*". The Society of Naval Architects & Marine Engineers. Star Symposium.

Frank, W. (1967)
"Oscillation of Cylinders in or Below the Free Surface of Deep Fluids". Naval Ship Research and Development Center. Washington, D. C. Report 2375.

Finkelstein, A. B. (1957)
"The Initial Value Problem for Transient Water Waves". Communications on Pure and Applied Mathematics, Vol X, pg 511 -522.

Frank, W., Salvesen, N. (1970)
"The Frank Close-Fit Ship-Motion Computer Program". Department of the Navy, Naval Ship Research Center, Washington, D.C. Report 3289.

G&M/ VTT (1985)
"*MV ARCTIC* Dedicated Field Tests. Test Results and Analysis". Transport Canada TP6270E by German and Milne Inc and Technical Research Center of Finland.

Garrison, C. J. (1973)
"Hydrodynamics of Large Objects in the Sea Part I-Hydrodynamic Analysis". Naval Postgraduate School, Monterey, California.

Gerritsma, I. R. J., Beukelman, W. (1968)
"Analysis of the Modified Strip Theory for the Calculation of Ship Motions and Wave Bending Moments". The Netherlands Ship Research Center TNO.

Gerritsma, I. R. J., Beukelman, W. (1964)
"The Distribution of the Hydrodynamic Forces on a Heaving and Pitching Shipmodel in Still Water". Technological University Delft, Netherlands. Fifth Symposium on Naval Hydrodynamics.

Gerritsma, I. R. J., Beukelman, W. (1963)
"Distribution of Damping and Added Mass Along the Length of a Ship Model". The Netherlands Ship Research Center TNO for Shipbuilding and Navigation.

Ghoneim, G. A. M., Johansson, B. M., Smyht, M.V., Grinstead, J. (1984)
"Global Ship Ice Impact Forces Determined from Full-Scale Tests ad Analytical Modeling of the Icebreakers *Canmar Kigoriak* and *Robert LeMeur*". The Society of Naval Architects & Marine Engineers, No 92.

Gray, W. O., Maybourn, R. (1981)
"*Manhattan's* Arctic Venture-A Semitechnical History. The Society of Naval Architects & Marine Engineers. STAR Symposium.

Grim, O. (1957)
"A Method for a More Precise Computation of Heaving and Pitching Motions Both in Smooth Water and in Waves". Hamburg Model Basin (HSVA).

Hakala, M. K. (1985)
"Numerical Modeling of Fluid-Structure and Structure-Structure Interaction in Ship Vibration". The Technical Research Center of Finland, Pub 22.

Haussling, H. J., VanEsseltin, R. T. (1975)
"Finite-Difference Methods for Transient Potential Flows with Free Surfaces". David W. Taylor Naval Ship Research and Development Center, Bethesda, Maryland.

Hearnshaw, J. D., German, J. G., Benjamin, A., Stirling, J., Timonin, P., (1981)
"Data Collection System on Board the Ice Strengthened Cargo Vessel *MV Arctic* for Evaluation of Ship Performance in Ice. The Society of Naval Architects & Marine Engineers. STAR Symposium.

Howard, D., Menon, B. (1987)
'Investigation of the Added Mass Phenomenon with a Flexible Model of the *MV Arctic*: Volume 3 - Model Experiments on Open Water and Ice". Fleet Technology Ltd. for the Transportation Development Center. TP8797E.

Howard, D., Daley, C., Menon, B. (1989)
"Parametric Modeling of a 150,000 Tonne Tanker. Hydroelastic Response During Multi- Year Ice Impacts". Fleet Technology Ltd. for the Canadian Coast Guard-Northern. Vol 1, I72163C.

International Association for Hydraulic Research Committee on Ice Problems and US National Science Foundation - Sponsors (1986)
"IAHR Symposium on Ice. Iowa City. August 18-22, 1986". Institute of hydraulic Research.

Johansson, B., Keinonen,A., Mercer, B., Stubbs,J. (1981)
"Technical Development of an Environmentally Safe Arctic Tanker". The Society of Naval Architects & Marine Engineers. STAR Symposium.

John, F. (1950)
"On the Motion of Floating Bodies : Simple Harmonic Motions". Communications on Pure and Applied Mathematics, Vol 3, pg45-101.

John, F. (1949)
"On the Motion of Floating Bodies". The Institute for Mathematics and Mechanics, New York University.

Kashteljan, V. I., Poznjak, I. I., Ryvlin, A. J. (1968)
"Ice Resistance to Motion of a Ship". Sudostroenie, Leningrad, Ch I to V. Translated by Marine Computer Application Corporation (MARCOM).

Karppinen, T. O. (1983)
"Comparison of Theoretical Seakeeping Predictions with Model Test Results for a Wide Beam Fishing Vessel". Arctic and Marine Research Institute, National Research Council, Ottawa, Canada.

Kellogg, O.D. (1953)
"Foundations of Potential Theory". Dover Publications Inc. (Originally published in 1929 by B.J. Stringer Ltd.)

Kheysin, D.E. (1966)
"Determination of Contact Forces Acting in the Zone of Impact of a Ship with Ice". Problemy Artiki I Antarktiki. 22, pg 96-102.

Kheysin D.E., Likhomanov, V.A (1971)
"An Experimental Determination of the Specific Energy of Mechanical Crushing of Ice by Impact". Problemy Arktiki I Antarktiki, Vol 41, pg 55-61.

Kheysin, D.E., Likhomanov, V.A., Kurdyumov, V.A. (1973)
"Determination of Specific Breakup Energy and Contact Pressures Produced by the Impact of a Solid Against Ice". Problemy Artiki I Antarktiki, Vol 22, pg 210-218.

Kolsky, H. (1963)
"Stress Waves in Solids". Dover Publications.

Korsmeyer, T. F. (1988)
"The First Order & Second Order Transient Free-Surface Wave Radiation Problems. Massachusetts Institute of Technology.

Kry, P.R. (1978)
"Ice Statistical Prediction of Effective Ice Crushing Stresses on Wide Structures". Proceedings IAHR Ice Symposium, Lulea, Sweden.

Laskow, V. (1982)
"Ship-Ice Interaction Models. Designer's Approach". Dome Petroleum Presented at the Arctic Section of SNAME.

Lau, C.S. (1985)
"Applications of Boundary Element Method to Time Dependent Problems". The City University, Boston Spa, Wetherby W. Yorks. U.K.

Lee, Chang-Ho. (1988)
"Numerical Methods for Boundary Integral Equations in Wave Body Interactions". Massachusetts Institute of Technology, Department of Ocean Engineering.

Lee, Choung Mook. (1968)
"The Second-Order Theory of Heaving Cylinders in a Free Surface". Journal of Ship Research, Vol 12, pgs 313 - 327.

Lewis, F.M. (1929)
"The Inertia of the Water Surrounding a Vibrating Ship". The Society of Naval Architects & Marine Engineers, Vol 37, pg 1-20.

Likhomanov, V.A., Kheysin D.E. (1971)
"Experimental Investigation of Solid Body Impact on Ice". Problemy Arktiki I Antarktiki. Vol 38, pg 105-111.

Longuet-Higgins, M. S., Cokelet, E. D. (1976)
"The Deformation of Steep Surface Waves on Water ". Proc. R. Soc. Lond. A 350, 1-26(1876).

Maskell, S. J., Ursell, F. (1970)
"The Transient Motion of a Fluid Body". Journal of Fluid Mechanics, Vol 44, pg 303 - 313.

McCallum, J. S. (1989) and The Subcommittee for the Revision of the Arctic Shipping Pollution Prevention Regulations.
"Proposal for the Revision of the Arctic Shipping Pollution Prevention Regulations". Canadian Coast Guard-Northern, TP9981.

Maattanen, M. (1978)
"On Conditions for the Rise of Self-Excited Ice Induced Autonomous Oscillations in slender Marine Pile Structures". Winter Navigation Research Board, Report No 25, Helsinki, Sweden.

Maeda, H. (1980)
"On the Theory of Coupled Ship Motions and Vibration". The University on Michigan,_ Department of Naval Arch. & Marine Engineering for the American Bureau of Shipping .

Matlock, H., Dawkins, W.P., Panak, J.T. (1969)
"A Model for the Prediction of Ice-Structure Interaction". Proceedings of the First Offshore Technological Conference, Houston ,Tx.

Matlock, H., Dawkins, W.P., Panak, J.T. (1969)
"Analytical Model for Ice-Structure Interaction". Proceedings for ASCE, Journal Of Engineering Mechanics.

Matsuishi, K., Ikeda, J-I., Kawakami, H., Hirago, M. (1978)
"Ship-Ice Floe Collision Analysis Considering the Elastic Deflection of Hull Girder". The Society of Naval Architects & Marine Engineers, Vol 84-001-E.

Melville / VTT (1982)
"*MV ARCTIC* Dynamic Exciter Tests." Melville Shipping Ltd and The Technical Research Center of Finland.

Mookhoek, A. D., Voelker, R. P., DeBord, F. W. (1981)
"Summary of the Selected Technical Results from *Manhattan* Arctic Marine Project. The Society of Naval Architects & Marine Engineers, STAR Symposium.

Moore, W. H. (1994)
"The Grounding of *Exxon Valdez:* An Examination of the Human and Organizational Factors". The Society of Naval Architects & Marine Engineers, Vol 31; No 1.

Michel, B. (1978)
"Ice Mechanics". Les Presses de L'Universite Laval.

Michel, B., Toussaint, N. (1977)
"Mechanisms and Theory of Indentation of Ice Plates". Journal of Glaciology, Vol 19, No 81.

Milano, V. R. (1973)
"Ship Resistance to Continuous Motion in Ice". The Society of Naval Architects & Marine Engineers, Vol 31, No 1.

Minorsky, V.U. (1959)
"An Analysis of Ship Collision with Reference to Protection of Nuclear Powered Plants. Journal of Ship Research, Vol 3, pg 1-4.

Murthy, L. K. S., Connor, J. J., Brebbia, C. A. (1986)
"Ice Technology. Proceedings of the 1st International Conference, Cambridge, Mass. USA, June 1986". A Computational Mechanics Publication. Springer-Verlag.

Naegle, J.N. (1980)
Ice Resistance Prediction & Motion Simulation for Ships Operating in the Continuous Mode of Icebreaking". PhD Dissertation, Naval Architecture and Marine Engineering.

Newman, J. N. (1977)
"Marine Hydrodynamics". The MIT Press.

Noble, P.G., Allan, R.J., Dunne, M.A., Johnson, B. (1971)
"Ice Effect Trials in Arctic Waters on CCGS *Louis S. St. Laurent*". The Society of Naval Architects & Marine Engineers, Annual Meeting. No. 10.

Oksanen, P. (1983)
"Friction and Adhesion of Ice". The Technical Research Center of Finland, Pub 10.

Orsero, P., Armand, J.L (1977)
"A Numerical Determination of the Entrained Water in Ship Vibrations". International Journal for Numerical Methods in Engineering. Vol 13, pg 35-48.

Papanikolaou, A. (1991)
"Discussion on Venkat & Spaulding: Numerical Simulation of Nonlinear Free-Surface Generated by a Heaving Body of Arbitrary Cross Section". Journal of Ship Research. Vol 35, No 3.

Parissis, G. (1966)
"Second-Order Potentials & Forces for Oscillating Cylinders on a Free Surface". MIT Dissertation Report 66-10.

Pei, Fang Wang. (1981)
"The Radiation Condition and Numerical Aspects of Second-Order Surface Wave Radiation and Diffraction". Massachusetts Institute of Technology, Department of Ocean Engineering.

Peterson, M. J. (1982)
"Dynamics of Ship Collisions". Ocean Engineering, Vol 9, No. 4.

Phillips, L. D., Daley, C. G., Basu, R. (1986)
"Continuation of the Parametric Model Study of *MV Arctic.* Hydroelastic Response during Multi-Year Ice Impacts". ARCTEC Canada Ltd. for the Canadian Coast Guard-Northern. Transport Canada Report TP7976E.

Phillips, L.D., Menon, B.C. (1987)
"Investigation of Added Mass with a Flexible Model of the *M. V. Arctic*". Vol 2:Time Domain Analysis of Hull Response During Ramming. Arctec Canada Ltd. Transport Canada Report TP 8797E.

Popov, Y.N., Faddeev, O. V., Kheysin, D. E., Yakovlev, A. A. (1968)
"Durability of Ships Designed for Ice Passage". University of Lenningrad.

Porter, W.R. (1960)
"Pressure Distributions, Added Mass, Damping Coefficients for Cylinders Oscillating in a Free Surface. Institute of Engineering Research in Berkely, 82-16.

Potash, R. L. (1971)
"Second-Order Theory of Oscillating Cylinder". Journal of Ship Research, pg 295 -324.

Prandtl, L., Teitjens, O. G. (1934)
"Fundamentals of Hydro- and Aeromechanics". Dover Publications Inc.

Press, W. H., Teukolsky, S. A., Vetterling, W. T., Fannery, B. P. (1987)
"Numerical Recipes in C. The Art of Scientific Computation". Cambridge University Press, second edition.

Riska, K. (1987)
"On the Mechanics of Ships Ramming Massive Ice Floes". Technical University of Finland, Helsinki.

Riska, K., Daley, C. (1986)
"Physical Modeling of Ship/Ice Interaction, Report I. Ministry of Transport Canada and Technical Research Center of Finland. Joint Research Project Arrangement III. Transport Canada Report TP8238E.

Riska, K., Frederking, R. (1987)
"Ice Load Penetration Model Report 1. Constituents for Structure-Ice Interaction Modeling ". Ministry of Transport Canada and Technical Research Center of Finland. Joint Research Project Arrangement I.

Riska, K., Frederking, R. (1987)
"Ice Load Penetration Model Report 2. Modeling Ice Load during Penetration into Ice". Ministry of Transport Canada and Technical Research Center of Finland. Joint Research Project Arrangement I.

Risse, M. (1973)
"Calculation of Elastic Ship Vibrations by the Finite-Element Method. Parts A & B. The British Ship Research Association, Wallsend, Northumberland.

Sayer, P., Ursell, F. (1977)
"Integral-Equation Methods for Calculating the Virtual Mass in Water of Finite Depth". The Proceedings of the Second International Conference on Numerical Ship Hydrodynamics, September 19-21, 1977, University of California, Berkely.

Sen, D., Pawlowski, J. S., Lever, J., Hinchey, M. J. (1989)
"Two-Dimensional Numerical Modeling of Large Motions of Floating Bodies in Waves". Fifth International Conference on Numerical Ship Hydrodynamics. Hiroshima, Japan.

Sinha, N.K. (1978)
"Methodology of Columnar-Grained Ice . Experimental Mechanics Philosophical Magazine, Vol 40, pg 825-842.

Slocum, S. (1983)
"Theoretical Evaluation of Nonlinear Springing Excitation and Response". University of Michigan. Department of Naval Architecture and Marine Engineering.

Stoker, J.J. (1957)
"Water Waves. The Mathematical Theory with Applications". Interscience Publications Vol. xxviii.

Spivak, M. (1965)
"Calculus on Manifolds". W.A. Benjamin.

Sunder, S.S. (1986)
"An Integrated Constitutive Theory for the Mechanical Behavior of Sea Ice: Micromechanical Interpretation.." Ice Technology Proceedings of the First International Conference, Cambridge, Mass.

Sunder, S.S. (1986)
"Ice Load Prediction during Indentation." Ice Technology Proceedings of the First International Conference, Cambridge, Mass.

Tan, C. L. (1987)
"The Boundary Element Method. A Short Course". Department of Mechanical & Aeronautical Engineering, Carleton University, Ottawa, Canada.

Telste, J. G. (1985)
"Calculation of Fluid Motion Resulting from Large-Amplitude Forced Heave Motion of a Two-Dimensional Cylinder in a Free Surface". David W. Taylor Naval Ship Research and Development Center, Bethesda, Maryland.

Thompson, W. T. (1981)
"Theory of Vibration with Applications". Prentice-Hall Inc, Second Edition.

Timoshenko, P.T. (1953)
"The Collected Papers." Parts 1 & 2, Mcgraw-Hill Book Co. Inc.

Tricomi, F.G. (1985)
"Integral Equations". Dover Publications Inc. (Originally published 1957.)

Ursell, F. (1949)
"On the Rolling Motion of Cylinders in the Surface of a Fluid". Quarterly Journal of Mechanical and Applied Mathematics, Manchester, England.

Ursell, F. (1948)
"On the Heaving Motion of a Circular Cylinder on the Surface of a Fluid". Quarterly Journal of Mechanical and Applied Mathematics, Vol II, Part 2, Manchester, England.

Ursell, F. (1953)
"Short Surface Waves Due to an Oscillating Immersed Body". Proceedings of the Royal Society of London, Series A, Mathematical and Physical Sciences, Vol 220.

Ursell, F. (1964)
"The Decay of the Free Motion of a Floating Body". Journal of Fluid Mechanics. Vol 19

Varsta, P. (1983)
" On the Mechanics of Ice Load on Ships in Level Ice in the Baltic." Technical Research Center of Finland, Pub. No. 11, Espoo.

Vaughan, H. (1986)
"Ice-Breaking Ships & Operational Loads. Ice Technology Proceedings of the First International Conference. Cambridge, Mass.

Vaughan, H. (1986)
"Flexural Response of Ice-Breaking Ships to Impact Loads". The Royal Institution of Naval Architects.

Vaughan, H. (1983)
"Global Response of Icebreakers Ramming Heavy Ice". The Society of Naval Architects & Marine Engineers. No 17.

Vaughan, H. (1982)
"Fatigue and Fracture of Structural Elements under Random Loads ". The Royal Institution of Naval Architects.

Venkat, K. N., Spaulding, M. L. (1990)
"Numerical Simulation of Nonlinear Free-Surface Flows Generated by a Heaving Body of Arbitrary Cross Section". Journal of Ship Research, June, pg 92 - 104.

Wang, X. M., Spaulding, M. L. (1988)
"A Two-Dimensional Potential Flow Model of the Wave Field Generated by a Semisubmerged Body in Heaving Motion". Journal of Ship Research. June, pages 83 - 90.

Wang, X. M. (1986)
" A Two Dimensional Nonlinear Hydrodynamic Model of the Wave Field Generated by a Heaving Body . University of Rhode Island, Ocean Engineering.

Wehausen, J. V. (1971)
"The Motion of Floating Bodies". Annual Review of Fluid Mechanics, Vol 3, pg 237 - 268.

Wehausen, J. V. (1967)
"Initial-Value Problem for the Motion in an Undulating Sea of a Body with Fixed Equilibrium Position". Journal of Engineering Mathematics, Vol 1, pg 1 - 17.

Wehausen, J. V., Laitone E.V. (1962)
"Surface Waves". Encyclopedia of Physics, Vol 1, pg 446-778.

White, R. M. (1968)
"Dynamically Developed Force at the Bow of an Icebreaker". PhD Dissertation Massachusetts Institute of Technology.

Yeung, Y. (1982)
"The Transient Heaving Motion of Floating Cylinders." Journal of Engineering Math, Vol 16, pg 97-119